FILE COPY ONLY PIBS 3375

ENVIRONMENTAL RESEARCH

REMOTE DETECTION OF HYDROCARBON FUEL CONTAMINANTS IN THE SUBSURFACE

RAC Project No. E561G

MINISTRY OF ENVIRONMENT AND ENERGY

Ontario

ISBN 0-7778-4679-9

REMOTE DETECTION OF HYDROCARBON FUEL CONTAMINANTS IN THE SUBSURFACE

RAC Project No. E561G

Report prepared by:

J.D. Redman, S.M. DeRyck and A.P. Annan
Department of Earth Sciences
University of Waterloo
Waterloo, Ontario, N2L 3G1

Liaison Officer: Dr. S. Emami

OCTOBER 1995

Cette publication technique n'est disponible qu'en anglais.
Copyright: Queen's Printer for Ontario, 1995

This publication may be reproduced for non-commercial purposes with appropriate attribution.

PIBS 3375

REMOTE DETECTION OF HYDROCARBON FUEL CONTAMINANTS IN THE SUBSURFACE

Project: E561G.

J.D. Redman, S.M. D^{e}Ryck
and A.P. Annan

July, 1994

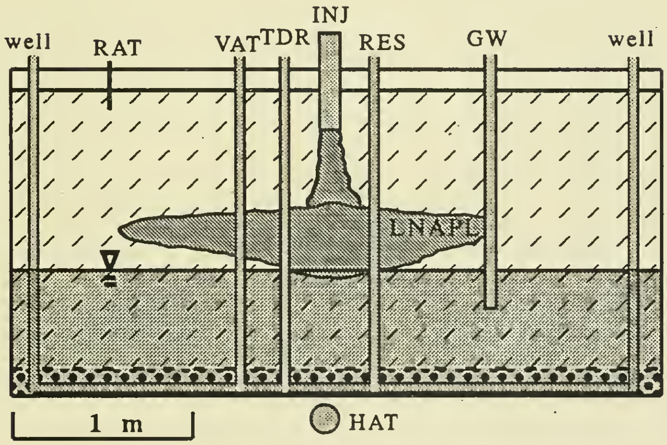

Department of Earth Sciences
University of Waterloo
Waterloo, Ontario, N2L 3G1.

Acknowledgement: The research described in this report was funded by the Ontario Ministry of Environment and Energy through the Cleansweep program.

ACKNOWLEDGEMENT AND DISCLAIMER

This report was prepared for the Ontario Ministry of Environment and Energy as part of a Ministry funded project. The views expressed in this report are those of the author and do not necessarily reflect the views and policies of the Ministry of Environment and Energy, nor does mention of trade names or commercial products constitute endorsement or recommendation for use. The Ministry, however, encourages the distribution of information and strongly supports technology transfer and diffusion.

Any person who wishes to republish part or all of this report should apply for permission to do so to the Environmental Research Program, Science and Technology Branch, Ontario Ministry of Environment and Energy, 2 St. Clair Avenue West, 14th Floor, Toronto, Ontario, Canada, M4V 1P5.

TABLE OF CONTENTS

ABSTRACT 1

1. INTRODUCTION 2

2. ELECTRICAL PROPERTIES OF SOIL-LNAPL MIXTURES 4

2.1 BACKGROUND 4

2.2 MODELLING OF ELECTRICAL PROPERTIES 5
2.2.1 Properties of Soil Constituents : Matrix, LNAPL, Water and Air 5
2.2.2 Electrical Properties of Composite Mixture 7

2.3 LABORATORY MEASUREMENTS 9
2.3.1 Background 9
2.3.2 Experimental Procedure 9
2.3.3 Results: Two-Phase Experiment 10
2.3.4 Results: Three-Phase Experiment 11

3. MODELLING EM AND GPR RESPONSE OF AN LNAPL POOL . 15

3.1 Background 15

3.2 Fluid Saturations: Water, LNAPL and Air 15

3.3 Electrical Properties Variation Across Interface 18

3.4 Surface EM Response 20

3.5 Borehole EM Response 24

3.6 GPR Response 26

4. MONITORING A CONTROLLED KEROSENE INJECTION 37

4.1 Introduction 37

4.2 Test Cell 37

4.3 Monitoring Techniques 41
  4.3.1 Water Table, Effluent Water Volume, and Soil Temperature 43
  4.3.2 Surface EM 43
  4.3.3 Ground Penetrating Radar (GPR) 43
  4.3.4 Dielectric Permittivity Monitoring 47
  4.3.5 DC Resistivity 47
  4.3.6 Neutron Logging 48
  4.3.7 Radon Soil Gas 48
  4.3.8 Borehole TV Camera 51

4.4 Monitoring and Injection Procedure 51

4.5 Monitoring Results 55
  4.5.1 Water Table, Effluent Water Volume, and Soil Temperature 55
  4.5.2 Surface EM 57
  4.5.3 Ground Penetrating Radar (GPR) 59
  4.5.4 Dielectric Permittivity Monitoring 67
  4.5.5 DC Resistivity 70
  4.5.6 Neutron Logging 79
  4.5.7 Radon Soil Gas 85
  4.5.8 Borehole TV Camera 87
  4.5.9 Kerosene Saturation Stratigraphy from Soil Cores 87

4.6 Discussion 89

5. DISCUSSION 91

5.1 Implications for the Detection of LNAPLs 91

5.2 Recommendations for Future Research 93

5.3 Publications Resulting from Funding 93

6. REFERENCES 95

TABLE of APPENDICES 98

ABSTRACT

Hydrocarbon fuel spills and leakage from underground storage tanks are a common source of groundwater contamination. In order to remediate contaminated sites, it is necessary to locate the spilled fuel within the subsurface. This site characterization has traditionally been performed by sampling groundwater in wells and collecting soil cores for laboratory analysis. In order to reduce the number of core and water samples required and to improve site characterization, many attempts have been made to use remote geophysical techniques for delineating the fuel contaminated zone. Although in principal these techniques should provide useful information, they have often been unsuccessful.

Our research objective was to provide a sound physical basis to explain the change in geophysical response observed when hydrocarbon fuels are spilled into the subsurface. A better understanding of the underlying cause for these changes will aid the evaluation of the potential effectiveness of geophysical methods at a particular site and the interpretation of survey data obtained with these methods.

In order to understand the geophysical response that can be expected at a spill site, the induced change in geophysical response for a controlled hydrocarbon fuel spill was measured, laboratory measurements of the electrical properties of contaminated soil were performed and the response of a hydrocarbon fuel pooled at the water table was modelled mathematically. The controlled fuel (kerosene) spill was performed in a 1.7-m deep by 3.6-m diameter cylindrical test cell containing a local sandy soil. Five separate kerosene injections were performed to give a total injected volume of 343 litres. Geophysical surveys were performed before, during and after each injection. The following techniques were used: ground penetrating radar, a surface electromagnetic method (EM38), surface DC resistivity, in situ DC resistivity monitoring, in situ dielectric permittivity monitoring, radon gas sampling, neutron logging, and borehole television monitoring.

1. INTRODUCTION

Hydrocarbon fuel spills are a common source of groundwater contamination. If these contaminated sites are not remediated, the spilled fuels will act as a long term source of contamination due to their slow dissolution into the local groundwater. However, to successfully remediate these sites, it is necessary to determine the distribution of the spilled fuel within the subsurface.

Previous work (Olhoeft, 1986; Keech, 1988; Pitchford et al, 1989; Borner et al, 1993; Vanhala et al, 1993, Daniels et al, 1992) has indicated that electrical geophysical methods may provide the means for the detection and delineation of these subsurface pools. The results from these previous studies at accidental spill sites were important in demonstrating that geophysical methods can in some cases provide useful information on the subsurface distribution of the spilled fuels. A limitation of these previous studies was the impossibility of characterizing the subsurface contaminant distribution and soil physical properties in sufficient detail to fully understand the observed responses, or to predict how successful these techniques would be at other contaminated sites. To improve our understanding of the application of electrical geophysical techniques to these problems, we have performed field and laboratory studies in which we measured the in situ physical properties during and following the injection of a hydrocarbon fuel. Theoretical modelling studies have also been used to predict the geophysical response due to a subsurface spill and to understand the factors that determine the magnitude of the anomalous response due to hydrocarbon fuel contaminants in the subsurface.

The objective of our research was to provide a sound physical basis to explain the change in geophysical response observed when hydrocarbon fuels are spilled into the subsurface. A better understanding of the underlying cause for these changes allows us to evaluate the effectiveness of geophysical methods (in particular those methods based on electrical properties) and improve the interpretation of survey data obtained with these methods.

To improve our understanding of the physical basis for the observed changes in geophysical response, we performed controlled laboratory and field studies of soils contaminated with hydrocarbon fuels. The laboratory studies focused on the electrical properties of soil-water-air-fuel mixtures. In the field experiment, we injected 343 litres of kerosene into a large test cell and observed the induced changes using the following techniques; in situ dielectric permittivity and resistivity probes; surface resistivity; ground penetrating radar; neutron logging; surface electromagnetic methods and radon soil gas monitoring. Theoretical modelling of a pooled hydrocarbon fuel in the subsurface was performed for the resistivity, ground penetrating radar(GPR) and electromagnetic (EM) techniques.

In previous experiments (Redman, 1992, Annan et al, 1992, and Schneider et al 1992), similar to those described here, a dense non-aqueous phase liquid (DNAPL) was injected into a natural sandy aquifer and monitored with geophysical techniques. In contrast to DNAPLs, hydrocarbon fuels belong the light non-aqueous phase liquid (LNAPL) class of organic contaminants, and do not migrate below the water saturated zone. Common examples of LNAPLs are gasoline, kerosene (or jet fuel), lubricating oils, and diesel fuel. Common DNAPLs are tetrachloroethylene(dry cleaning fluid), trichloroethylene and carbon tetrachloride.

When an LNAPL is spilled into the subsurface, it will move downwards through the unsaturated zone leaving behind a residual (isolated blobs of LNAPL) until it encounters either an impermeable horizon or the water table. An LNAPL will then accumulate at the top of and within the capillary water saturated zone above the water table, creating a zone we will refer to as an LNAPL pool. DNAPLs, on the other hand will continue to move below the water table until they encounter an impermeable horizon where they will accumulate and form a DNAPL pool. The *pooled* zone is the region in which a NAPL exists not as separate isolated blobs, but as a continuous phase that is connected by way of pore throats or films surrounding grains.

Even though DNAPLs and LNAPLs have roughly similar electrical properties, they present quite different problems in terms of geophysical detection because of the way they distribute themselves in the subsurface. DNAPL pools are usually below the water table in contrast to LNAPL pools that are situated near the water table, at the interface between the unsaturated and saturated zones. This makes the geophysical detection of LNAPLs, with electrical techniques, more difficult since this interface is usually complicated and variable depending on recent infiltration events and movement of the water table.

Since most of the geophysical methods we address depend on electrical properties of the subsurface, the first part of this report will discuss the following:

1. The results and implications of laboratory studies of the electrical properties of soil-water-kerosene-air mixtures.

2. Modelling of the electrical properties of soil-water-kerosene-air mixtures.

3. The electrical properties stratigraphy of a water table zone contaminated with a hydrocarbon fuel pool.

4. Theoretical models of the response of electrical geophysical methods to a hydrocarbon fuel contaminated water table.

The second part of the report describes a large scale field experiment in which a range of geophysical and other techniques were used to monitor the injection of 343 litres of kerosene into a large test cell.

2. ELECTRICAL PROPERTIES OF SOIL-LNAPL MIXTURES

2.1 BACKGROUND

The term soil is used in this discussion in the broad sense and refers to unconsolidated material (regolith and overburden) that may contain organic material. The laboratory measurements that are presented were performed on a sand soil but the results are also relevant to porous rocks. The theoretical modelling of electrical properties is relevant to both rocks and soils. The particular theoretical results presented are for a material with a porosity of 0.4 which clearly applies to soils. The same models with different parameters can be used to predict the electrical properties of rocks. Usually hydrocarbon fuel spills occur in the near surface and do not penetrate very far below the water table and therefore often contaminate the overburden as opposed to the underlying bedrock.

Laboratory measurements are useful for determining the effect a contaminant has on a the electrical properties of a specific soil type and provide ground-truth for theoretical mixing laws. In practice, it is not possible to characterize the electrical properties of contaminated soils for all possible soil types and pore fluids (i.e. mixtures of immiscible organic liquids, air and water) by performing laboratory measurements. Theoretical mixing laws however can be used to predict the electrical properties of a broad range of these contaminated soil types.

To predict the change in geophysical response (for electrical methods) induced by an LNAPL it is necessary to also know both the electrical properties of an LNAPL contaminated soil and the distribution of the LNAPL in the subsurface. This distribution can be obtained from core sample measurements at specific sites or can be predicted for different soils using theoretical models. In section 3.2 a theoretical model is used to predict the relative saturation of the three fluid phases (LNAPL, water and air) within the pore space of an LNAPL contaminated water table interface. From these fluid saturations the electrical properties stratigraphy across the water table interface is determined using the mixing laws.

The term dielectric permittivity, when used in this report, is the relative dielectric permittivity (often also referred to as the dielectric constant) unless specified otherwise. The electrical properties of material can be expressed in terms of the complex dielectric permittivity, the complex conductivity, or as a combination of both of these.

In this discussion, the electrical properties of mixtures are computed in terms of complex dielectric permittivity which is more convenient for GPR modelling. For modelling the response of EM methods to LNAPL pools, it is more convenient to use the real part of the conductivity σ_r (at frequency f) which is derived from the imaginary part of the complex conductivity $\mathbf{K}_i$ as:

$$\sigma_r = -2\pi f K_i$$

The imaginary part of the conductivity is generally quite small at the low frequencies used in DC resistivity and EM techniques. The highest frequency EM method discussed is the EM39 borehole induction logger which has an operating frequency of 39.2 kHz.

2.2 MODELLING OF ELECTRICAL PROPERTIES

2.2.1 Properties of Soil Constituents : Matrix, LNAPL, Water and Air

The electrical properties of the soil matrix or grains are reasonably well known and are best expressed as dielectric permittivity since their conductivity is extremely low and for the purposes of modelling is assumed to be zero. Typical values of dielectric permittivity for soil mineral grains lie in the range of 3 to 15. For a more detailed discussion of the permittivity of rocks and minerals see Olhoeft (1981) and Campbell (1969). We have used a value of 5.1 which was measured on the Borden sand that was used both in laboratory and field experiments.

LNAPLs in general have very low conductivity and for the purposes of modelling are assumed to have a conductivity of zero. Their dielectric permittivities are quite low compared to water as shown in Table 2.1.

Table 2.1: Dielectric permittivities for typical LNAPLs.

Kerosene	2.09[3]
Crude Oil	2.2 [1]
Gasoline	1.95 [2]
Mineral Oil	2.1 [2]

[1] at approximately 1 GHz (Shen et al , 1985)
[2] at 300 MHz (Musil and Zacek, 1986)
[3] at 3000 MHz (Von Hippel, 1961)

The electrical properties of typical pore water are well known and depend on temperature, ionic species and their concentration, and frequency. An excellent description of these properties is given in Olhoeft (1981). The DC conductivity of water containing number of ionic species of different concentration can be estimated (Fuoss and Hsia, 1967). DC conductivity increases by approximately 2% per °C. For a more accurate estimate of temperature dependence and concentration dependence see Ucok et al. (1979).

A relationship that gives the complex dielectric permittivity of water, excluding the contribution from DC conductivity, is given in Hasted (1973). Using this relationship, and incorporating the DC conductivity into the imaginary part of the complex dielectric permittivity, the complex dielectric permittivity of water as a function of temperature T (degrees Kelvin) and ω, the angular frequency, is given by:

$$K(\omega,T)=n^2+\frac{K_s(T)-K_h}{1+(i\omega\tau_1(T))^{1-\alpha}}+\frac{K_h-n^2}{1+i\omega\tau_2}-\frac{i\sigma}{\omega\epsilon_0}$$

Where:

$$K_s(T)=295.68-1.228T+2.094\cdot 10^{-3}T^2-1.41\cdot 10^{-6}T^3$$

$$\tau_1(T)=5.62\cdot 10^{-15}e^{\frac{.118}{8.62\cdot 10^{-5}T}} \qquad \tau_2=4.2\cdot 10^{-14}$$

$$n=1.342 \qquad \alpha=.012 \qquad \epsilon_0=8.85\cdot 10^{-12}f/m$$

σ - DC Conductivity (S/m)

$K_h=4.2$ - High frequency permittivity

The DC conductivity σ depends on specific ionic species and their concentration. $K_s(T)$ and K_h also depend on specific ion species and their concentration, but ignoring this dependence results in an error of less than 1% in the estimate of permittivity over the frequencies from DC to 1 GHz for water with ionic concentration less than .05 moles/litre (DC conductivity of .5 S/m).

The electrical properties of typical pore water at 10°C are summarized in Figures 2.2.1 and 2.2.2 for a range of ionic concentrations. The concentrations are shown as their equivalent DC conductivity. The electrical properties of a typical pore water are relatively frequency independent below 100 MHz but the high frequency properties should be considered when modelling GPR responses. At lower frequencies (less than 100 kHz), used with surface and borehole EM techniques and DC resistivity, the conductivity is frequency independent and has only a small imaginary part.

2.2.2 Electrical Properties of Composite Mixture

Mixing formulae can be used to estimate the electrical properties of composite mixtures. These mixing formulae and their application to NAPLs are discussed in Endres and Redman (1993). For the specific case of soils containing only two fluid phases, the model of Feng and Sen (1985), can be used. However, to model the vertical profile of electrical properties through of an LNAPL pool, situated at the water table interface, a model that can deal with 4 separate phases (LNAPL, water, air and soil grains) is required. Models to deal specifically with this case are not presently available.

For the modelling discussed in this report, the more general Bruggeman-Hanai-Sen (BHS) model (Sen et al, 1981) has been used to estimate the electrical properties. The relative dielectric permittivity of a mixture of two phases is calculated with this model by solving the following equation for K_m :

$$\left[\frac{\kappa_m-\kappa_e}{\kappa_b-\kappa_e}\right]\left[\frac{\kappa_b}{\kappa_m}\right]^c = \phi$$

K_e - permittivity of embedded phase
K_b - permittivity of background phase
K_m - permittivity of mixture
c - constant depending on grain shape of embedded phase (1/3 for sphere)
ϕ - porosity (fraction of sample occupied by background phase)

This model calculates the electrical properties of the mixture formed by embedding inclusions of one phase in a background media formed by the other phase. When more than two phases are involved, the model can still be used by first mixing two of the phases and then embedding the resulting mixture in a third phase and repeating this process until all phases are incorporated. The electrical properties of the LNAPL-water-air-grain mixture, were estimated with this repeated embedding procedure in the following sequence:

1. The electrical properties of the air phase was embedded in water was determined.

2. The electrical properties of the LNAPL phase embedded in mixture from step 1 was determined.

3. The electrical properties of the soil grain phase embedded in the mixture from step 2 was determined to give electrical properties of 4 phase composite.

This particular sequence is used since it preserves the continuity of the water phase throughout the matrix. This is important since most soils and rocks are water wet and the water phase is connected throughout the matrix. A grain shape parameter (c) of 1/3, appropriate for spherical grains, was assumed to be reasonable for the soil modelled.

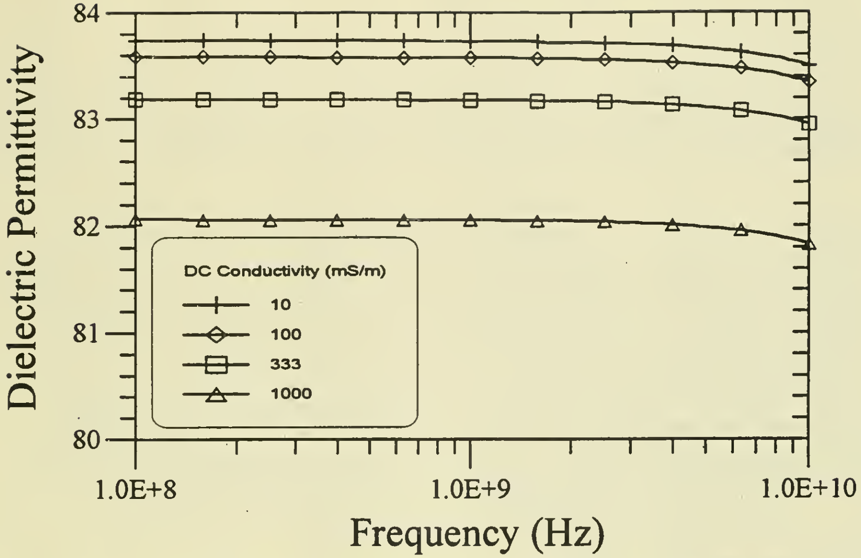

Figure 2.2.1: Real part of relative dielectric permittivity of water with varying ionic concentration. Ionic concentration is expressed in terms of low frequency (DC) conductivity of water.

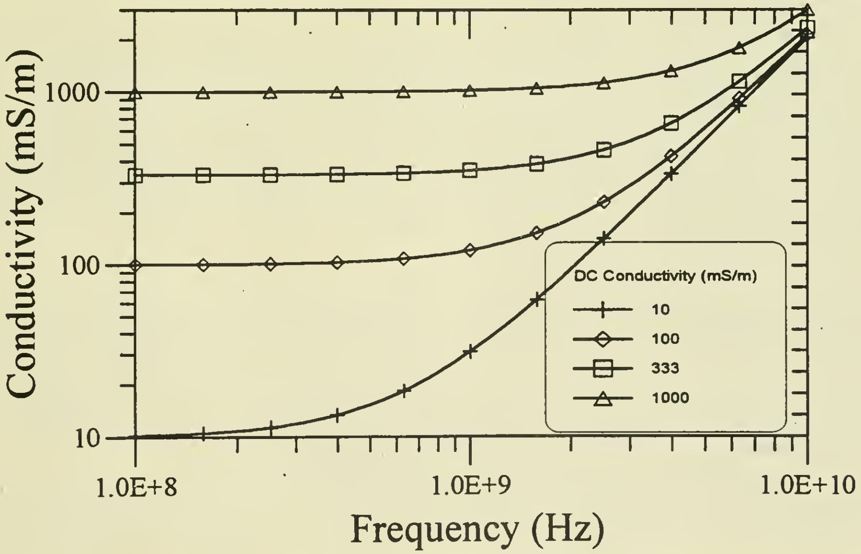

Figure 2.2.2: Conductivity of water (real part) with varying ionic concentration. Ionic concentration is expressed in terms of low frequency (DC) conductivity of water.

2.3 LABORATORY MEASUREMENTS

2.3.1 Background

The DC electrical conductivity of a standard sand (Ottawa graded sand - ASTM C778-87) was measured for a range of water-kerosene-air saturations (Westbroek, 1993). A two-phase fully liquid saturated and a three-phase partially liquid saturated experiment were performed.

In the two-phase experiment, the sand was initially saturated with water and then the electrical conductivity was measured as kerosene was injected into the sample displacing water. When no further kerosene could be injected, the process was reversed with water displacing kerosene. This process resulted in residual kerosene saturation of 0.16.

The three-phase experiment began with a liquid saturated sample containing residual kerosene (0.16 of the pore volume contained kerosene and 0.84 was water). The electrical conductivity was then measured as water was removed from the bottom of the sample allowing air to enter from the top. The relative saturation of the three fluid phases (air, water and kerosene) was measured throughout each of these experiments.

2.3.2 Experimental Procedure

The sand sample was put into a glass sample holder (Figure 2.3.1) designed for measuring the relationship between saturation and capillary pressure, and between saturation and electrical conductivity. In order to create a uniformly packed sample, the dry sand was put into the holder using a special packing technique (Wygal, 1963). In this technique, the dry sand was allowed to fall from a height of about 1.0 m through crossed screens into the sample holder. The current and potential electrodes were in place before the packing occurred. To ensure complete saturation of the sample, CO_2 gas was passed through the bottom of the sample and the fritted glass disk. De-aired water was then introduced slowly to the sample from the bottom. The water used in the experiment was deionized water mixed with 1.0 mg/litre of KCl. This resulted in water with a measured conductivity of 100 mS/m at 20°C (80 mS/m when corrected to 10°C).

The sample holder, constructed of glass, had a fine fritted glass disk (1 μm pore size) at the bottom, and a removable top with a Viton O-ring. The glass disk, when wetted with water only allowed water to pass through for the range of capillary pressures used. The injection port was connected to an LNAPL (kerosene) reservoir (Figure 2.3.2) and the outlet port to the water reservoir. Each of the reservoirs were burettes which were used to measure relative volumes of effluent and influent with a repeatability of 0.1 ml.

Since electrical conductivity is quite temperature sensitive (+2%/ °C), the sample holder was maintained at a constant temperature of 10°C in a modified refrigerator. Throughout the 1000 hours of the experiment the temperature varied by a maximum of ±0.5°C.

Stainless-steel mesh current electrodes and platinum wire potential electrodes were embedded within the sand during the packing procedure to allow for a four-terminal electrical conductivity measurement technique. The voltage from the current sense resistor, after passing through a preamplifier, was connected to the reference input on the Hewlett-Packard impedance analyzer (HP4192A). The voltage between the potential electrodes, after passing through another preamplifier was connected to the signal input on the 4192A. The impedance analyzer was computer controlled with software that used the measured relative magnitude of the current and voltage to compute the conductivity.

The capillary pressure(pressure between the kerosene and water phase) was increased by lowering the elevation of the water reservoir in 2-3 cm increments and keeping the elevation of the kerosene reservoir constant. After each change in elevation the system was allowed to equilibrate for 12 hours. Measurements of electrical conductivity, taken during one of these changes in capillary pressure, indicate that it took about 4 hours to stabilize within a few percent of the conductivity measured after 12 hours.

After the 12 hour period, the electrical conductivity, the temperature, the water volume in the water reservoir (a burette), the kerosene volume in the kerosene reservoir and the capillary pressure were measured. The complete experiment lasted about 1000 hours.

2.3.3 Results: Two-Phase Experiment

Initially the fully water saturated sample had a conductivity of 14.3 mS/m. A capillary pressure of about 10 cm of water was required before any kerosene entered the sample (Figure 2.3.3). As the capillary pressure increased further, kerosene displaced water from the pore space and the conductivity decreased, as expected since kerosene is effectively non-conducting compared with typical pore water. The conductivity continued to decrease until no further water could be displaced by the kerosene. At this point the water saturation was 0.16 (kerosene saturation 0.84) and the conductivity had decreased substantially to 0.71 mS/m.

After this initial phase of the experiment, the capillary pressure was reduced to zero. During this process the conductivity increased as water moved back into the sample displacing the kerosene. All of the kerosene was not displaced. A residual kerosene saturation of 0.19 remained in the sample.

For data collected during the initial part of the experiment in which the kerosene saturation increased from 0.0 to 0.84, there are two distinctive regimes in the conductivity versus saturation relationship. The same two regimes are also seen in the capillary pressure versus saturation relationship. The first regime is between kerosene saturations of 0.0 and 0.35 and the second is from 0.35 to 0.84.

The first regime may result from a non-uniform distribution of kerosene in the sample that is more likely to occur at low capillary pressures. Since the sample is 5.06 cm long, the top of the sample has a capillary pressure that is 1.4 (cm of water) greater than the bottom. This effect could result in a non-uniform kerosene distribution and such a distribution would affect the conductivity versus saturation relationship. It is also possible that there were two distinctive populations of pores with the larger ones being filled first.

We suspect that the first regime is not related to a non-uniform distribution of kerosene, but we believe that the second regime gives the relationship between saturation and conductivity that is representative of what would be observed in naturally contaminated soils. For both of these regimes there is linear dependence of the logarithm of conductivity on saturation. This is consistent with an Archie's law (Archie, 1942) type relationship in which the effective porosity (available for electrical conduction) is reduced relative to the amount of kerosene in the sample. This same relatively simple relationship was seen when tetrachloroethylene was injected into a Borden sand sample (Voralek, 1991).

In the second part of the two-phase experiment, in which the kerosene saturation was reduced from 0.84 to 0.19, the conductivity was substantially lower for the same saturation observed during the first part of the experiment. This observed hysteresis is quite an interesting result and may relate to the specific way is which the kerosene and water in distributed at the pore scale.

2.3.4 Results: Three-Phase Experiment

The three-phase experiment followed the final part of the two-phase experiment. At this point, the kerosene saturation was 0.19 and the remainder of the pore space was filled with water. The pooled kerosene was removed from the top of the sample. The level in the water reservoir was then lowered in a series of steps resulting in water being removed from the top of the sample and air entering from the top. The air displaces water reducing the water saturation but the kerosene saturation remained at 0.19 throughout the experiment. The results of the three-phase experiment (Figure 2.3.4) are quite similar to the two-phase experiment except that the hysteresis is not as pronounced. The effect of air in reducing the conductivity is almost the same as kerosene, as was expected since both are non-conducting compared to the water they displace.

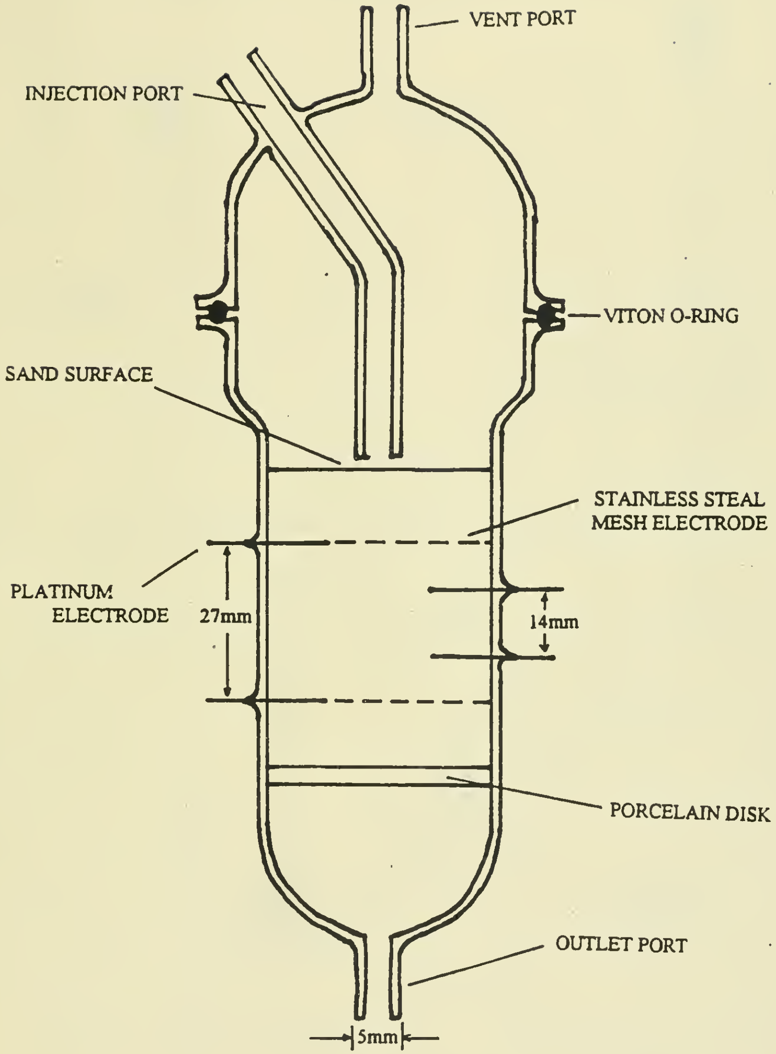

Figure 2.3.1: Cross section of glass sample holder used for injecting kerosene into sand sample and for measuring electrical conductivity of sand sample containing water, air and kerosene.

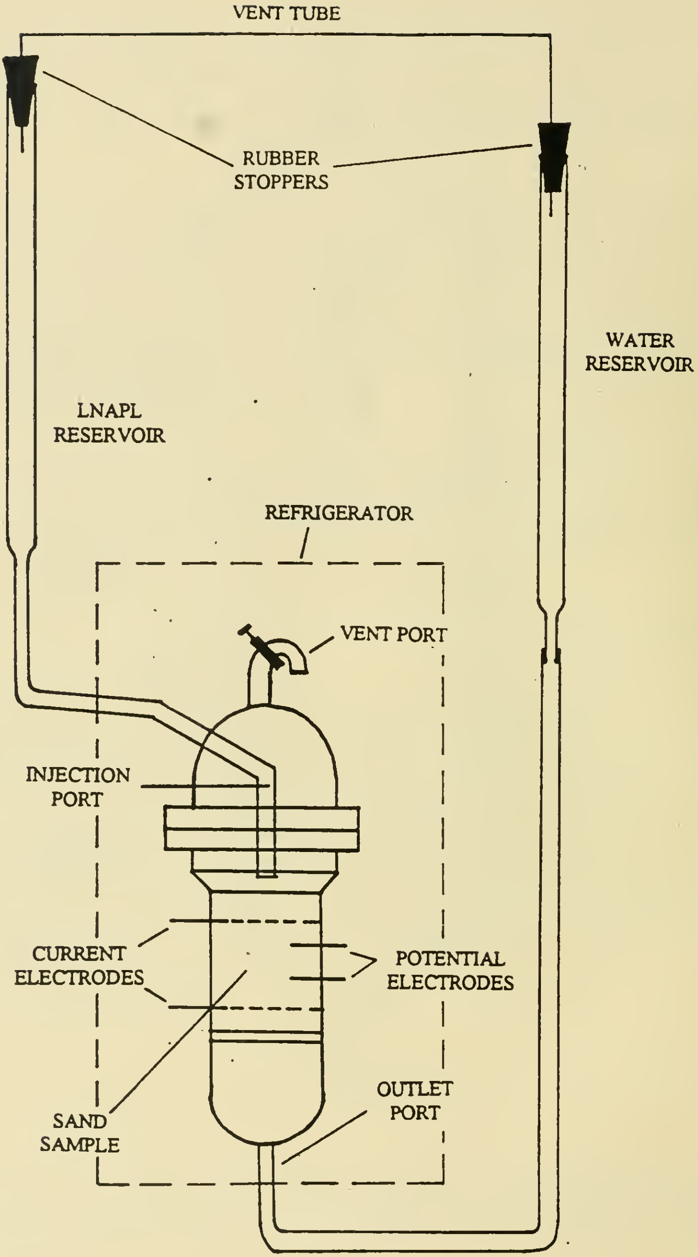

Figure 2.3.2: Schematic of complete experimental apparatus used for injecting known volume of kerosene into sand sample and for measuring electrical conductivity of sample.

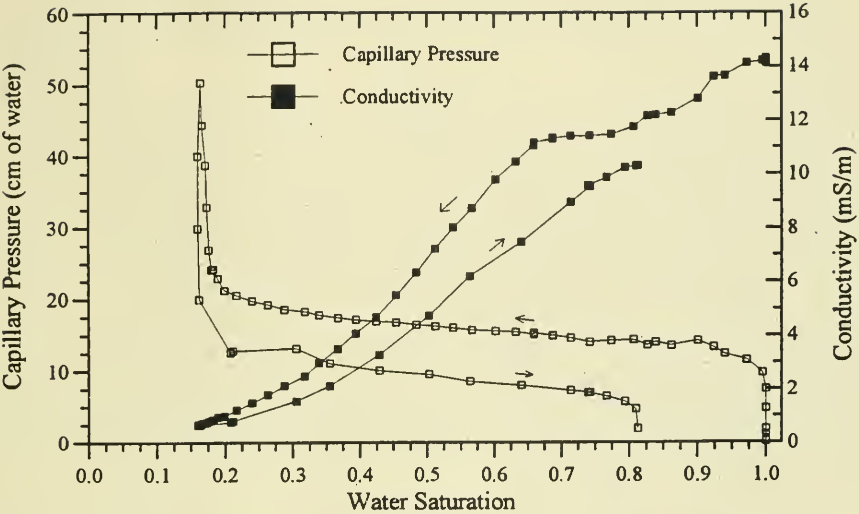

Figure 2.3.3: Electrical conductivity and capillary pressure dependence on saturation for two phase experiment. Arrows indicate direction in which experiment progressed.

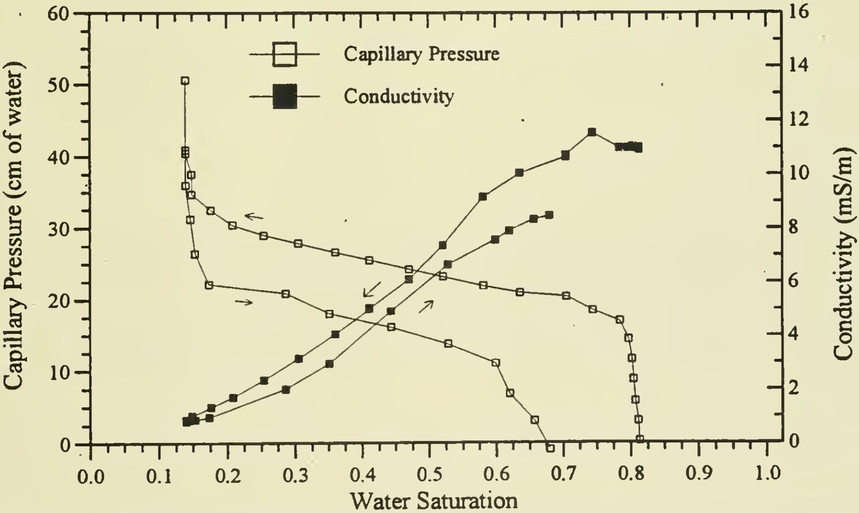

Figure 2.3.4: Electrical conductivity and capillary pressure dependence on saturation for three phase experiment. Arrows indicate direction in which experiment progressed. Initial saturations were: water .813, kerosene .187 and air 0.0.

3. MODELLING EM AND GPR RESPONSE OF AN LNAPL POOL

3.1 Background

An LNAPL that is spilled or leaked from a storage tank will move downwards until it encounters an impermeable horizon or a water saturated zone. If the spill is sufficiently large, it will then form a zone of pooled LNAPL. To remediate such a contaminated site it is important to delineate this pooled zone in the subsurface. The LNAPL may sufficiently alter the electrical properties of that zone such that it is detectable with surface geophysical techniques. The models discussed in the following sections look at the changes induced in borehole and surface EM, resistivity, and GPR responses due to a pooled LNAPL.

The first step in this modelling process, which is discussed in section 3.2, is to calculate the relative saturation of water, LNAPL, and air from the surface through the LNAPL pool and into the water saturated zone. Knowing these saturations, the vertical profile of electrical properties is then calculated as described in section 3.3. In the remaining sections the EM, GPR and resistivity responses that would result from this stratigraphy are discussed.

3.2 Fluid Saturations: Water, LNAPL and Air

The relative saturation of the three pore fluids (water, LNAPL and air) are calculated for a pooled LNAPL using a variation of the model described in Lenhard and Parker (1990). They use the following model of van Genuchten (1980) that describes the relationship between capillary head **h** and saturation S for two phase systems (n, m and α are soil parameters defined in Table 3.1):

$$S(h)=(1+(\alpha h)^{n})^{-m} \qquad h>0$$

$$S(h)=1 \qquad h\leq 0$$

The water and total liquid saturation are assumed to be independent functions of the LNAPL-water and air-LNAPL capillary head and are calculated using heads scaled with the coefficients β_{aL} and β_{Lw}. The values given for gasoline in Lenhard and Parker(1990) are used in this analysis. The pressure differences between the air and LNAPL phase h_{aL} and between the LNAPL and water phase, h_{Lw} are defined as a function of elevation z in terms of the parameters Z_{aw} and t_L as follows:

$$h_{Lw}(z)=(1-\rho_L)\,(z-z_{aw}+\rho_L t_L)$$

$$h_{aL}(z)=\rho_L(z-z_{aw}-t_L(1-\rho_L))$$

Z_{aw} - the elevation at which the gauge water pressure is zero which is equivalent to the water table elevation in a screened well outside the zone of contamination.

t_L - the difference between the elevation (Z_{aL}) at which the gauge LNAPL pressure is zero and the elevation (Z_{Lw}) at which the LNAPL and water pressures are equal. In the model of Lenhard and Parker (1990) this is assumed to be the thickness of the LNAPL in a fully screened well. For the example given in this paper, the soil parameters were taken for a sand (G.E. No. 2 sand, porosity of .37) described in van Genuchten and Nielsen (1980).

ϱ_L- Ratio of LNAPL to water density.

θ_m- Residual water content.

Table 3.1 Parameters used in modelling LNAPL and water saturations.

α	.0227
n	4.11
m	4.80
θ_m	.091
β_{Lw}	1.45
β_{aL}	3.20
ϱ_L	.73

It is assumed in the modelling that there is no residual LNAPL in the unsaturated zone. The residual LNAPL would likely be limited to the zone immediately below where the spill occurred, would be quite small in lateral extent compared to the pool and would have only a small effect on the electrical properties.

The modelling results (Figure 3.2.1) show that the pooled zone of LNAPL extends above and below the water table (elevation Z_{aw}= -1.0 m). The average saturation and thickness of the pool increases as t_L is increased from 0.0 m to 1.25 m. For the largest value of t_L, the LNAPL pool within the formation has a thickness of 1.1 m and a relatively high saturation of 0.7.

By looking at the change in total liquid (LNAPL plus water) saturation with respect to the water saturation with no LNAPL present it can be seen (Figure 3.2.2) that the LNAPL mostly displaces water from the capillary fringe. As well, a smaller fraction of the pooled LNAPL displaces air within the unsaturated zone and in the capillary zone. This is consistent with what we observed in the LNAPL injection experiment (see section 4). In this experiment the injected kerosene formed a pool at the water table and displaced water principally from the capillary fringe.

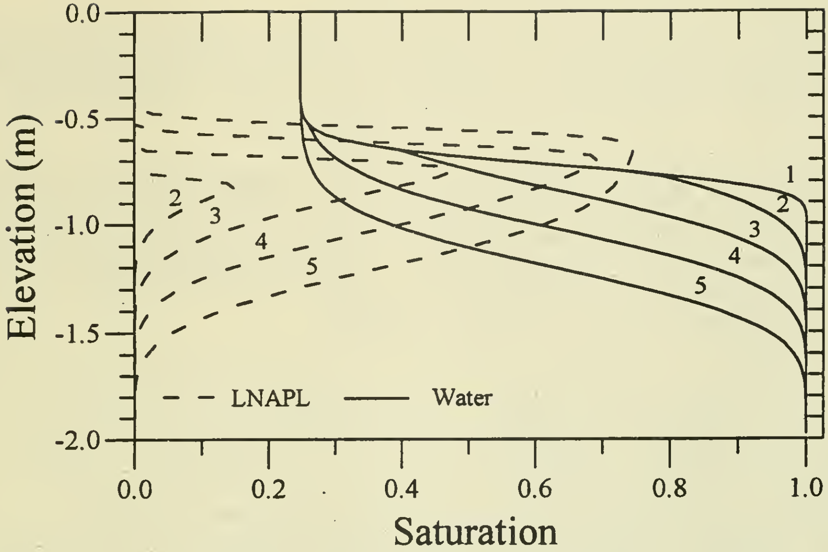

Figure 3.2.1: LNAPL and water saturation for a range of values for parameter t_L which determines thicknesses of LNAPL pool in sand. Case: 1 - 0.0 m; 2 - 0.50 m; 3 - 0.75 m; 4 - 1.0 m; 5 - 1.25 m.

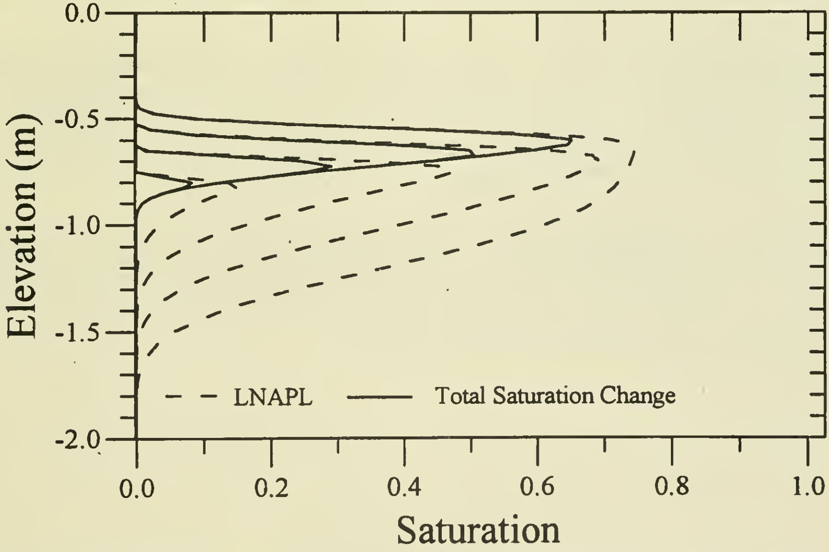

Figure 3.2.2: LNAPL saturation and change in total liquid saturation (water plus LNAPL) for same range of values for parameter t_L. Change in total liquid saturation is with respect to case 1 with no LNAPL present.

3.3 Electrical Properties Variation Across Interface

The BHS model was used to calculate the electrical properties of an LNAPL pool using the method described in section 2.2.2. The variation in water, LNAPL and air fluid saturations from the surface and through the LNAPL pool into the fully water saturated zone were computed using the method previously described in the section 3.2.

The results of this modelling (Figure 3.3.1 and 3.3.2) are presented as high frequency (200 MHz) dielectric permittivity relevant to GPR modelling and low frequency conductivity (10 Hz) relevant to EM modelling and DC resistivity. In this model the LNAPL has a relative dielectric permittivity of 1.95, the soil grains 5.1. Both of these phases are assumed to have zero conductivity. The water conductivity is 44.6 mS/m and is chosen such that the soil within the saturated zone has a conductivity of 10 mS/m.

Model 1 (Figure 3.3.1), with no LNAPL present, has a relative dielectric permittivity (real part) of 7.2 in the residually saturated zone near the surface and this increases to 24.3 within the saturated zone. This interface zone between the low to high permittivity at the water table usually gives a significant reflection event in GPR cross sections. As the pool thickness t_L increases, the depth of this interface zone increases and it becomes more gradational. Thus GPR events will occur at later times in these zones and may be of lower amplitude because of the more gradational interface. These effects are discussed in more detail in section 3.6. The imaginary part of the dielectric permittivity is small and negative for all of the models shown but is important in determining the depth of penetration for GPR.

The low frequency conductivity is 1.2 mS/m in the residually saturated zone near the surface and 10 mS/m within the saturated zone. As water is displaced from the tension saturated zone by the LNAPL the conductivity of this zone decreases. Thus the zone in which the conductivity rises to the saturated zone values moves deeper. These effects should be detectable with EM and resistivity techniques and are discussed in sections 3.4, 3.5 and 3.7.

As long as the unsaturated zone is sufficiently thick that residual saturation is reached within this zone, then the form of the electrical properties variation across the capillary fringe and LNAPL pool is independent of the depth of the water table. This is the case because it is the elevation of a point with respect to the water table, not the depth, that determines the relative saturation of the three pore fluids at that point.

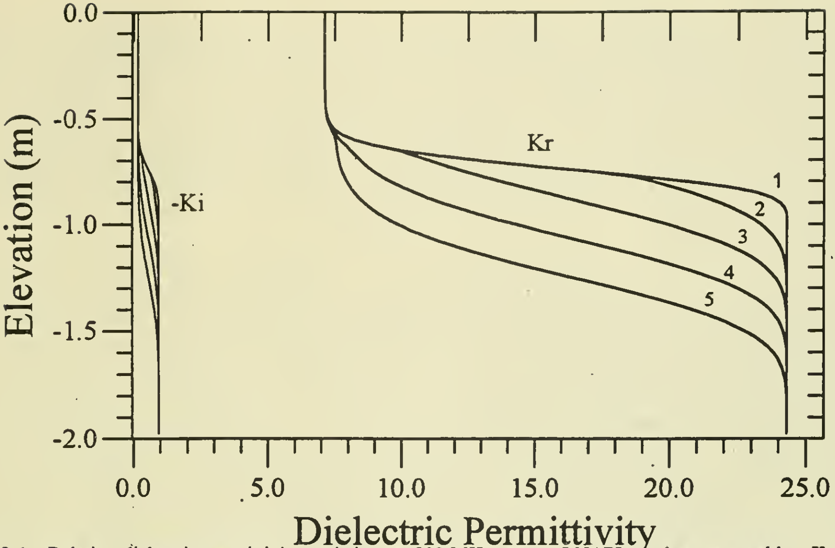

Figure 3.3.1: Relative dielectric permittivity variation, at 200 MHz, across LNAPL pool at water table. Kr is real part and Ki imaginary part (N.B. Ki has negative sign.). Water table is at 1.0 m and LNAPL pool thickness t_L within the formation is: 1 - 0.0 m; 2 - 0.50 m; 3 - 0.75 m; 4 - 1.0 m; 5 - 1.25 m.

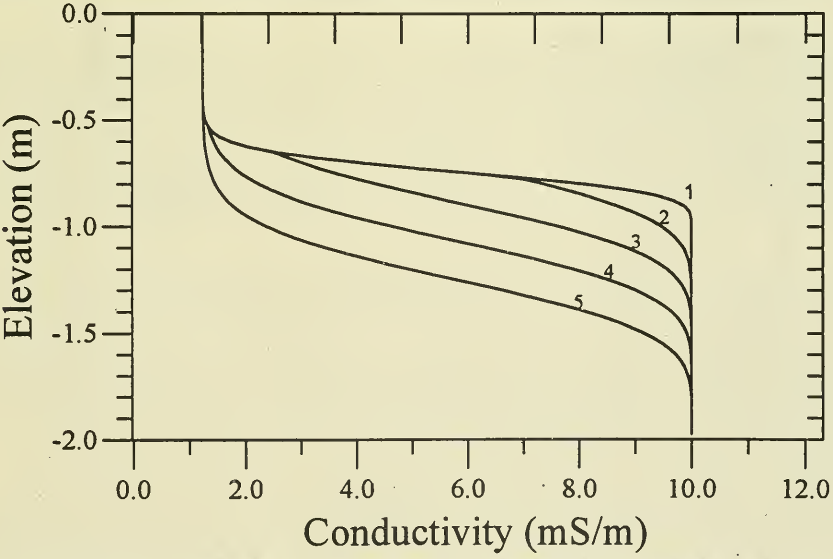

Figure 3.3.2: Conductivity (real part) at 10 Hz across LNAPL pool at water table. Water table is at 1.0 m and LNAPL pool thickness t_L, within the formation, is: 1 - 0.0 m; 2 - 0.50 m; 3 - 0.75 m; 4 - 1.0 m; 5 - 1.25 m.

3.4 Surface EM Response

Modelling of the surface EM response observed over an LNAPL contaminated water table was performed for both vertical and horizontal dipole orientations using the low induction number approximation (McNeill, 1980). The modelling is relevant to EM tools such as the Geonics EM38, EM34 and EM31. Modelling results are presented for coil separations of 3.7 m and 1.0 m that correspond to the coil spacings for the EM38 and EM31 respectively. The coils were assumed to be 1.0 m above the surface for the 3.7 m coil separation and at the surface for the 1.0 m coil separation which corresponds to the normal usage of the EM31 and EM38 respectively.

The vertical variation in electrical conductivity across an LNAPL contaminated water table was computed using the method discussed previously in section 3.3. The LNAPL was assumed to be nonconducting and the pore water conductivity was chosen to give a saturated zone conductivity of 5.0 mS/m in one case and 50 mS/m in the other case. The soil modelled is the standard GE sand discussed in section 3.2. Typical profiles of electrical conductivity for this interface are shown in Figure 3.3.2. All electrical conductivity models were calculated at 14.6 kHz (EM38 operating frequency) for the 1.0 m coil separation and at 9.8 kHz (EM31 operating frequency) for the 3.7 m coil separation. For these particular conductivity models, the maximum difference in conductivity between 9.8 kHz and 14.6 kHz for the conductivity profiles is less than 0.02% so normally, as in this case, this frequency dependence can be ignored. To perform the EM modelling , a 300 layer earth model (each layer 0.025 m thick) was produced from the vertical profiles and EM response was calculated for these models using the technique described in McNeill (1980).

The modelling results presented (Figures 3.4.1- 3.4.3) show the dependence of the apparent conductivity measured with typical EM systems above an LNAPL contaminated water table for a range of LNAPL pool thicknesses. Examples are shown for the water table at a depth of 1.0 m and 2.0 m and for a low conductivity soil (5.0 mS/m in the saturated zone) and for a high conductivity soil (50 mS/m in the saturated zone). The average LNAPL saturations in the pooled zone, as a function of the pool thickness, is given on Figures 3.4.1 and 3.4.2, since, as shown in Figure 3.2.1, the saturation varies considerably through the LNAPL pool.

In the first two models (Figure 3.4.1), the saturated zone conductivity was 50 mS/m with the water table at 1.0 m and 2.0 m. In the third and fourth less conductive models (Figure 3.4.2), the saturated zone conductivity was 5 mS/m with the water table at 1.0 m and 2.0 m. Models were computed for two coil separations 1.0 m (EM38) and 3.7 m (EM31). Since the conductivity models are scaled by the conductivity of the pore water, which is constant for each model profile, the shape of the conductivity models does change for the conductive and resistive models shown in Figures 3.4.1 and 3.4.2. It follows then that the apparent conductivity versus LNAPL pool thickness models are also scaled by the pore water conductivity. Thus the results shown for the resistive environment are exactly the same as the conductive model except that the apparent conductivities are reduced by a factor of ten.

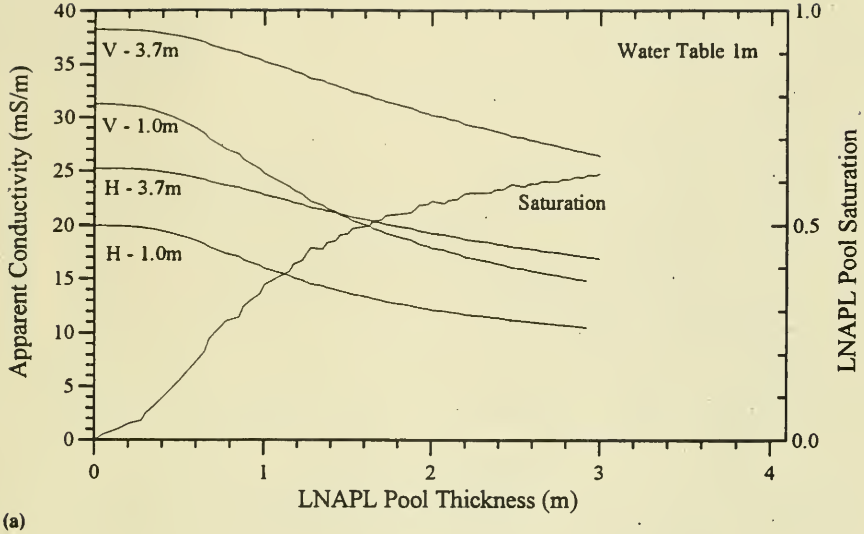

(a)

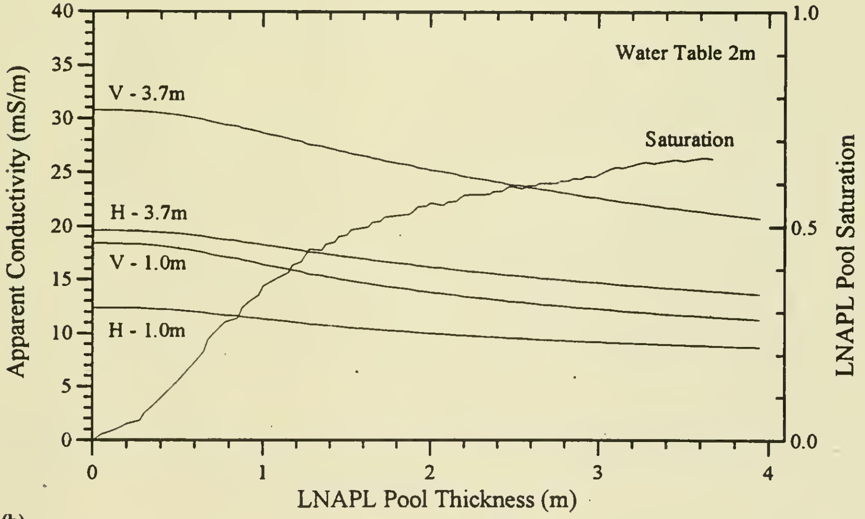

(b)

Figure 3.4.1: Modelling of EM response to an LNAPL pool at the water table in a relatively conductive environment (50 mS/m below the water table). In case (a) the water table is at a depth of 1.0 m and in case (b) the lower plot the water table is at 2.0 m. The coil orientation and separation is shown for each model (eg. V-3.7m is vertical coil orientation with a coil separation of 3.7 m)

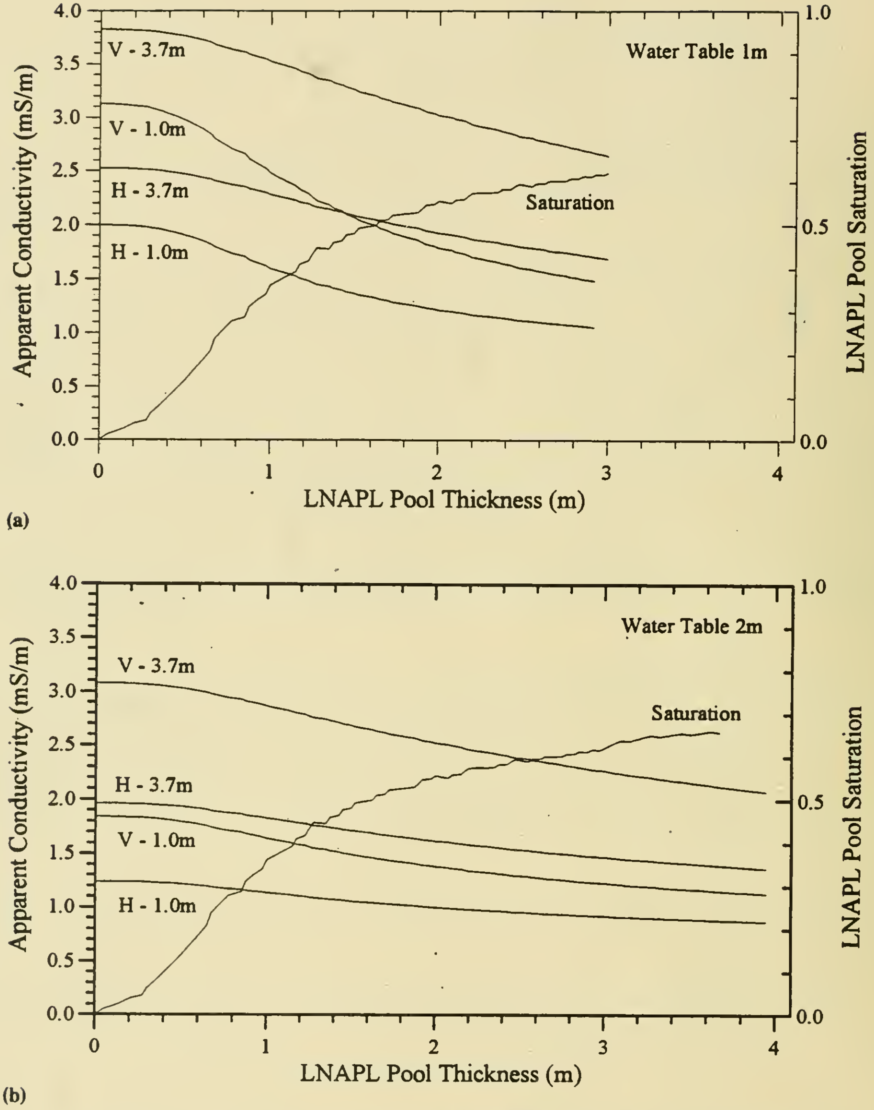

Figure 3.4.2: Modelling of EM response to an LNAPL pool at the water table in a relatively resistive environment (5 mS/m below the water table). In case (a) the water table is at a depth of 1.0 m and in case (b) the lower plot the water table is at 2.0 m. The coil orientation and separation is shown for each model (eg. V-3.7m is vertical coil orientation with a coil separation of 3.7 m).

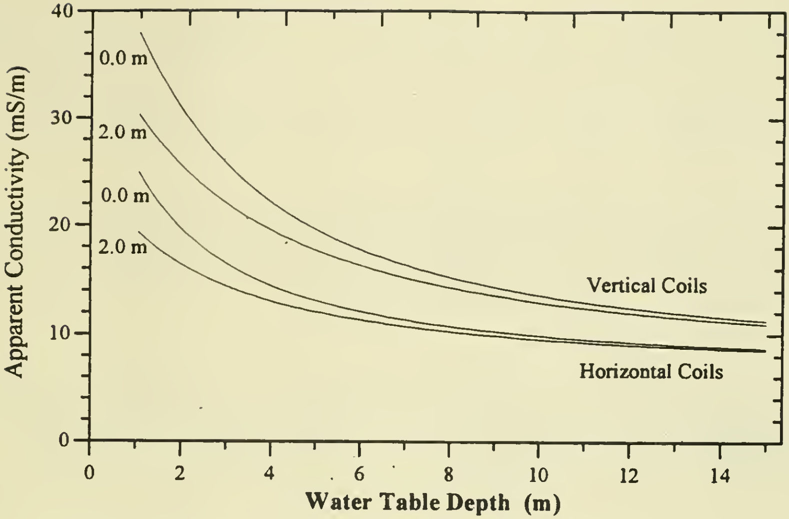

Figure 3.4.3: Modelling effect of water table depth on EM response to an LNAPL contaminated water table. Results are shown for the case of no LNAPL contamination (0.0 m) and for a 2.0 m thick pool.

In the less conductive models (Figure 3.4.2), the change in apparent conductivity measured at the surface is only about 1.5 mS/m for an LNAPL pool thickness of 3 m with the water table at 1 m. Since these instruments have a sensitivity of about 1 mS/m, this change would not be detectable. In the more conductive environment, (Figure 3.4.1) the anomalous response is substantially larger and would likely be detectable if other background changes due to natural heterogeneities and variations in water table elevation were not large.

The effect of varying the depth of the water table (Figure 3.4.3), on which the LNAPL pool lies, shows that the change in apparent conductivity for a 2.0 m thick LNAPL pool compared to no LNAPL pool (0.0 m) varies from 8 mS/m for the water table at 1 m to 2 mS/m at 6 m depth (for vertical coils). Thus below about 4-5 m in depth even this relatively thick pool would not be seen for a 3.7 m coil separation.

There are a number of limitations in this modelling approach. It is assumed that the change in pore water chemistry due to the presence of the LNAPL does not significantly alter it's electrical conductivity. This may not be the case is some instances. In this modelling it assumed that the LNAPL is nonconducting. In some cases, however, LNAPLs may associated with other waste that is high in inorganic ions resulting in an increase in electrical conductivity.

3.5 Borehole EM Response

The response of the EM39 borehole induction logger was computed for a layered earth model consisting of an LNAPL pool situated at the water table interface. The layered earth conductivity models (Figure 3.5.1a) consisted of 400 layers (layer thickness of 0.025 m) and were the same as those discussed in section 3.4 except that the water table is at a depth 4.0 m. The response function described in McNeill (1986) was then used to calculate apparent conductivity profiles (Figure 3.5.1b) that would be observed in a borehole that passed through the modelled LNAPL contaminated zone. Model results for a relatively conductive environment (50 mS/m below the water table) are shown. The model for a more resistive environment (5 mS/m below the water table) is not shown since it is exactly equivalent to the more conductive model except that the apparent conductivities are reduced by a factor of 10.

The model results (Figure 3.5.1b) extend to the surface giving rise to the reduction in apparent conductivity that is observed near 0.0 m were the conductivity drops to zero. It requires a quite significant LNAPL pool to substantially reduce the apparent conductivity and the changes that result from the presence of the LNAPL pool would be difficult to distinguish from a reduction in the water table elevation since the shape of the profile is not modified substantially.

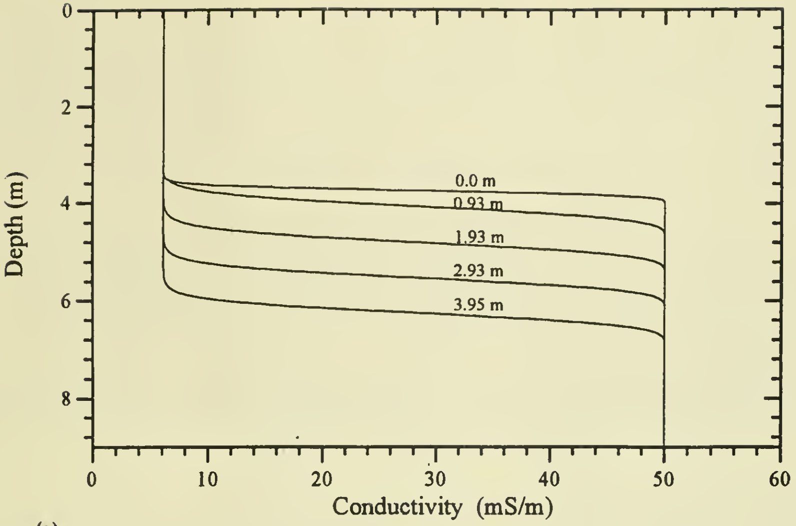

(a)

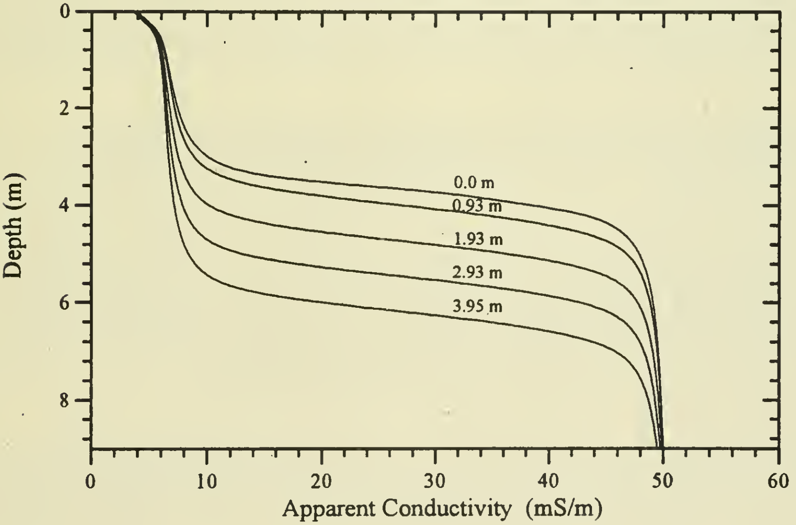

(b)

Figure 3.5.1: The layered earth conductivity model for an LNAPL pool at the water table (4.0 m), in a relatively conductive environment, is shown in the upper plot (a) for a range of LNAPL pool thicknesses. The modelled apparent conductivity profiles that would be measured in a borehole with the EM39 is shown in (b). The average LNAPL saturation within the LNAPL pool of the given thickness is: 0.0 m - 0.0; 0.93 m - .326; 1.93 m - .547; 2.93 m - .681; 3.95 m - .648.

3.6 GPR Response

The GPR response of an LNAPL pool at the water table was modelled for the following GPR frequencies: 50, 100, 200, 400 and 800 MHz. At each of these frequencies a vertical profile of the electrical properties variation (from the surface, through the LNAPL pool, and into the saturated zone) was computed for a range of LNAPL pool thicknesses. The method used to compute these electrical properties models was discussed previously in section 3.3.

A layered earth model was then constructed with a constant layer thickness (0.001 m) and with the electrical properties of each layer expressed as the real part of the dielectric permittivity and the attenuation coefficient (in units of dB/m). Models were computed for each GPR measurement frequency, for a range of LNAPL pool thicknesses, and for the depth interval from 0.0 m to 3 m (5 m at 50 MHz). The water table was at a depth of 2 m for all modelled frequencies except for 50 MHz where it was placed at 4 m so that the reflection event from the water table interface could be distinguished from the incident wave. An example of these models, for a range of LNAPL pool thicknesses, is shown in Figure 3.3.1.

The number of layers in the initial models was minimized to decrease the computation time. This was done by removing all layers in which the relative dielectric permittivity increased by less than 0.01 (0.02 at 50 MHz - see Table 3.6.1) . The number of layers in the resulting models at each frequency ranged from 396 to 840 depending on the LNAPL pool thickness. The maximum difference in dielectric permittivity between adjacent layers in these resulting layered earth models is shown in Table 3.6.1.

The GPR response, in terms of a synthetic (model) radargram, was computed using techniques similar to those used in the petroleum industry for calculating synthetic seismograms (Wuenschel, 1960). In this modelling process, the layered earth model consisting of layer thicknesses and their electrical properties was converted into an equivalent layered model (equal travel time model) in which the travel time in each layer is identical. Through this conversion process, each layer in the original model is subdivided into many layers in the equal travel time model. The number of these equal time layers within each electrical properties model layer depends on the time step chosen and on the velocity in the layer. The reflection and transmission coefficients at the boundaries of each layer and the attenuation coefficient for each layer define the equal travel time model.

The equal travel time models at 400 MHz (Figures 3.6.1 and 3.6.2) for a range of pool thicknesses show that the increase in dielectric permittivity and attenuation that occurs at the water table moves to later times and becomes more gradational as the LNAPL pool thickness increases. Also at intermediate pool thicknesses (0.5, 0.6 and 0.7 m) there is a sharp change in the slope of the curves that is coincident with the top of the modelled LNAPL pool.

The radargram is computed by exciting the equal travel time model with a vertically incident plane wave impulse. The impulse is propagated through the model in time steps equal to the propagation time through each layer. At each boundary between layers, the up-going and down-going events are determined from the appropriate transmission, reflection and attenuation coefficients. This process is repeated until the impulse response is computed for the time interval desired. The time step used in the modelling depended on the model frequency (Table 3.2).

Table 3.2: Parameters used in radargram time step modelling.

Frequency (MHz)	Water Table Depth (m)	Maximum Kr Difference[1]	Minimum Kr Difference[2]	Time Step (ns)
50	4	0.10	0.02	0.1
100	2	0.10	0.01	0.025
200	2	0.10	0.01	0.005
400	2	0.90	0.01	0.005
800	2	0.90	0.01	0.005

1. Maximum difference in relative dielectric permittivity (Kr) between adjacent layers in electrical properties model.
2. Minimum difference in relative dielectric permittivity (Kr) between adjacent layers.

The impulse response for each model was convolved with a the Ricker wavelet R(t) (centre frequency f_c) to produce the final radargrams:

$$R(t) = (1-2(\pi f_c t)^2)\, e^{(-\pi f_c t)^2}$$

The following simplifying assumptions are made in computing the radargrams. First, it is assumed that the media is not dispersive. Secondly, to account for the dependence of velocity on frequency, the electrical properties profile was calculated for each model at the centre frequency of the wavelet. Finally, the wavelet is attenuated to account for conductivity losses but spreading losses are not included.

In the modelling results presented (Figures 3.6.3-3.6.5) the amplitude scale is larger at early times (given in the figure captions), to permit both the air wave and reflected event from the water table interface to be clearly displayed.

At 50 Mhz (water table at 4 m) the amplitude of the reflected event from the water table interface decreases in amplitude and moves to later times as the LNAPL pool thickness increases. The same general character is observed in the 100 MHz radargrams except that the change in shape of the interface is apparent in the more complicated wavelet returned for greater LNAPL pool thicknesses. At 200 MHz the reflected event moves to earlier times as the pool thickness increases. At 400 MHz there is an increase in amplitude of the reflected event at intermediate thicknesses due to the more rapid increase in permittivity at the top of the pool that can be seen in Figure 3.6.1. This effect is also distinctive in the 800 MHz radargrams (Figure 3.6.5). The peak frequency in the reflected wavelet shifts to lower frequencies compared to incident wavelet.

The two-way travel time, from the surface to the water table interface, was computed from the travel time difference between the peak of the incident wavelet and the wavelet reflected from the water table. The travel time for the uncontaminated interface is about 30 ns. The travel time decreases by 3 ns for an 1.3 m LNAPL pool thickness. For pool thicknesses less than 0.3 m the change is less than 0.1 ns.

The amplitude of the reflection event from the water table interface, for an incident wavelet with an amplitude of 1.0, depends on both the GPR frequency and the LNAPL pool thickness (Figure 3.6.6). The amplitude of the reflected event does not change for the range of cases from a pool thickness of 0.0 m up to approximately 0.4 m. For intermediate thicknesses, the amplitude increases and then is substantially reduced for thicknesses greater than 0.8 m. The amplitude of the events also decrease with increasing wavelet centre frequency. As has been observed previously for field data and modelled in Annan et al (1990), the gradational nature of the water content change at the water table makes it difficult to see this interface with GPR. The presence of the LNAPL, in this case, causes this interface to become even more gradational, further reducing the amplitude of the reflected event.

The amplitude spectra for the incident wavelet are compared with the reflected events (Figures 3.6.7 - 3.6.11) for incident wavelets with a range of centre frequencies. These model results clearly show how the reflected event has a lower frequency content than the incident wavelet at the surface. Also the LNAPL pool thickness is an important factor in controlling the amplitude and centre frequency of the reflected wavelet's spectra. Amplitude spectra computed for the case of an incident 400 MHz wavelet, show that the reflected wavelet has a centre frequency of 117 MHz for no LNAPL pool (0.0 m) and a centre frequency of 264 MHz for a 1.3 m thick pool.

This modelling shows that a thick LNAPL pool is required to substantially change the amplitude and character of the event from the water table. Since the presence of the LNAPL causes a more gradational change in dielectric permittivity across the water table, the amplitude of the event from the water table will be reduced. Depending on the radar frequency used, the event from a contaminated water table may arrive earlier or later than the event from an uncontaminated water table. The anomalous response depends strongly on the thickness of the LNAPL pool and on the GPR frequency used. There appears to be little effect observed when the pool thickness is less than about 0.3 to 0.4 m.

There are a number of limitations inherent in this modelling process. In most situations, the LNAPL distribution will be more complicated due to the specific history of the spill, natural heterogeneity in the subsurface, infiltration events and fluctuations in the water table. Vapours from even small LNAPL spills can affect the water content distribution in the capillary fringe. Some of these effects may enhance the anomalous response, while others will make it more difficult to observe significant changes over contaminated sites.

The modelling results show that the effects of the LNAPL are most apparent in the peak amplitude and frequency content of the reflected wavelet while the effects on travel time are relatively small except for exceptionally thick pools.

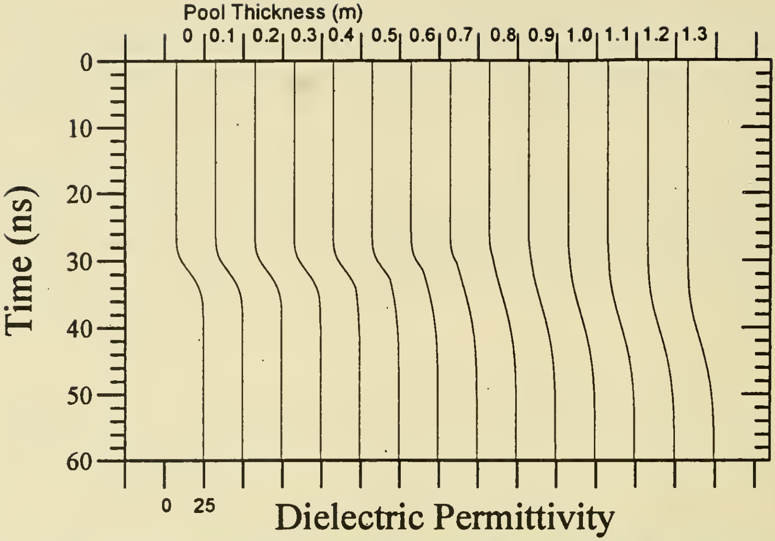

Figure 3.6.1: Relative dielectric permittivity versus time (two-way travel time) models at 400 MHz for a range of LNAPL pool thicknesses. Each model profile is offset by 25 units on the horizontal axis with a full scale of 25 for each profile, as shown.

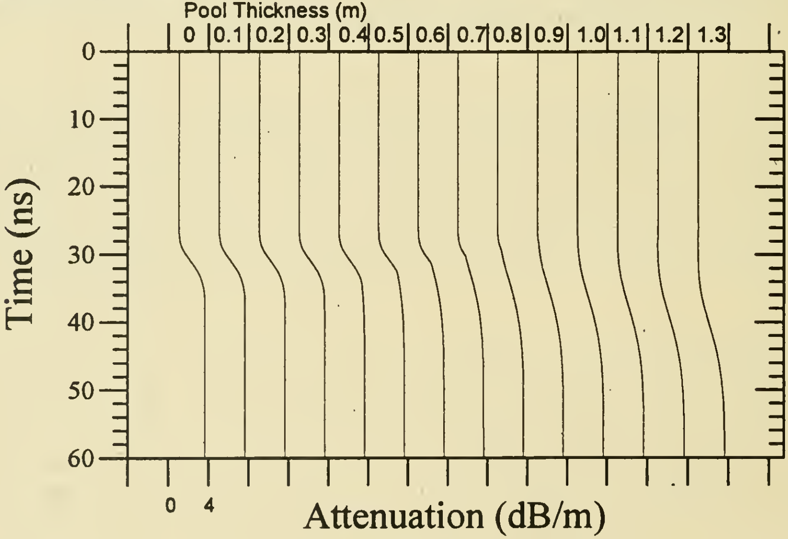

Figure 3.6.2: Attenuation versus time (two-way travel time) models at 400 MHz for a range of LNAPL pool thicknesses. Each model profile is offset by 4 units on the horizontal axis with a full scale of 4 for each profile, as shown.

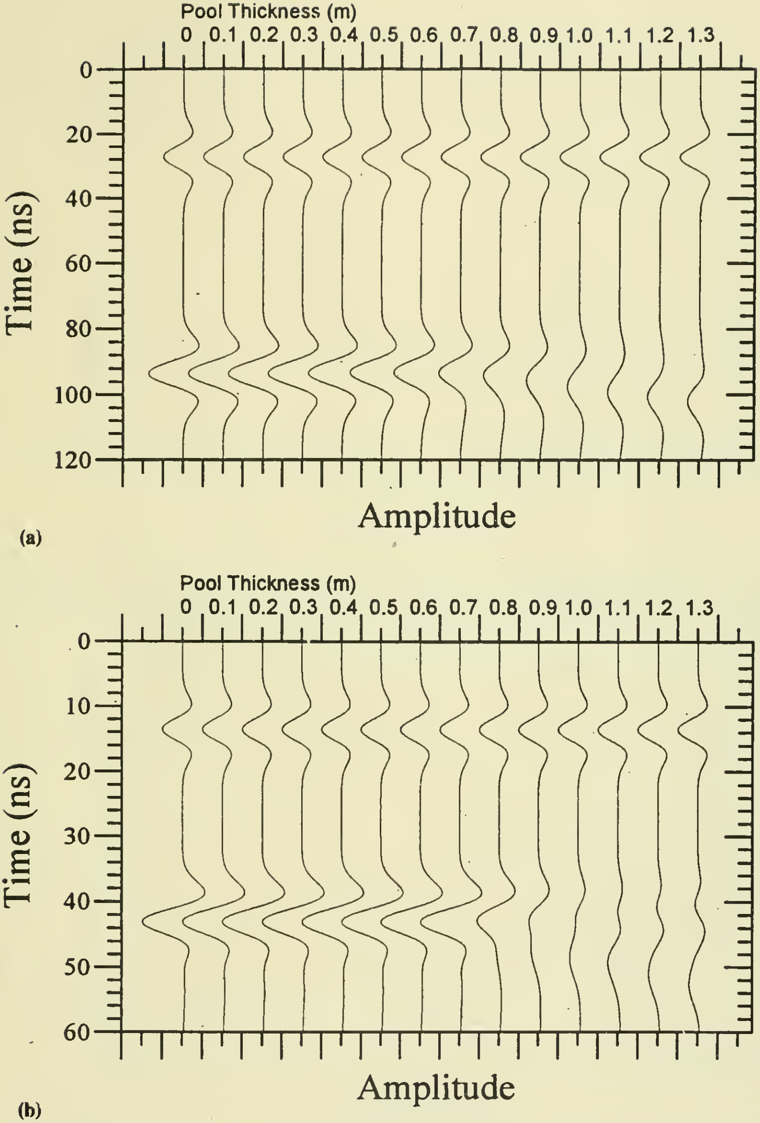

Figure 3.6.3: Radargrams for wavelet with a centre frequency of (a) 50 MHz and (b) 100 MHz for a range of LNAPL pool thicknesses. To fully display the event reflected from the surface and from the water table simultaneously, on the upper plot (a), all amplitudes for times greater than 60 ns have been multiplied by a factor of 10 and on the lower plot (b), all amplitudes for times greater than 25 ns have been multiplied by a factor of 20.

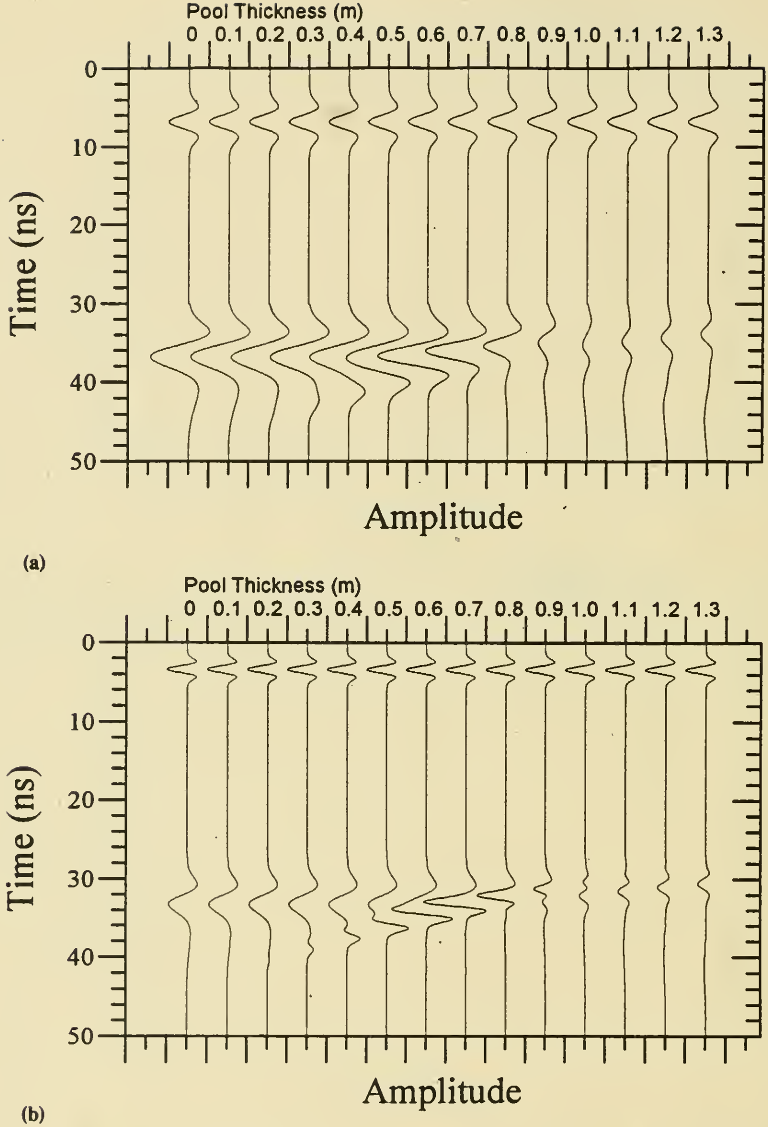

Figure 3.6.4: Radargrams for wavelet with a centre frequency of (a) 200 MHz and (b) 400 MHz for a range of LNAPL pool thicknesses. To fully display the event reflected from the surface and from the water table simultaneously, on the upper plot all amplitudes for times greater than 30 ns have been multiplied by a factor of 40 and on the lower plot (b), all amplitudes for times greater than 25 ns have been multiplioed by a factor of 100.

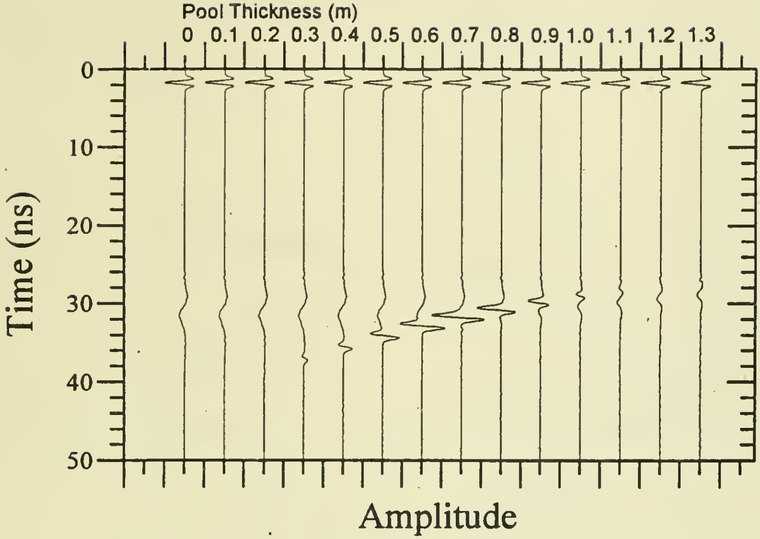

Figure 3.6.5: Radargrams for wavelet with a centre frequency of 800 MHz for a range of LNAPL pool thicknesses. To fully display the event reflected from the surface and from the water table simultaneously all amplitudes for times greater than 20 ns have been multiplied by a factor of 200.

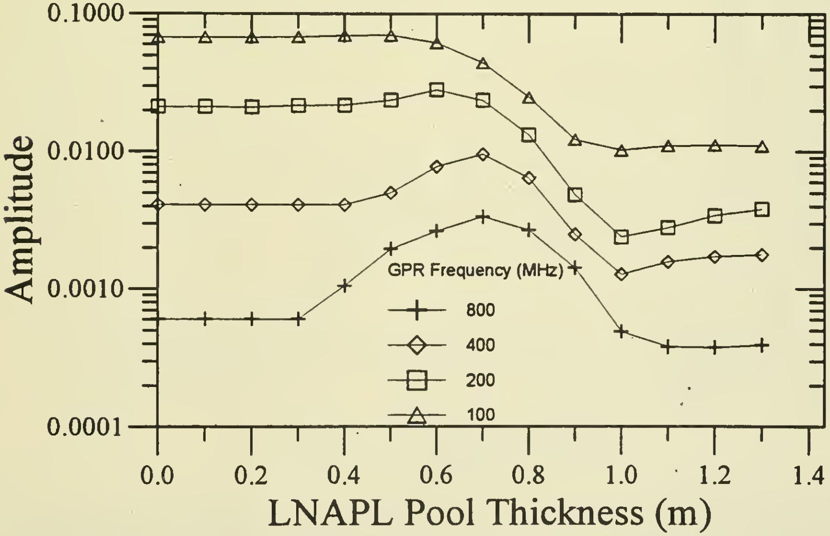

Figure 3.6.6: Amplitude of event reflected from the LNAPL contaminated water table interface for incident wavelet with an amplitude of 1.0 and with the centre frequencies indicated.

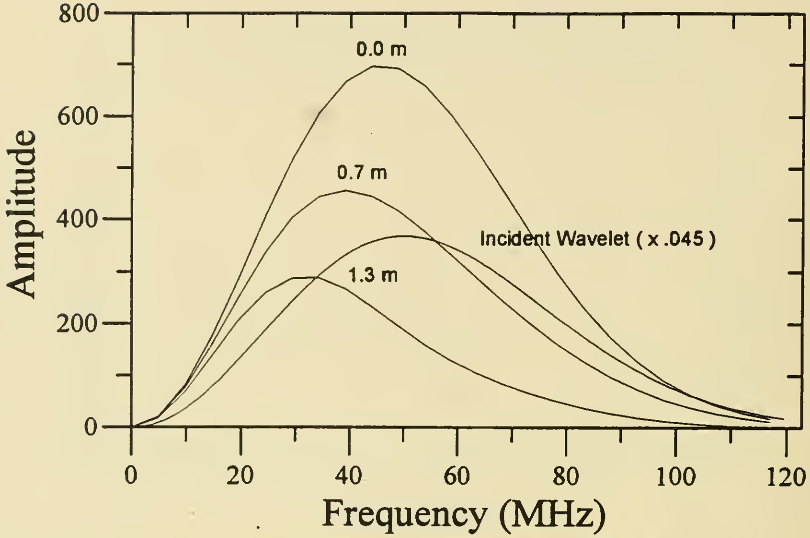

Figure 3.6.7: Amplitude spectra for event reflected from LNAPL contaminated water table for a range of LNAPL pool thicknesses. The amplitude spectra (reduced by factor indicated) of the incident wavelet with a 50 MHz centre frequency is also shown .

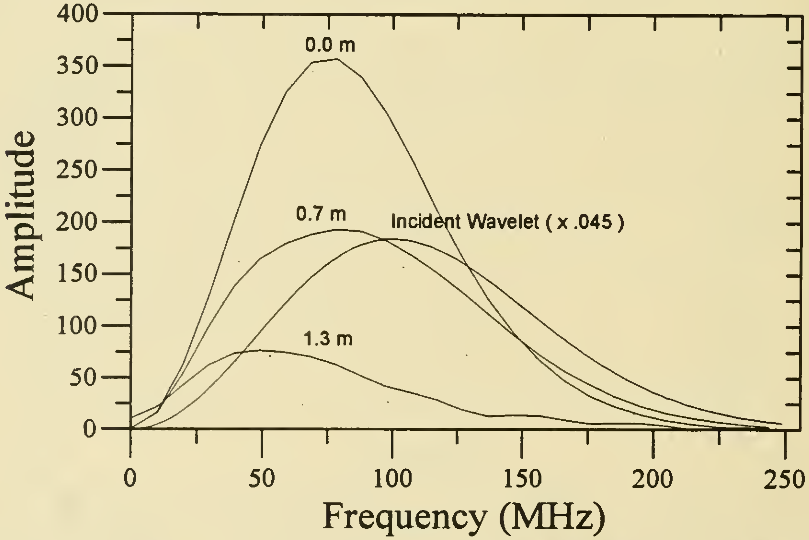

Figure 3.6.8: Amplitude spectra for event reflected from LNAPL contaminated water table for a range of LNAPL pool thicknesses. The amplitude spectra (reduced by factor indicated) of the incident wavelet with a 100 MHz centre frequency is also shown .

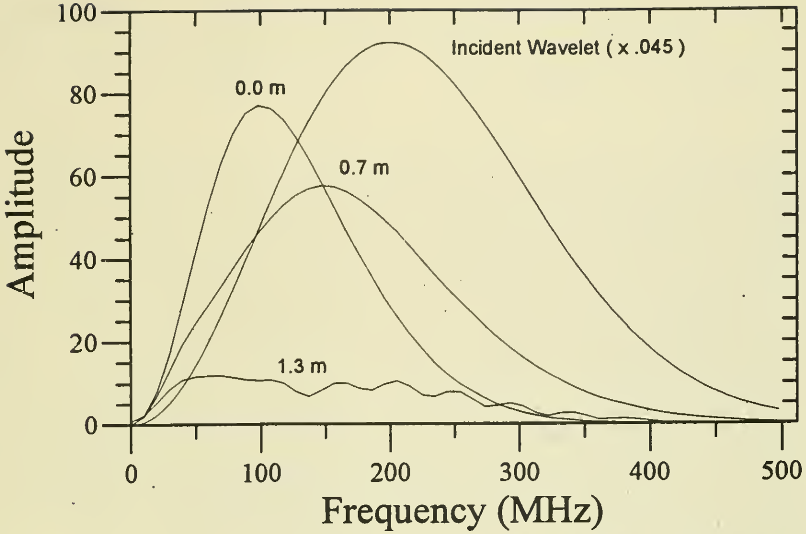

Figure 3.6.9: Amplitude spectra for event reflected from LNAPL contaminated water table for a range of LNAPL pool thicknesses. The amplitude spectra (reduced by factor indicated) of the incident wavelet with a 200 MHz centre frequency is also shown .

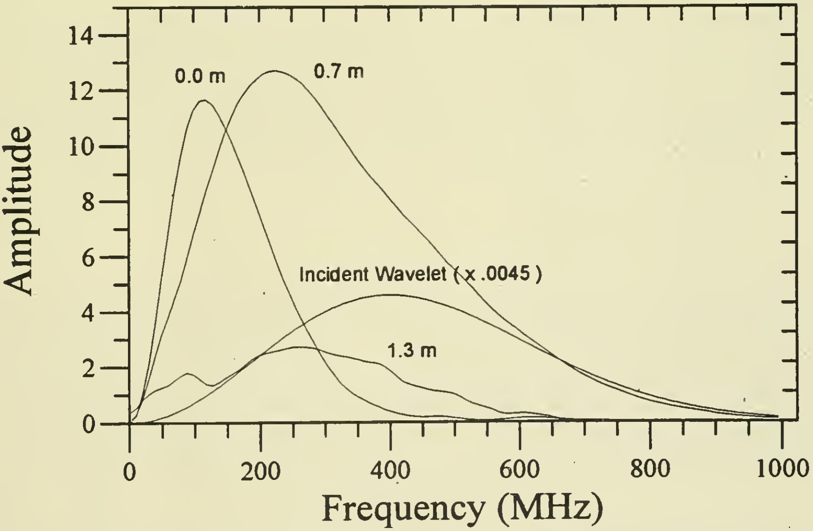

Figure 3.6.10: Amplitude spectra for event reflected from LNAPL contaminated water table for a range of LNAPL pool thicknesses. The amplitude spectra (reduced by factor indicated) of the incident wavelet with a 400 MHz centre frequency is also shown .

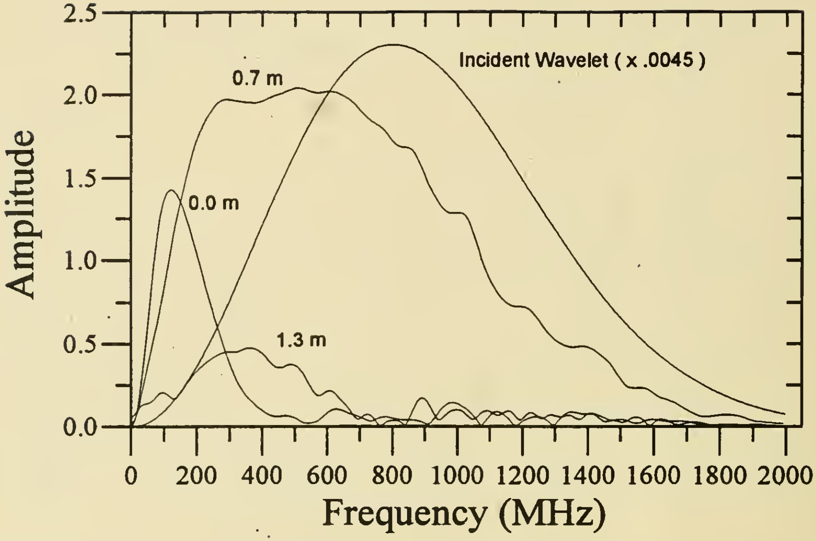

Figure 3.6.11: Amplitude spectra for event reflected from LNAPL contaminated water table for a range of LNAPL pool thicknesses. The amplitude spectra (reduced by factor indicated) of the incident wavelet with a 800 MHz centre frequency is also shown .

4. MONITORING A CONTROLLED KEROSENE INJECTION

4.1 Introduction

Light nonaqueous phase liquids (LNAPL's) are a common subsurface contaminant. There are many different methods which have been used to detect and monitor these contaminants one of which is geophysics. In order to better understand the capabilities and limitations of geophysical techniques used in the investigation of LNAPLs, a controlled kerosene injection experiment was conducted during the summer and fall of 1992 at Canadian Forces Base Borden. By controlling many of the factors which could affect the geophysical readings, the changes in physical properties which occurred due to the kerosene could be identified and monitored. In so doing, we could learn about the responses of the geophysical equipment and perhaps even observe the behaviour of the LNAPL in this simple environment.
One accepted conceptual model of an LNAPL spill (Figure 4.1.1) depicts a spill which occurs at or near the surface within the unsaturated zone of a homogeneous porous medium. The LNAPL moves down through the unsaturated zone exhibiting little lateral spreading. The LNAPL continues moving down until it reaches the top of the saturated zone where, since by definition it is immiscible in water, the LNAPL begins to pool. This immiscible phase pool spreads along the top of the saturated zone until its mass becomes large enough to displace water. As the immiscible phase pool increases, it may even cause a depression of the water table.

As well as the immiscible phase LNAPL pool, there will also be vapour phase LNAPL above the saturated zone and a dissolved phase plume within the saturated zone. This dissolved phase plume is shown to spread in the groundwater flow direction. In the case of this experiment, there was essentially no groundwater flow and as a result we would expect the dissolved phase plume to be symmetric about the pool itself. The only induced groundwater flow that may have occurred was due to a small amount of pumping.

4.2 Test Cell

The monitoring instrumentation was installed in a 3.6 m diameter, 1.7 m deep, cylindrical polyethylene tank. (Figures 4.2.1 & 4.2.2) The cell was equipped with a system of 2" SCH 40 (0.008 slot) Timco well screens which ran horizontally along the bottom of the tank and were buried within a 12 cm layer of gravel. The well screens were attached to two 2" SCH 40 PVC vertical wells through which the water table could be monitored and controlled. The balance of the instrumentation consisted of two ½" SCH 40 PVC piezometers, a 2½" SCH 40 PVC vertical access tube, 2" SCH 40 PVC vertical resistivity and dielectric permittivity monitoring probes and seven 63.5 mm tubing glass sections.

The piezometers were screened over the bottom 10 cm and extended into the top of the gravel layer. All of the probes were sealed on the bottom and also extended into the gravel

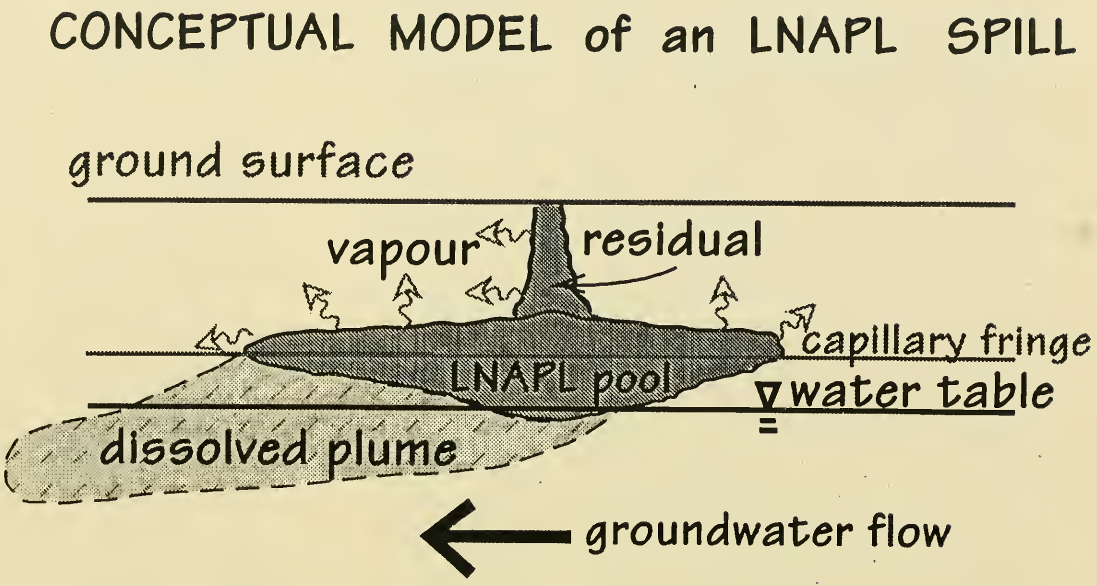

Figure 4.1.1
This figure is a conceptual model for an LNAPL spill in an aquifer with groundwater flow.

CROSS SECTION

INSTRUMENTATION

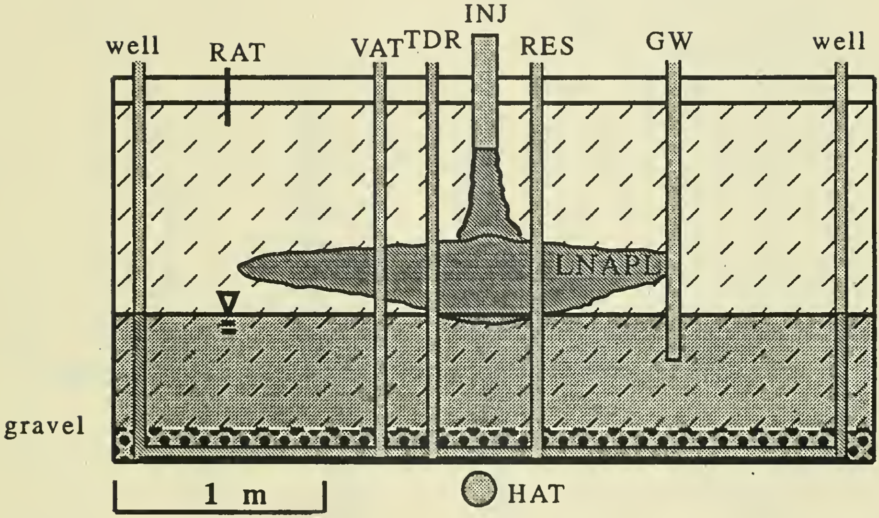

RAT : radon access tube
VAT : vertical access tube
TDR : dielectric permittivity probe (time domain reflectometry)
INJ : injection point
RES : resistivity probe
GW : observation well
HAT : horizontal access tube

Figure 4.2.1
Cross section of instrumentation in test cell with water table at 1.1 m.

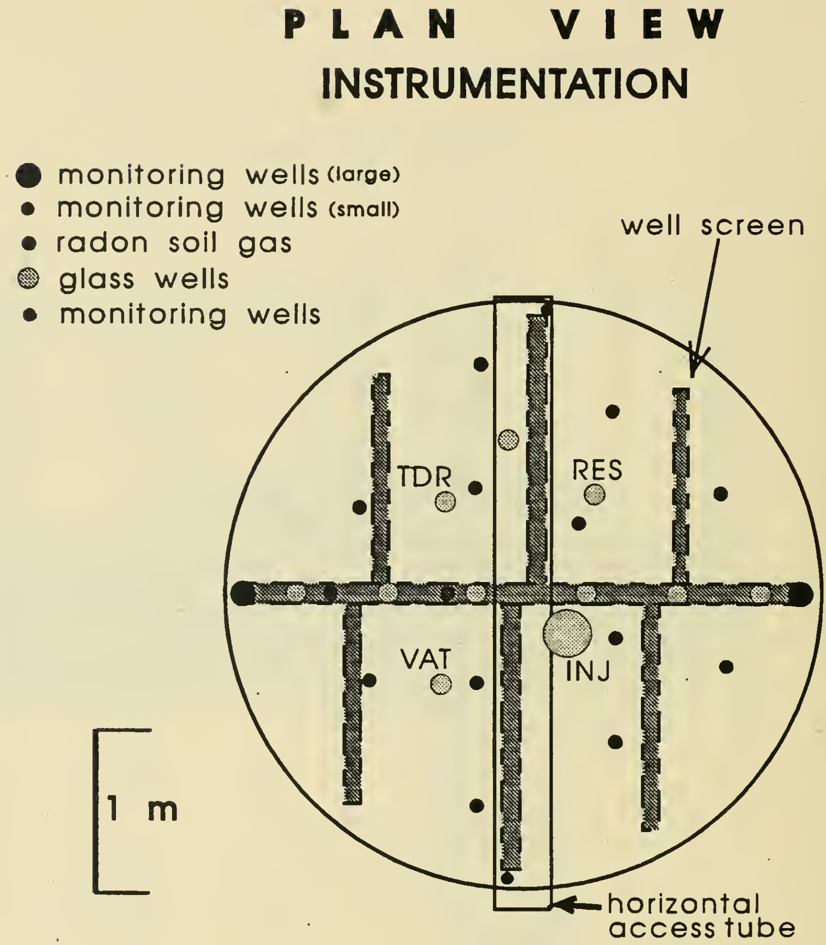

TDR : dielectric permittivity probe (time domain reflectometry)
RES : resistivity probe
VAT : vertical access tube
INJ : injection point

Figure 4.2.2
Plan view of instrumentation in test cell.

with the exception of the glass wells. Although sealed on the bottom, the glass only penetrated to a depth of 1.3 m with the top 10 cm consisting of a 2" SCH 40 PVC extension. Six of the glass wells were positioned in a line across the cell with the seventh on a perpendicular line. A 12" SCH 35 gasketed sewer pipe was used as a horizontal access tube which was buried below the tank and extended from one side of the tank to the other.

The test cell was packed with Borden sand after all of the probes had been installed. The sand pile was initially at residual water content. The packing procedure involved passing the sand through a 1 cm mesh in order to sieve out leaves and roots and then conveying it into the tank. The sand within the tank was then raked until an even 20 cm layer was created. Hand tampers were used to compact the sand layer which had a final thickness of 10-15 cm. The surface was then raked lightly to encourage blending with the next layer. The water table was raised as the tank was packed so that the top of the saturated zone was just below the sand surface. The packing of the test cell was coordinated with the building of a sand berm around the outside of the cell to serve the dual purpose of structural support and thermal insulation. The final depth of the sand pack (including gravel) was 1.7 m.

The injection point was a 1.6 m length of 5" diameter SCH 35 sewer pipe which was driven down to 30 cm below ground surface (bgs). The sand inside the injection point stand pipe was removed and replaced with approximately 30 cm of clean coarse gravel. This gravel layer prevented the sand at the point of injection from being disturbed by the injection of the kerosene.

4.3 Monitoring Techniques

The following conventional monitoring and geophysical techniques were used in the experiment.

- Water level monitoring,
- Effluent water monitoring,
- Monitoring temperature within the sand pack and wells,
- Electromagnetics (surface),
- Ground Penetrating Radar (GPR)
  (reflection, transillumination, and tomography),
- Dielectric Permittivity (TDR, *time domain reflectometry*)
  (borehole),
- DC Resistivity (surface and borehole),
- Neutron logging,
- Radon soil gas monitoring,
- Borehole television observations.

Each instrument required its own survey design in order to obtain the best results. Therefore, although an attempt was made to use common survey grids, there are still a number of different grids and station locations. (Figure 4.3.1)

PLAN VIEW

NUMBERING CONVENTIONS

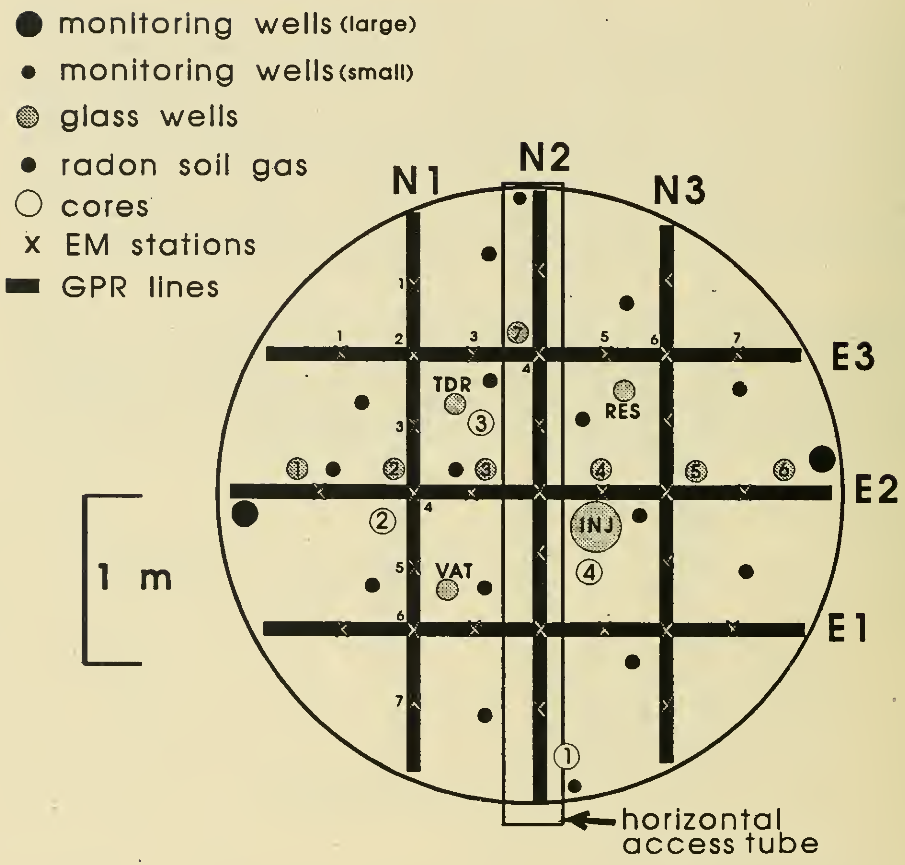

TDR : dielectric permittivity probe (time domain reflectometry)
RES : resistivity probe
VAT : vertical access tube
INJ : injection point

Figure 4.3.1 Plan view of test cell describing the numbering conventions used for various surveys.

In an attempt to simplify the reporting of the monitoring schedule as well as the results, the events of the experiment are reported in days and hours. That is, day zero is assumed to be the day that the packing of the test cell was complete which was August 19, 1992. Day one began at 00:00 hours on August 20, 1992.

4.3.1 Water Table, Effluent Water Volume, and Soil Temperature

Water level measurements were made throughout the experiment in the four monitoring wells. (Figure 4.3.1.1) During the course of the experiment, any effluent water was captured and measured. (Appendix A.1) This effluent water could then also be tested for any dissolved kerosene constituents. In addition to these measurements, the temperature of the cell was monitored occasionally using a thermistor. The thermistor was placed in the surface resistivity electrode holes for surface measurements and in the wells for depth measurements. As a result, the measurements at depth may be greatly affected by the air temperature.

4.3.2 Surface EM

The electromagnetic data were collected with the Geonics EM38 at seven stations along each of the six GPR grid lines. The grid overlaps such that alternate stations along any line corresponded to a station along a perpendicular grid line. (Figure 4.3.2.1) The electromagnetic data were collected on only three occasions: once while the sand pack was completely saturated, again just prior to the injections with a reduced water table, and finally after the last injection.

4.3.3 Ground Penetrating Radar (GPR)

Ground Penetrating Radar (GPR) was used to identify interfaces between regions of different dielectric properties. GPR reflection surveys were performed on a six line grid within the test cell. (Figure 4.3.3.1) These surveys were conducted with the Sensors and Software Pulse Ekko 1000 with both the 450 MHz and 900 MHz antennae. The antennae separations for the two frequencies were 0.25 and 0.165 m respectively. Data were also collected using the 450 MHz transmitter and the 900 MHz receiver at an antennae separation of 0.165 m. GPR transillumination surveys were performed using the 450 MHz antennae with the transmitter located within the horizontal access tube which ran under the tank and the receiver on the test cell surface. A tomographic survey was also conducted along one line after the final injection.

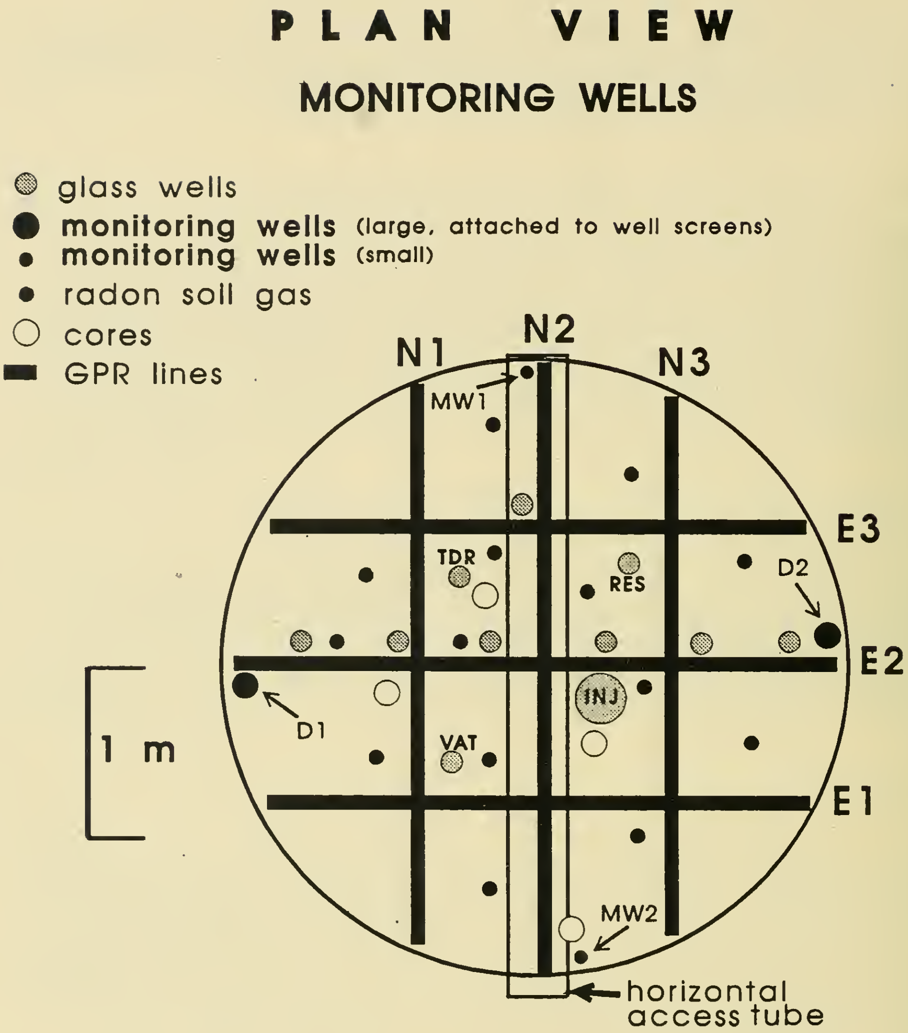

TDR : dielectric permittivity probe (time domain reflectometry)

RES : resistivity probe

VAT : vertical access tube

INJ : injection point

Figure 4.3.1.1 Plan view of test cell highlighting monitoring wells.

PLAN VIEW

EM STATIONS

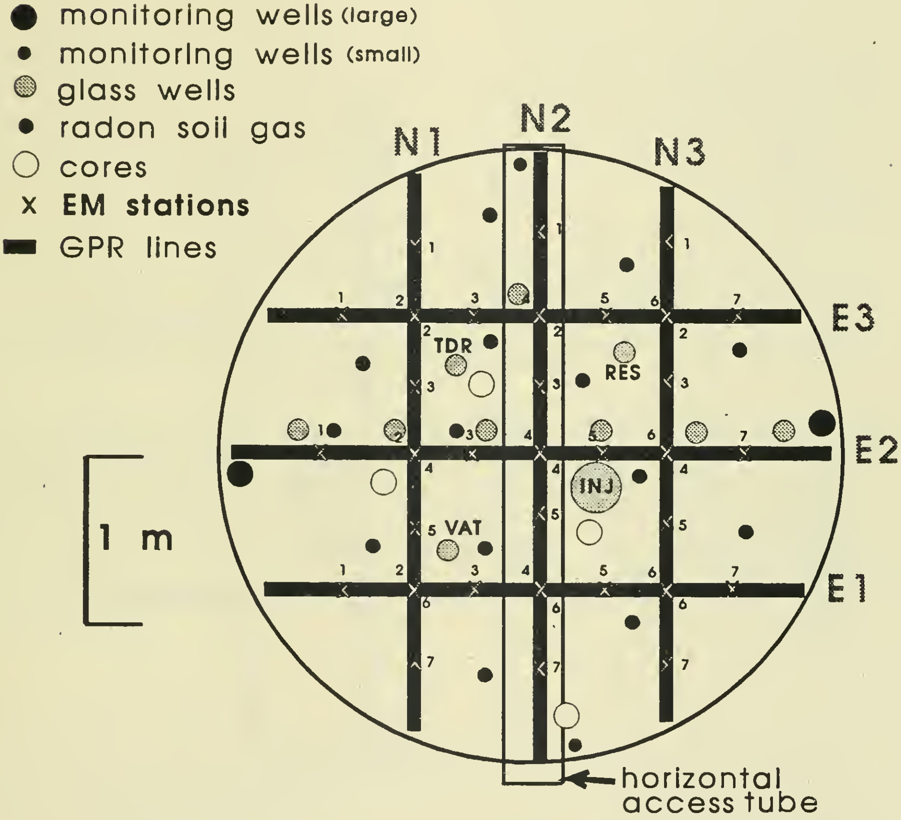

TDR	:	dielectric permittivity probe (time domain reflectometry)
RES	:	resistivity probe
VAT	:	vertical access tube
INJ	:	injection point

Figure 4.3.2.1 Plan view of test cell highlighting the grid station locations of the EM surveys.

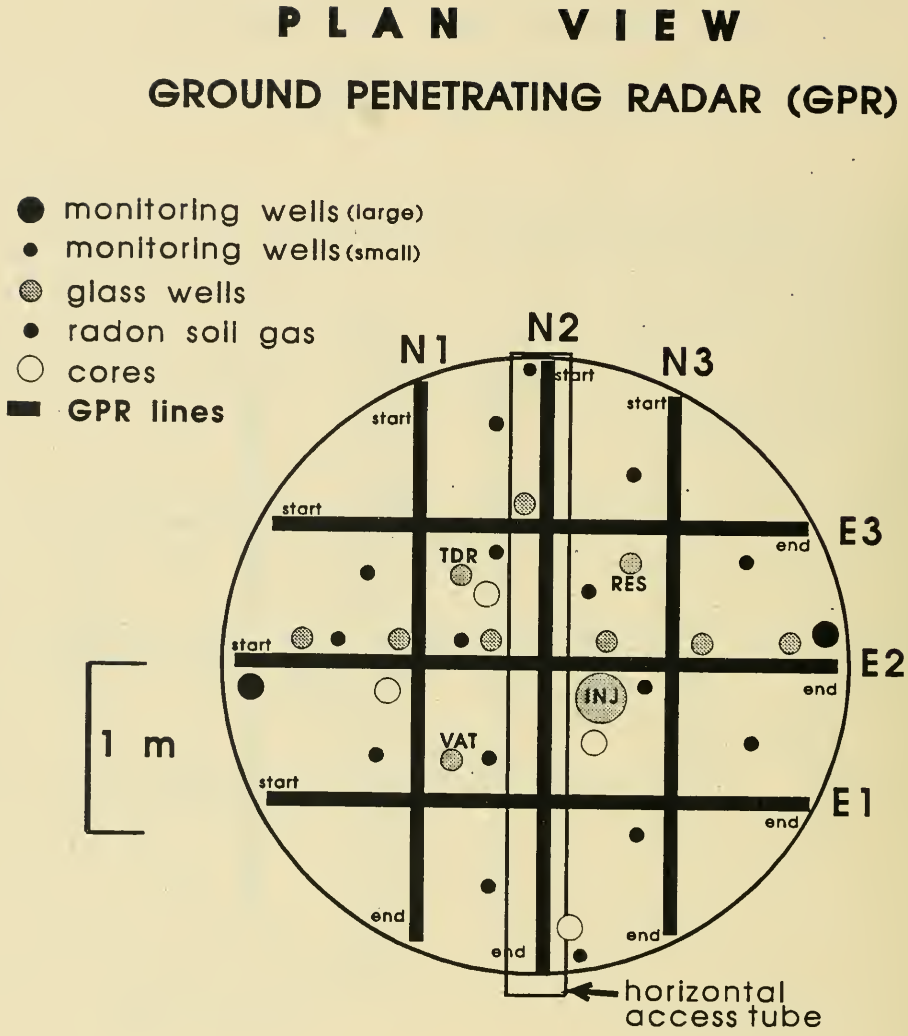

TDR : dielectric permittivity probe (time domain reflectometry)

RES : resistivity probe

VAT : vertical access tube

INJ : injection point

Figure 4.3.3.1 Plan view of test cell highlighting the GPR survey grid lines.

4.3.4 Dielectric Permittivity Monitoring

The multilevel dielectric permittivity probe enabled us to measure a high resolution (2.5 cm) vertical profile of dielectric permittivity and inferred water content. The probe consisted of 65 horizontal transmission lines (19 cm long), spaced 2.5 cm apart, and extending from the surface to within the gravel layer. Each transmission line was a pair of brass rods that were joined to a vertical PVC tube. A shielded cable was inserted into this tube, to contact the sequential pairs of rods that form the transmission line.

Since the probe was installed in the test cell before it was filled with sand, it was possible to pack sand carefully around each of the rods that formed the transmission lines. The probe is similar to the device described by Brewster et al (1992), that was used for monitoring tetrachloroethylene migration except that in this case the transmission lines were horizontal, giving better vertical resolution.

The Tektronix 1502B time domain reflectometer recorded the waveform reflected back from the start and end of each transmission line. This waveform was transferred to a computer, stored on disk and then analyzed at a later time to determine the EM wave velocity along each transmission line. The dielectric permittivity, computed from this velocity, is used to determine the volumetric water content from a standard empirical relationship (Topp, 1980) between water content and dielectric permittivity.

The Topp relationship applies to a mixture of soil grains, water and air. In this experiment, kerosene is also present as a pore fluid and has a small effect on the measured water content. Modelling of this effect using the BHS mixing law (see section 2.2.2) shows that the presence of the kerosene will cause the water content to be slightly over estimated. A kerosene saturation of 0.8 will result in maximum over estimation of water content of 1.5% while a saturation of 0.4 will result in an over estimation of only 0.8%. Since the maximum kerosene saturation observed in cores from the test cell was 0.35, this effect is relatively unimportant.

4.3.5 DC Resistivity

The DC Resistivity probe was designed to minimize interference with the GPR system (Schneider et al, 1993). It consisted of a vertical PVC tube which had a row of 63 electrodes along its length spaced 2.5 cm apart. For each set of resistivity measurements, an inner probe which contained the wiring was inserted into the PVC tube and measurements were obtained using Wenner arrays with potential electrode spacings of 2.5, 7.5, 17.5, 32.5, 42.5, and 47.5 cm. These measurements resulted in vertical profiles of apparent resistivity which, depending on the electrode spacing, sampled different volumes of the test cell. At a particular point, the volume measured approximates a half space of radius equal to the potential electrode spacing.

In addition to the borehole resistivity measurements, a surface array was also used. The surface resistivity arrays were located on the N2 and E2 lines of the GPR surface grid. The two lines were perpendicular and each consisted of 17 electrodes spaced 20 cm apart. Again, in order to avoid interference with the GPR, the electrodes were placed in the ground before every reading and removed following it. The position of the electrodes was marked so that the readings were taken in the same position every time. As in the borehole survey, automated measurements were obtained using Wenner arrays with potential electrode spacings of 20, 60 and 100 cm. The volume of the sand pack being measured about a point is approximated by a half space of radius equal to the electrode spacing. Therefore these data show apparent resistivities across the test cell at three different depths. The number of measurement points however is inversely proportional to the depth of investigation and as a result, the near surface readings offer the most detail.

4.3.6 Neutron Logging

The neutron probe used in this experiment was the Campbell Pacific Nuclear (CPN) Corporation Model 503DR Hydroprobe, Neutron Depth Moisture Gage. This neutron probe is normally used to measure water content based on thermalized neutron counts (Ellis, 1987) and responds to the total hydrogen content of the medium. The Neutron probe was used in each of the seven glass wells as well as in the vertical access tube. (Figure 4.3.6.1) The effective sampling volume is dependent on many factors including the well casing material, the medium and its saturation, as well as the source-detector assembly. The volume sampled is large; however, the primary target volume is determined by the source-detector assembly and can be approximated by a cylinder of height 12.7 cm (along the well axis) and radius less than 15 cm (Endres, 1993). Measurements in the vertical access tube were made at 5 cm intervals from the surface to the gravel layer in the vertical access tube and in the glass wells from the surface to 1.3 m.

4.3.7 Radon Soil Gas

Radon soil gas measurements were made with the Scintrex/EDA RDA-200. The measurements were taken from an surface array of 14 access tubes approximately 60 cm apart. (Figure 4.3.7.1) The tubes themselves were ¼" SCH 40 PVC tubes with ¼" PVC doweling plugs which could be removed during the sampling procedure. (Appendix G) The access tubes extended to 10 cm below the sand surface allowing for a sample of near surface soil gas. The RDA-200 measures total alpha counts which include contributions from both radon (Rn^{222}) and thoron (Rn^{220}). The radon and thoron counts, and the average counts per minute (CPM) are determined using the formulae:
Average CPM = (C1 + C2 + C3) / 3 Radon CPM = 0.87*C3 + 0.32*C2 - 0.34*C1
Thoron CPM = Average CPM - Radon CPM
(where C1, C2, and C3 are actual counts over three sequential one minute periods reduced by the background CPM).

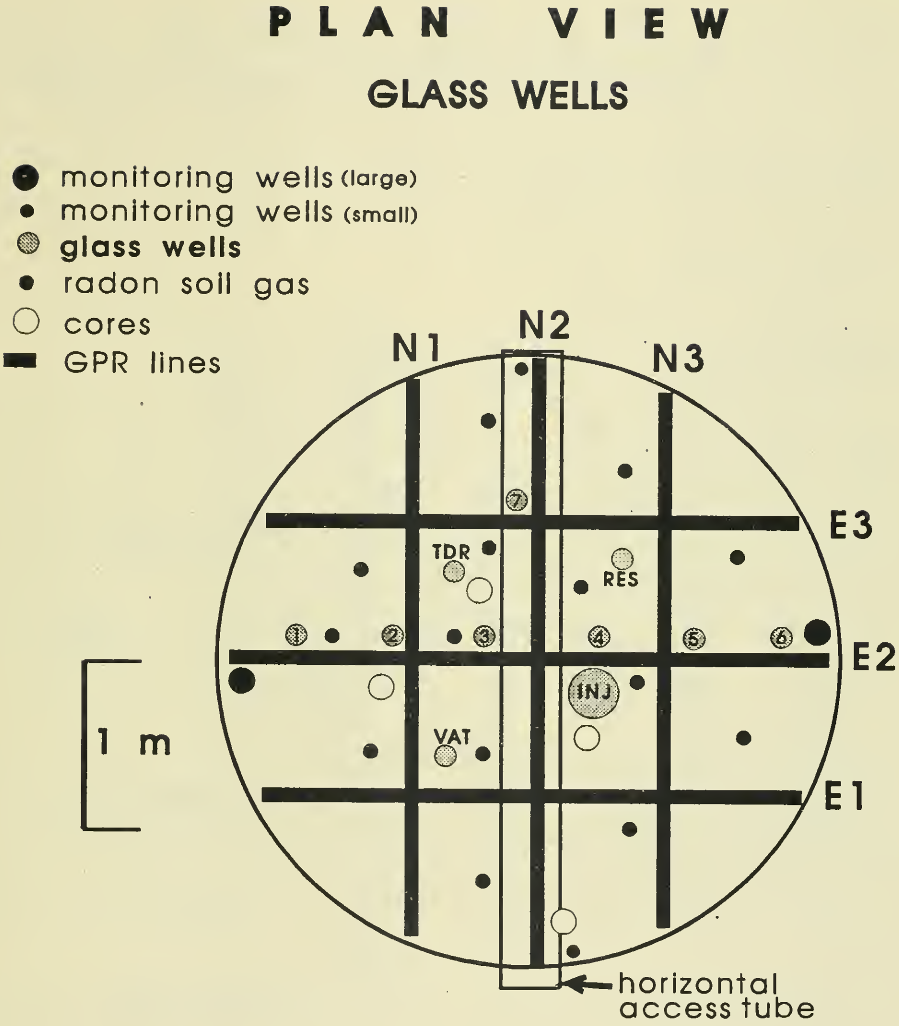

TDR : dielectric permittivity probe (time domain reflectometry)
RES : resistivity probe
VAT : vertical access tube
INJ : injection point

Figure 4.3.6.1 Plan view of test cell highlighting the seven glass wells used for Neutron logging..

PLAN VIEW

RADON SOIL GAS ACCESS TUBES

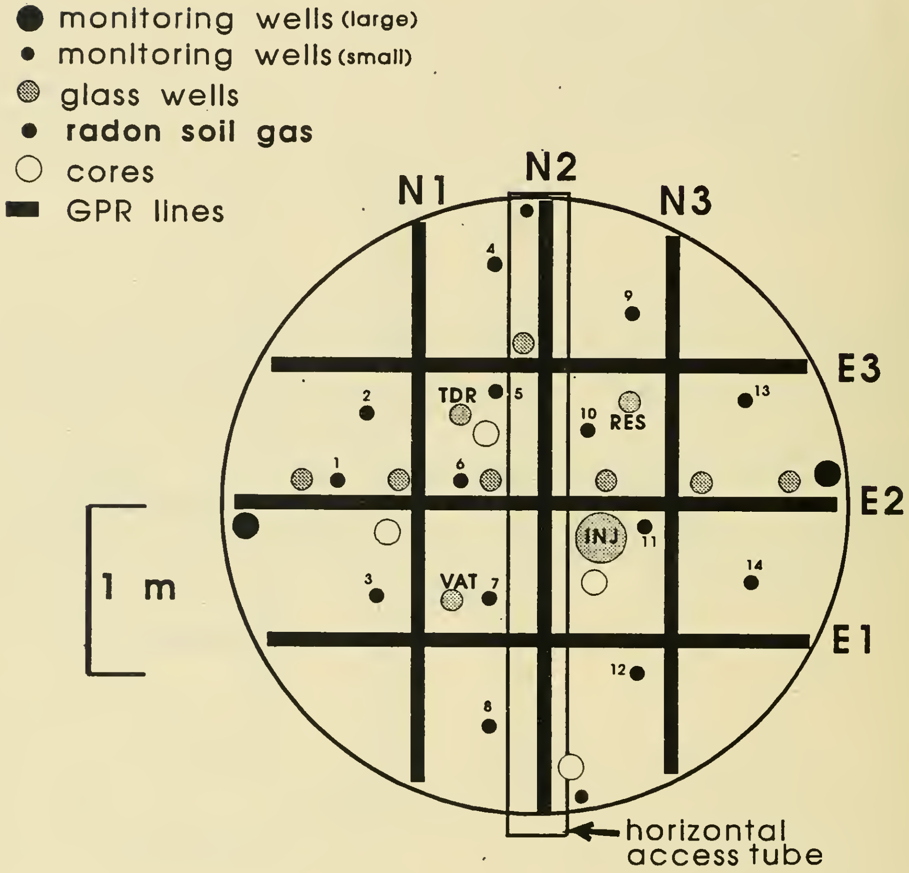

TDR : dielectric permittivity probe (time domain reflectometry)
RES : resistivity probe
VAT : vertical access tube
INJ : injection point

Figure 4.3.7.1 Plan view of test cell highlighting the location of the Radon Soil Gas monitoring points.

The soil gas sampling procedure was adapted from that of Scintrex to ensure that multiple readings taken in the same locations did not disturb the near surface portion of the sand pack. This was achieved using the permanent access tubes described above. These tubes differed from the standard RDA-200 sampling tube in two ways. Firstly they were made of PVC rather than metal so as not to affect the GPR. Secondly, they were much shorter since our source was extremely shallow and we needed to ensure that the measurement was within the unsaturated zone. Unfortunately, through the course of the experiment, some of the access tubes were damaged and no longer gave reliable data.

4.3.8 Borehole TV Camera

In an attempt to actually see the kerosene pooled within the test cell, a borehole television camera from the Oregon Graduate Institute (OGI) was used. The kerosene was clear and colourless therefore in order to distinguish it from the water it was mixed with Coumarin #7 fluorescent dye before injection. The concentration of the dye used was 12.5 mg/L, double that suggested by Dr. Rick Johnson who had used this dye successfully at the OGI. The camera was equipped with an ultraviolet light as well as a white light. The ultraviolet light would make the dye fluoresce and would therefore allow for easy detection of the dyed kerosene within the porous medium. The borehole television camera would be used to detect the depth and thickness of the kerosene pool at each of the glass well locations and would therefore allow us to monitor the development of the pool.

4.4 Monitoring and Injection Procedure

Following the packing procedure, soil porosity measurements were taken. (Appendix A.3) The test cell was saturated to the surface, then the water table was lowered to 1.1 m (bgs) for the start of the injections. The test cell was monitored while saturated and then again with the water table at 1.1 m until equilibrium was reached. For the purpose of this experiment, equilibrium is considered to be the point at which no changes could be detected using the monitoring instrumentation. The water table was maintained at 1.1 m for the duration of the injections.

The injection point was, as mentioned before, a 5" diameter 1.6 m long standpipe which extended to 30 cm below the ground surface. There was a total of 343 L of kerosene injected into the test cell in five separate injections. The injections were of 2, 10, 88, 100 and 143 L respectively. With the exception of the first, which was too small to warrant it, all of the injections were performed by gravity feed with a controlled flow rate. Therefore, the dyed kerosene entered the injection point stand pipe at a constant rate where it was allowed to form a standing head. The average injection rate of the kerosene was approximately 0.24 L/min. The injection rate for the final two injections which comprised 70% of the total injected volume of kerosene was 0.17 L/min.

During this initial portion of the experiment the water table was maintained at a constant level using a peristaltic pump. A polyethylene tube was attached to the pump and inserted to the desired depth, at this point 1.1 m, within one of the monitoring wells. Since the monitoring well was attached to the well screen system, water was removed via the bottom of the test cell where the well screens were set up. This pumping resulted in a small downward gradient of the groundwater. The pump was left running at all times so that as the water table started to rise, the displaced water was removed and pumped into a barrel for measurement and storage.

Coring was performed after water had stopped being displaced from the cell after the final injection. It was assumed that by this time the kerosene distribution was not changing significantly. A total of four cores were taken, three of which penetrated well below the water table. (Figure 4.4.1) These cores were divided into 5 cm segments and analyzed for kerosene content. (Appendix A.4)

Following the injections and coring, the water table was lowered to 1.4 m (bgs) and then raised again to 1.1 m. To lower the water table an additional polyethylene tube was placed in the well at 1.4 m and the pump was attached to it. The tube was clamped to ensure that the water removal was slowed to about 1.5 L/min. In order to raise the water table again two peristaltic pumps were used, one attached to the 1.4 m tube and one to the 1.1 m tube. The one attached to the 1.4 m tube drew water out of one of the storage barrels and pumped it into the well. The other pump, attached to the 1.1 m tube, was set to withdraw water at a faster rate than the first pump delivered it and pump it back into the storage barrel. This ensured that the water table could not get any higher than 1.1 m regardless of the water injection rate.

Due to the number of techniques being used and the incompatibility of some of the instruments, the monitoring could not be carried out on a continual basis. This may not be of consequence since the resolution of the data seems to indicate that more frequent monitoring would not have resulted in additional information. Monitoring using the geophysical equipment was performed at least twice for each injection; once preceding the injection and once immediately following each injection. This was followed by sporadic long term monitoring. (Appendix A.5)

In order to define locations within the test cell without the confusion which might occur due to the number of different grids used, an xy-grid was established. (Figure 4.4.2) The origin of the grid is close to the centre of the cell and the x and y axes are the E2 and N2 lines respectively with the positive portion of each axis being that portion which is closest to the injection point. (Appendix A.6) An elevation survey was also performed for vertical references. (Appendix A.7)

PLAN VIEW

CORES

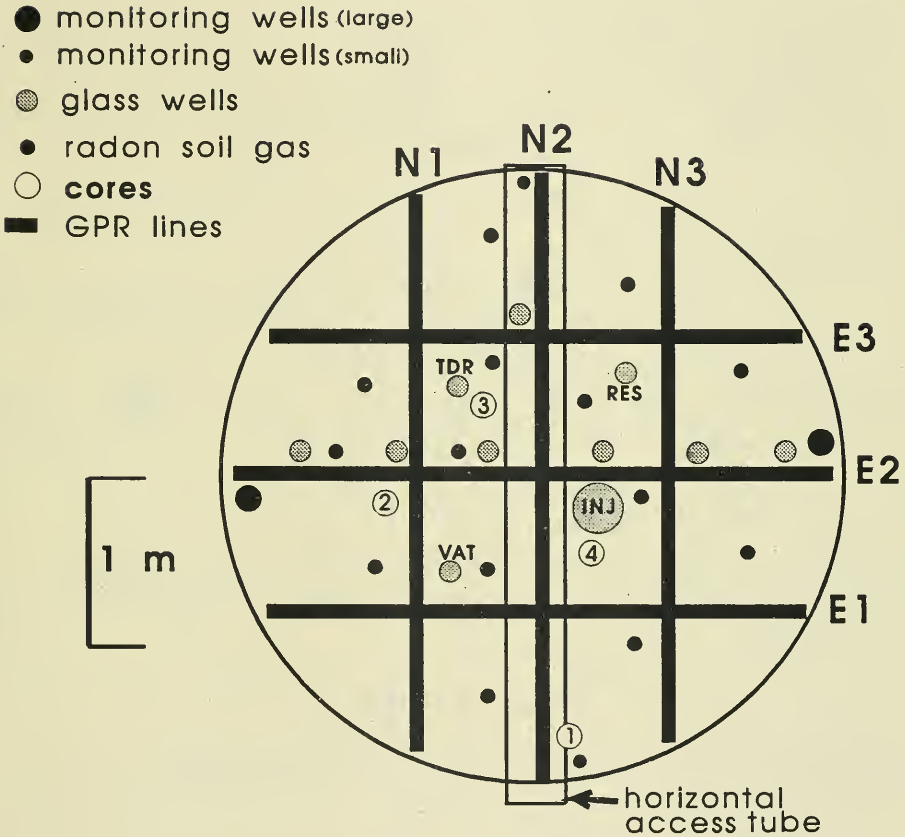

TDR : dielectric permittivity probe (time domain reflectometry)
RES : resistivity probe
VAT : vertical access tube
INJ : injection point

Figure 4.4.1 Plan view of test cell highlighting the locations where cores were taken.

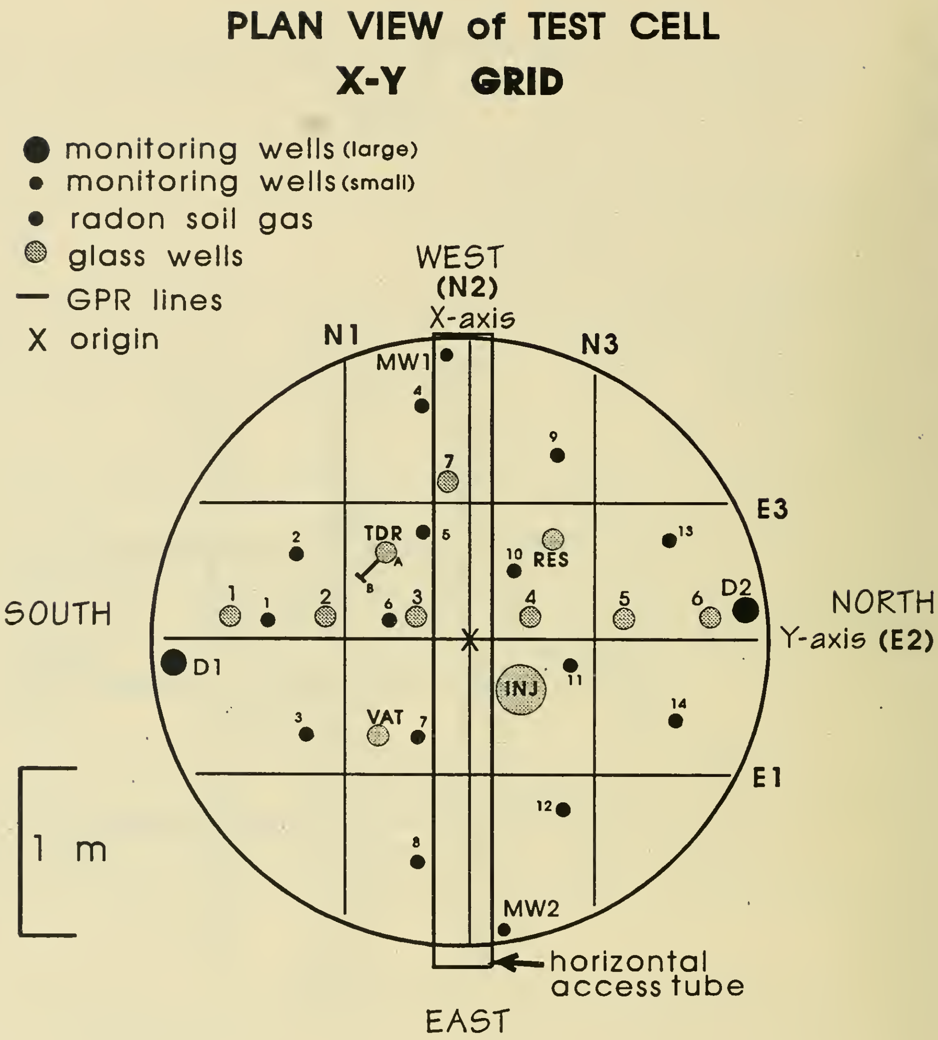

TDR : dielectric permittivity probe (time domain reflectometry)
RES : resistivity probe
VAT : vertical access tube
INJ : injection point

Figure 4.4.2 Plan view of test cell indicating the origin and orientation of the x-y grid surface.

4.5 Monitoring Results

In order to interpret the data, some of the physical properties of air, soil, water, and kerosene need to be known. These physical properties are either well known standards, measured or estimated values. Firstly, kerosene has a density of 0.8 g/cm^3. Kerosene has a dielectric permittivity of 2.1 whereas that of soil is 5.2, air is 1, and water is 80. The electrical conductivities of kerosene and air are both effectively zero, while the pore water conductivity is approximately 44.6 mS/m. The surface tension of water (water-air interfacial tension) is 73.6 dynes/cm while the air-oil interfacial tension of kerosene is 26.8 dynes/cm and the oil-water interfacial tension of kerosene is 38.6 dynes/cm. Finally, the measured porosity of the sand was 0.40 (Appendix A.3) and the average temperature of the sand pack during the experiment was 14°C.

The important dates and times of injections and of the lowering and raising of the water table are listed in Table 4.5.1.

Table 4.5.1: Record of injection days, times, and volumes, and the period during which the water table was raised and lowered.

INJECTION NUMBER	INJECTION DAY	INJECTION TIME	INJECTION VOLUME (litres)
1	33	06:30	2
2	38	17:30	10
3	45	14:30	88
4	57	08:30	100
5	65	07:00	143
completion or the lowering and raising of the water table	98 - 100		

Note that any data reported on the day of an injection were obtained just prior to the injection unless otherwise noted.

4.5.1 Water Table, Effluent Water Volume, and Soil Temperature

The water table level, injected volume of kerosene, and effluent water were closely related. (Figure 4.5.1.1) The addition of kerosene caused the distribution of water within the test cell to change resulting in effluent water. (Table 4.5.1.1) The most interesting data are that of the effluent water following the first kerosene injection. However, although only 2 L of kerosene were injected, 27.5 L of effluent water was collected. When the kerosene contacted the water, either in liquid or gas phase, the surface tension of the water was reduced. When the surface tensions are reduced, water is released from the capillary fringe, which is by definition under tension, and a new water content profile is established.

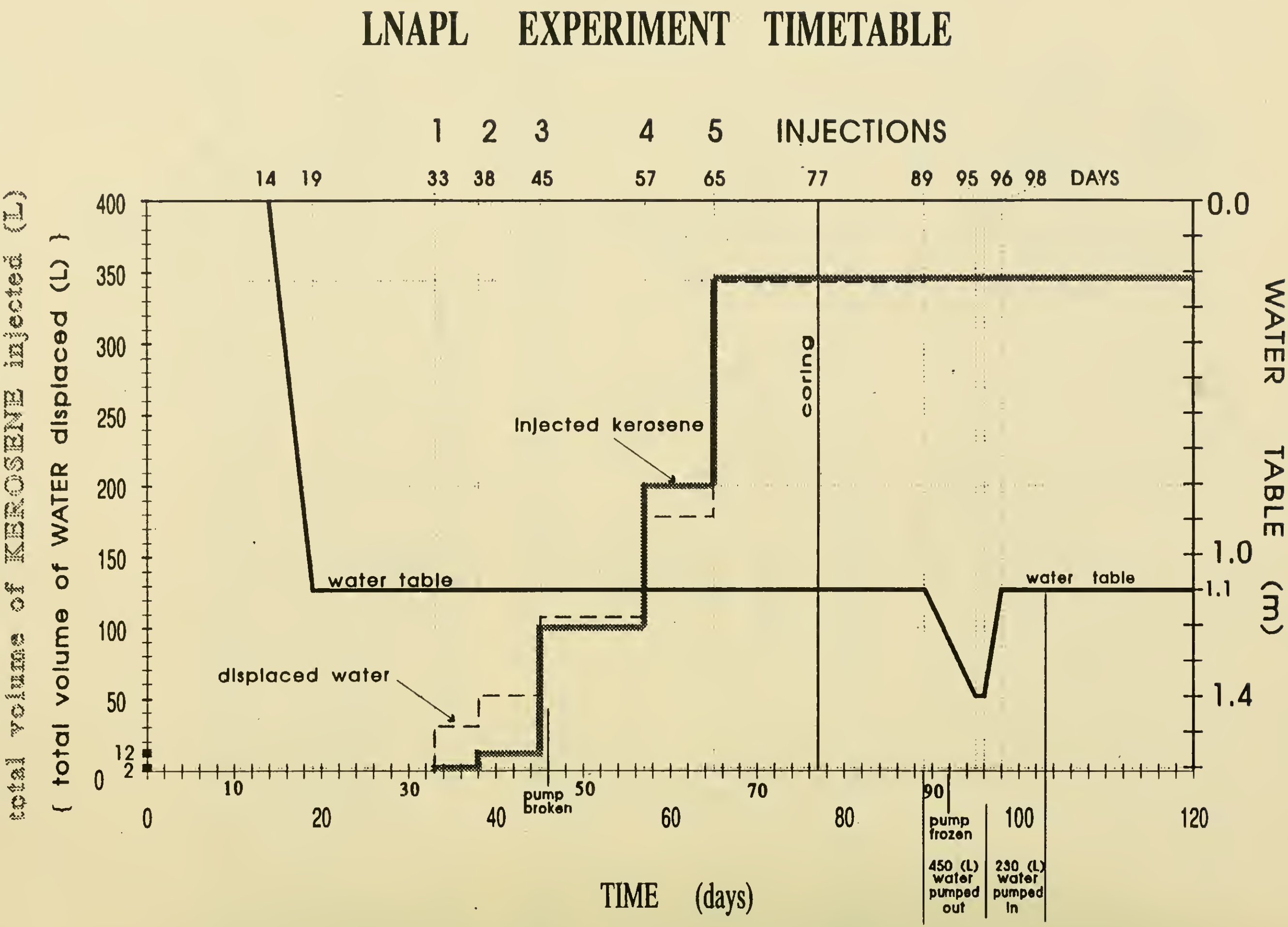
LNAPL EXPERIMENT TIMETABLE

Figure 4.5.1.1
Experiment timetable indicating changing kerosene and water volumes as well as the water table level.

Table 4.5.1.1: Kerosene injection summary.
* estimate of flow rate [L/min] = {volume of kerosene per injection [L]} / {duration of injection [min]}

INJECTION NUMBER	KEROSENE IN (L)	WATER OUT [effluent] (L)	TOTAL KEROSENE IN (L)	TOTAL WATER OUT (L)	FLOW METER RATE (L/min)	DURATION OF INJECTION (min)	ESTIMATE OF FLOW RATE* (L/min)
1	2	27.50	2	27.50	NA	NA	NA
2	10	23.75	12	51.25	0.29	NA	NA
3	88	56.25	100	107.50	0.29	360	0.24
4	100	72.00	200	179.50	0.16	620	0.16
5	143	161.74	343	341.24	0.17	840	0.17

The temperatures within the test cell (Appendix A.2) were seen to decrease throughout the experiment from approximately 18°C to 6°C due to seasonal changes. (Figure 4.5.1.2) Temperature changes had the most obvious affect on the effluent water when the pump lines froze. However, the duration over which the lines were frozen was short and was also between injection periods and therefore did not have a significant affect on the experiment. Following the experiment, there was a freezing event within the sand pack which was documented by a reduction in water table levels and changes in the TDR and neutron responses with depth.

4.5.2 Surface EM

The EM38 has two dipole modes of operation. The horizontal dipole mode of operation has a maximum relative sensitivity to near surface electrical conductivities. The sensitivities then decrease quickly with depth. The vertical dipole mode, on the other hand, is insensitive to near surface conductivities, increases with depth to a maximum relative sensitivity at 0.4 m and then decreases again with depth below this level. Therefore, we will use the horizontal dipole for information about the near surface conductivities and the vertical dipole for information about conductivities at depth within the test cell.

As previously mentioned, the test cell was modelled with a porosity of 0.37 (the measured porosity was approximately 0.40), a pore water conductivity of 44.6 mS/m, and a saturated electrical conductivity of 10.0 mS/m (which agrees with the measured saturated resistivity of 100 ohm.m). The change in pool thickness was modelled from 0 to 0.5 m as was determined to be the thickness of the kerosene following the final injection through TDR measurements and coring. The predicted change in apparent conductivities from prior to the injections to just following the final injection was 3.71 to 3.55 mS/m for the horizontal dipole mode and 5.81 to 5.55 mS/m for the vertical dipole mode.

All of the EM38 data were collected using both vertical and horizontal dipole modes of operation. (Appendix B) From the summarized data we find that the vertical and horizontal

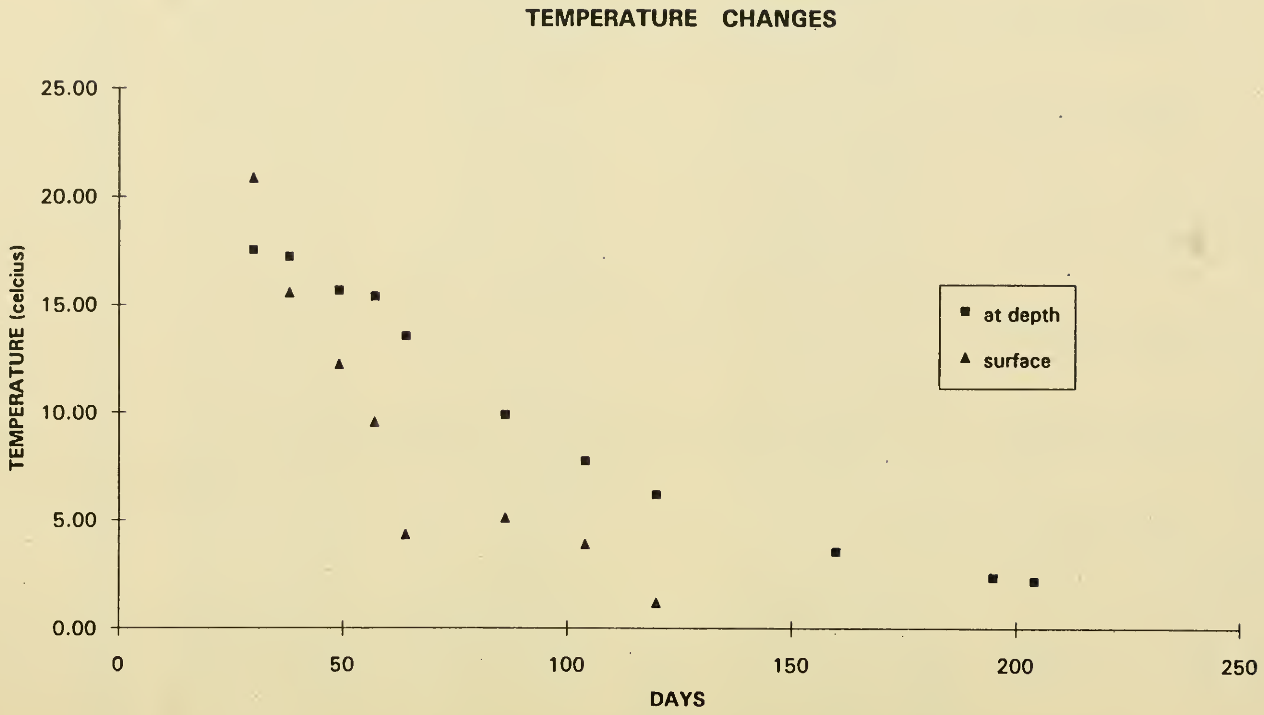

Figure 4.5.1.2 Temperature changes in the test cell time.

apparent conductivities are lower than what we would expect to see from the previously discussed modelling. Also, since we know water to have a high conductivity relative to sand, air or kerosene which are all low, we would expect higher water saturations to result in higher conductivities which is demonstrated in only one of the three data sets. These discrepancies with theory may be due to the fact that the readings themselves are bordering on the detection limit of the EM38 and that field measurements were noisy and difficult to make. Also, the small number of data sets made it impossible to check for repeatability or to apply data averaging.

The only apparent application for the EM38 data is a relative comparison of changing conductivities with time. The horizontal dipole mode, which gives information about near surface conductivities, shows that the readings when the test cell was saturated are definitely higher than those with the water table at 1.10 m. (Figure 4.5.2.1) Once the water table was lowered, the near surface measurements do not give us much interpretable information. Although the readings with kerosene appear higher than those without, which contradicts theory, the range of values is very small and stay between 1 and 4 mS/m. These values are close to the modelled values. The vertical dipole mode, which gives information about conductivities at a depth of approximately 0.4 m, shows the highest values when the test cell was saturated, intermediate values before kerosene was injected, and the lowest levels after the addition of kerosene. (Figure 4.5.2.2) These relationships agree with theory as do the conductivity values of 4 to 5 mS/m before the injections. The values after the injections of 2 to 3.5 mS/m do however seem low.

4.5.3 Ground Penetrating Radar (GPR)

The GPR surveys collected with the 450 MHz antennae repeatedly gave the best results. (Appendix C) On all the grid lines we see interface events representing the top of the gravel layer and the top of the saturated zone. The dipping events seen at the sides of the test cell are diffractions from the point where the saturated zone meets the walls of the test cell. By comparing the changes in the various interface events we can identify changes within the cell throughout the experiment.

The background data were taken with the water table at 1.10 m before any kerosene was added. It shows an event at 47 ns, which is the bottom of the tank, an event at 44 ns, which is the top of the gravel layer, and an event at 16 ns, which is the top of the saturated zone. (Figure 4.5.3.1) After injecting 100 litres of kerosene, the events at the bottom of the cell have been "pulled up" in the area to the right of centre within the test cell. (Figure 4.5.3.2) The injection point itself was located at (0.23 m, 0.21 m) on the x,y grid. Therefore, this "pull up" occurs due to a region of higher velocities (caused by lower dielectric permittivities) above the water table and in the vicinity of the injection point where kerosene has displaced water.

Further injections show that the zone affected by the kerosene was spreading toward the sides

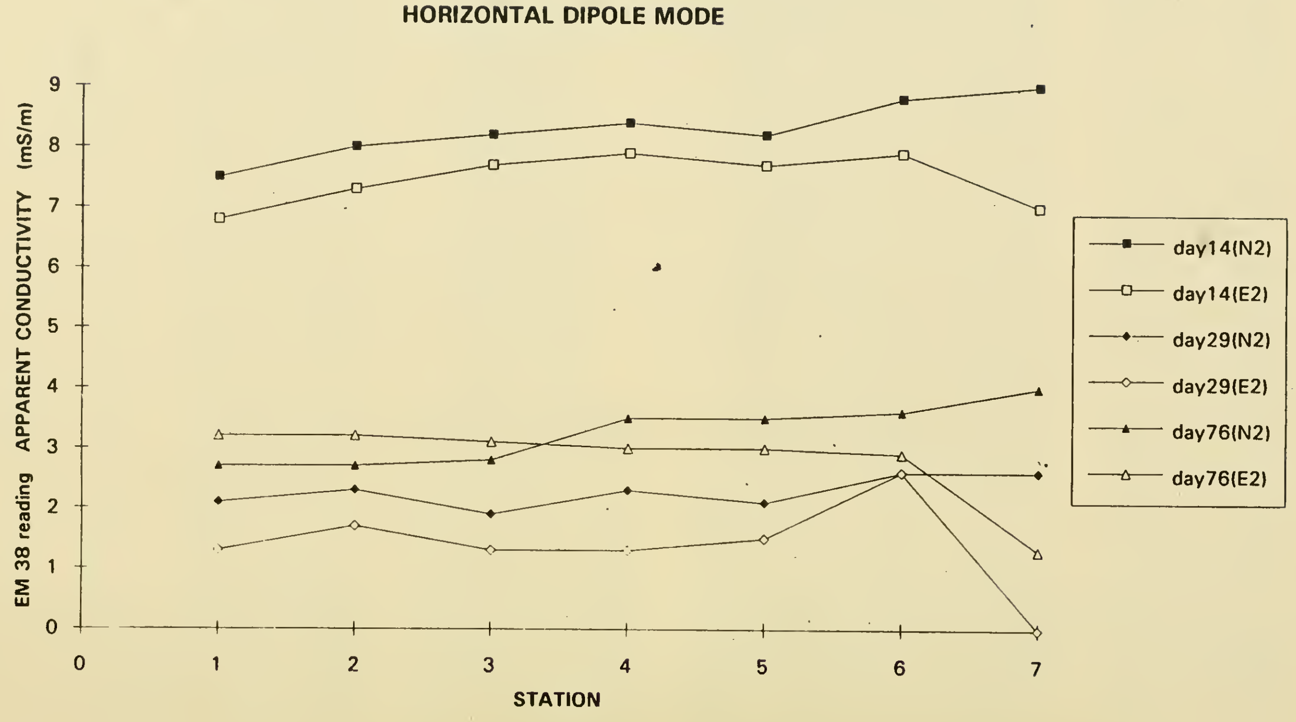

Figure 4.5.2.1 EM38 survey across test cell. Horizontal dipole results..

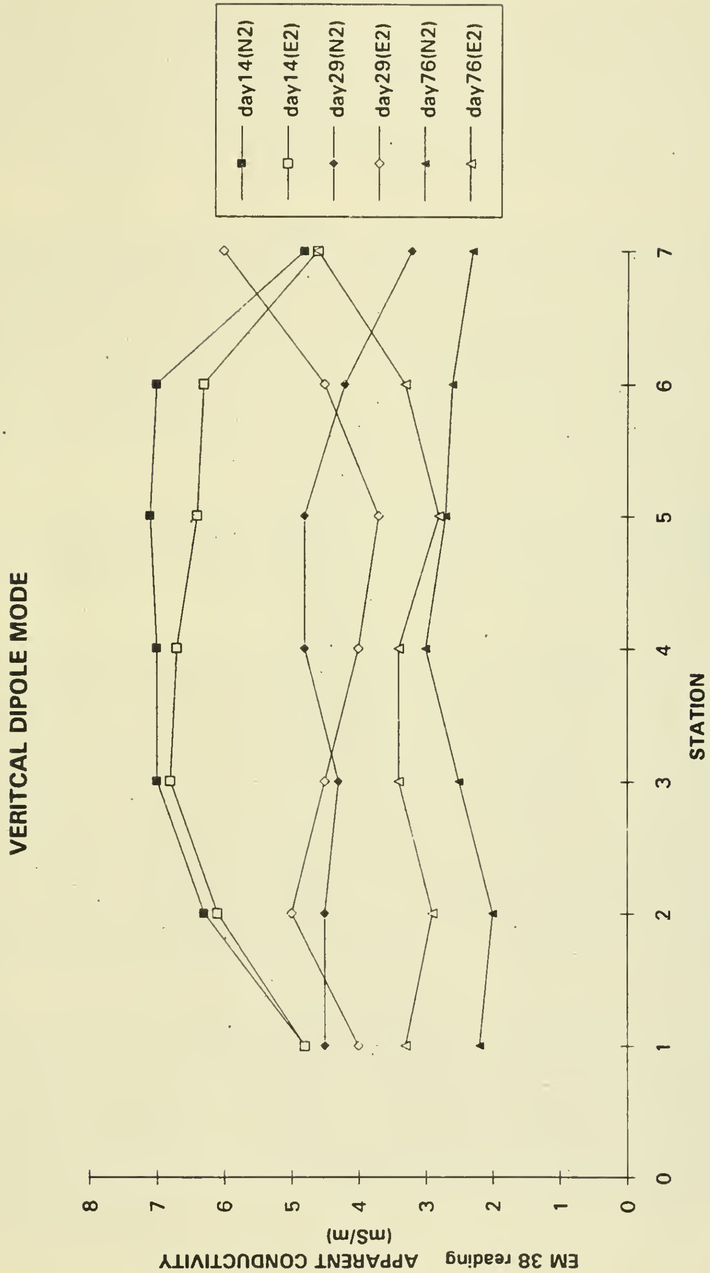

Figure 4.5.2.2 EM38 survey across test cell. Vertical dipole results..

of the test cell. (Figure 4.5.3.3 & 4.5.3.4) The observed reflection event from the bottom of the cell indicates that the kerosene affects the right side of the test cell first, and that with successive injections the "pull up" is greater indicating greater kerosene pool thicknesses. If we assume that the rate of lateral spreading of the injected kerosene along the top of the saturated zone was symmetric about the injection point, we would expect the kerosene to have intersected the right side of the cell sooner than the left due to the proximity of the injection point to that side. This does appear to be the case.

The depression of the saturated zone caused by pooling kerosene can be observed best by comparing the data following the final injection with the background data. (Figure 4.5.3.1 & 4.5.3.4) Since we know the water table to have been at 1.10 m, and the background capillary fringe to be approximately 0.30 m thick, then the thickness of the unsaturated zone (including transition zone) would be 0.80 m. From the pre-injection data, we see that the event caused by the top of the saturated zone occurs at 15 ns. From this we deduce that the background velocities in the unsaturated zone are approximately 0.106 m/ns. Following the final kerosene injection the same event occurs at 20 ns, 5 ns later than in the background data.

If we were to assume that the velocities in the unsaturated zone after the final injection were the same as before the injections, then the event would be located at a depth of 1.07 m. This would indicate almost a complete reduction or depression of the initial capillary fringe since we know the water table to be at 1.1 m.

Following the final injection of kerosene, although the water table was maintained at 1.1 m, the thickness of the capillary fringe was reduced. As previously stated, this is due to changing interfacial tensions and displacement of water by kerosene. If the depth to the saturated zone interface increased then, assuming the velocities were the same, the time to the interface should also increase, as is the case. However, since the unsaturated zone had increased in thickness, there would be a region which had previously been saturated with water which now contained air and/or kerosene. Since the dielectric permittivity of air and kerosene are much lower than water, this should mean that the average dielectric permittivity between the surface and the top of the saturated zone should decrease. A decrease in dielectric permittivity results in an increase in velocity. If the velocities in the unsaturated zone increased and we know the time to the interface to have increased, then we would expect the depth to the interface, using the background velocities, to be underestimated.

A final GPR reflection survey was performed on day 119. This data set cannot be compared directly with the previous data sets since it followed the lowering and raising of the water table. Although the water table was returned to its previous level of 1.10 m, there would have been redistributions of the water, air and kerosene within the system. Therefore, while it is not appropriate to compare actual events, it is possible to note that the higher velocity region which was causing “pull up” has now dissipated. The GPR measurements would show the same results whether the kerosene pool had spread laterally with time and become a more uniform layer or if the act of lowering and raising the water table had mixed the three

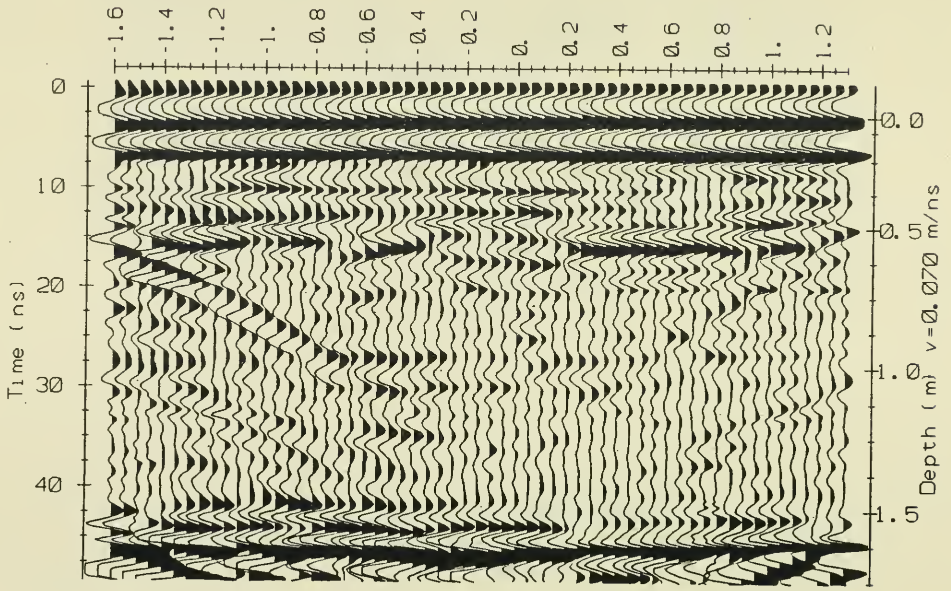

Figure 4.5.3.1 GPR survey across line N2 on day 23 using the 450 MHz antennae. Preinjection (background) data.

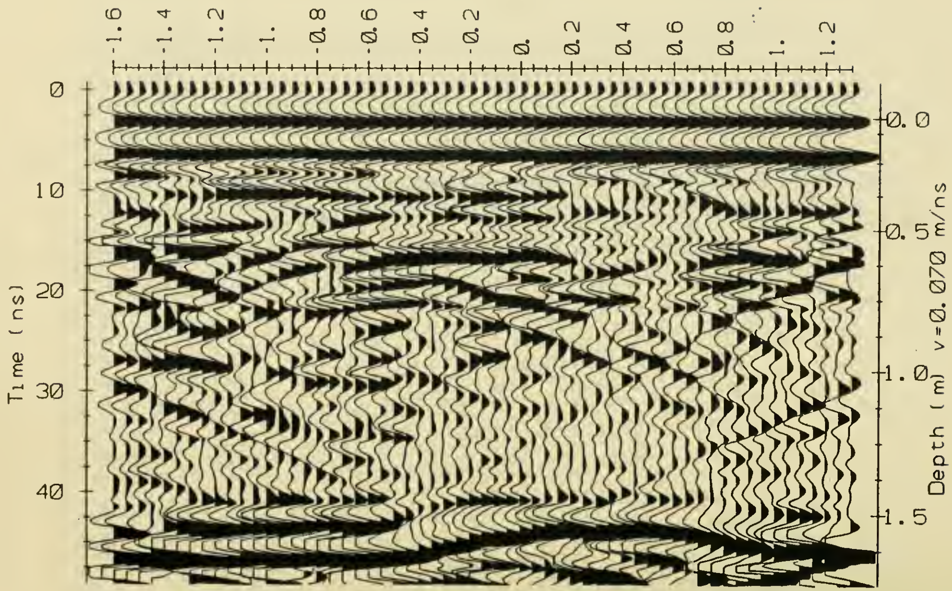

Figure 4.5.3.2 GPR survey across line N2 on day 49 using the 450 MHz antennae. Just prior to injection #4. The total volume of injected kerosene is 100 L.

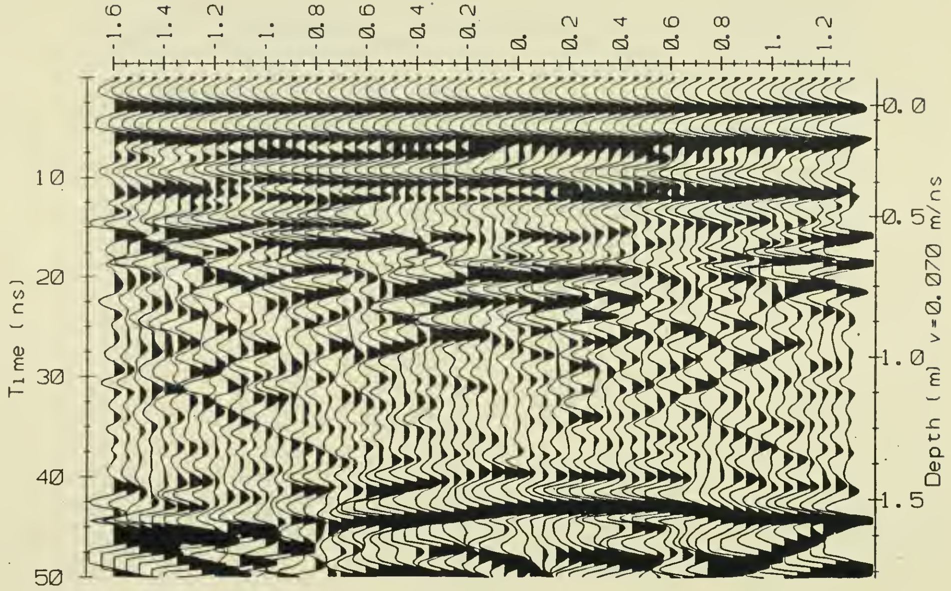

Figure 4.5.3.3 GPR survey across line N2 on day 63 using the 450 MHz antennae. Just prior to injection #5. The total volume of injected kerosene is 200 L.

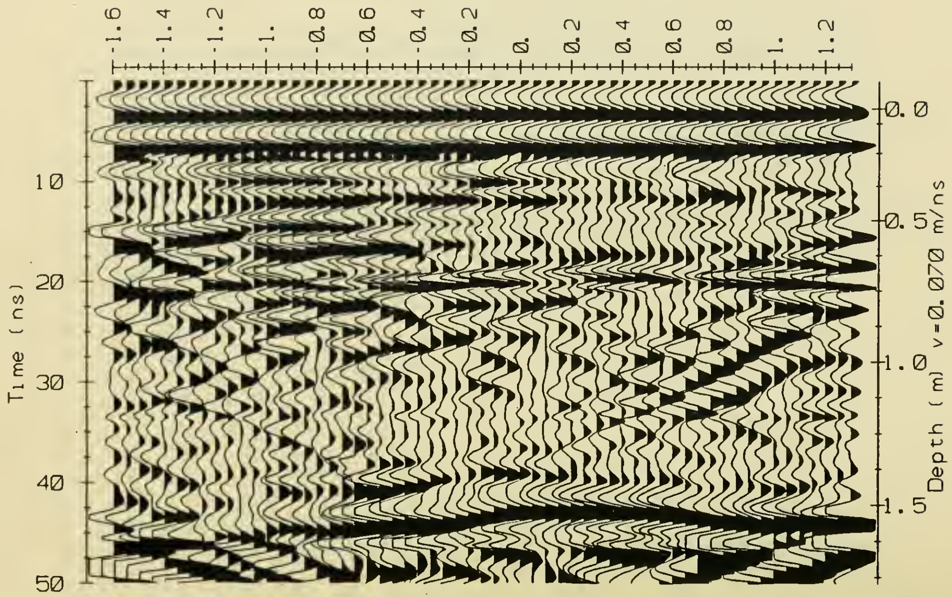

Figure 4.5.3.4 GPR survey across line N2 on day 69 using the 450 MHz antennae. Following final injection. The total volume of injected kerosene is 343 L.

fluid phases and redistributed them evenly across the cell. It is likely that the effect is due to a combination of these two processes.

4.5.4 Dielectric Permittivity Monitoring

There were 32 vertical profiles of dielectric permittivity measured periodically over the duration of the experiment (about 2800 hours). Profiles were measured at the start of the experiment with the water table at the surface, after the water table was lowered, just before and following each kerosene injection, and during the raising and lowering of the water table.

The water content profile (Figure 4.5.4.1) taken when the water table was at the surface shows a relatively uniform water content of 40% from the surface to the top of the gravel layer at the bottom of the tank. The deepest transmission line shows a significantly higher water content because it was within the higher porosity gravel layer. After the water content had equilibrated with the water table at a depth of 1.1 m, the capillary fringe was about 30 cm and the residual water content was 12% just below the surface. Profiles measured after each injection show the reduction in water content within the capillary fringe due to kerosene displacing water.

By looking at the change in water content (with respect to the profile taken just before the first injection with the water table at 1.1 m), it can be seen (Figure 4.5.4.2) that even after the injection of 2.2 litres of kerosene there was a small change in water content. We believe this may be due to dissolved phase kerosene changing the surface tension of the water just above the capillary fringe. For the effect to occur so quickly, the kerosene is probably transported in the vapour state from the injection point to the TDR probes.

As discussed in section 4.6, the neutron soil moisture probe showed there was only a small change in the total fluid content indicating that the changes observed with the TDR are in fact due principally to kerosene displacing water. Thus the profiles shown in Figure 4.5.4.2 represent the development of pooled kerosene within the capillary fringe. A direct comparison of kerosene saturation observed in cores compared to water loss (see section 5.5.9 and Figure 4.5.9.2) demonstrates that this assumption is valid.

The complete data set of TDR profiles has been contoured as a time and depth section (Figure 4.5.4.3). This type of presentation allows one to see more clearly the changes in time on a single vertical profile. The location in time and depth of the individual data points is indicated.

Notice the large change in water content particularly after the injections of 88, 100, and 150 litres of kerosene. When the water table was lowered and then raised again kerosene was trapped below the water table resulting the lower water content persisting after the water table is raised.

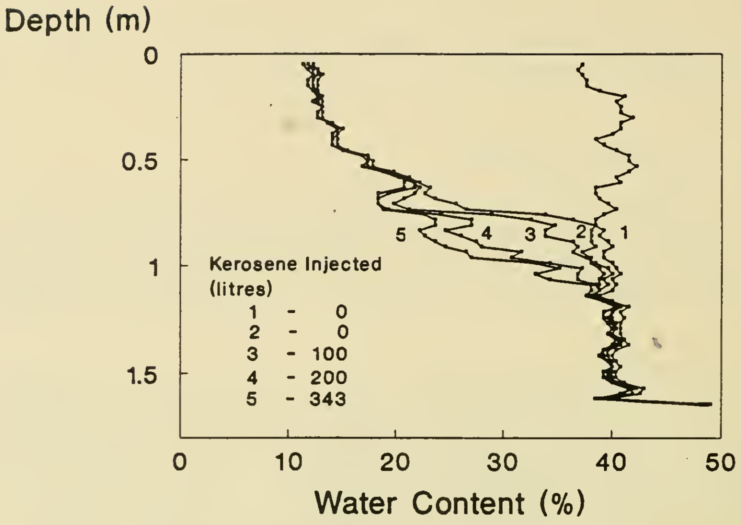

Figure 4.5.4.1: Water content profiles measured with multilevel dielectric permittivity probe before and following injections. Profiles: 1. Day 15 - fully saturated; 2. Day 33 - before 2.2 litre injection; 3. Day 56 - after 100 litres injected; 4. Day 64 - after 200 litres injected; 5. Day 69 - after 343 litres injected.

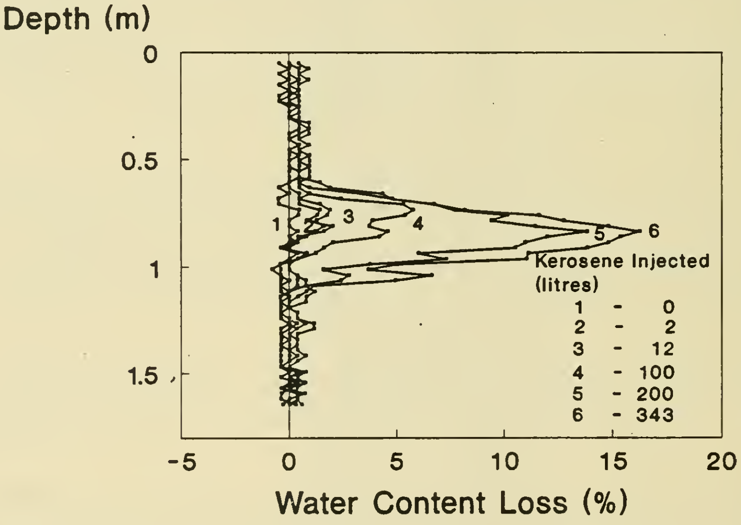

Figure 4.5.4.2: Loss in water content with respect to profile measured on day 30, before first injection. Measured with multilevel dielectric permittivity probe. Profiles: 1. Day 33 - just before 2.2 litre injection; 2. Day 38 - after 2.2 litre injection; 3. Day 42 - after 10 litre injection; 4. Day 56 - after 100 litres injected; 5. Day 64 - after 200 litres injected; 6. Day 69 - after 343 litres injected.

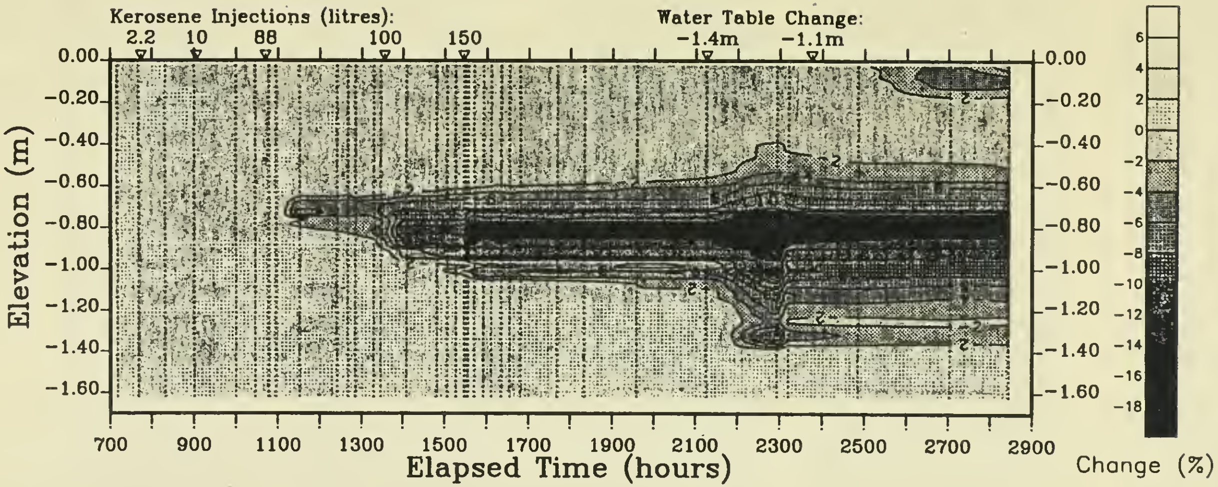

Figure 4.5.4.3: Change in water content with respect to profile measured on day 33 (768 hours), contoured on a time versus depth section. The complete set of water content profiles, measured with the multilevel dielectric permittivity probe, are shown versus time. The development of the kerosene pool at the location of the probe can be seen after the 88 litre injection and following all subsequent injections.

The TDR data have been presented as water content inferred from the measured dielectric permittivity. Clearly the dielectric permittivity decreases substantially after the larger injections and during the raising and lowering of the water table. The effect of these changes was observed in GPR sections and is discussed in section 4.3.2.

4.5.5 DC Resistivity

The DC resistivity borehole surveys showed the saturated resistivity to be approximately 100 ohm-m (which is equal to a conductivity of 10 mS/m). The resistivity profiles give information about the apparent resistivities at different distances away from the probe. This distance away from the probe for which survey gives information is determined by the current electrode spacing. For a Wenner array this "TARGET" distance is actually equal to the potential electrode spacing. These potential electrode spacings, as mentioned before, are 2.5, 7.5, 17.5, 32.5, 42.5, and 47.5 cm. The number of data points however decreased for the larger electrode spacings and, since the data did not change drastically with distance, the 2.5 cm spacings resulted in the most complete and detailed results.

The vertical resistivity profiles, as mentioned, consistently show readings of 100 ohm-m below the saturated zone before any kerosene was added. Above the saturated zone, the resistivities increase with decreasing water saturation to a maximum of 1300 ohm-m near the surface. These results are what would be expected as water content decreases from the top of the saturated zone to the ground surface. Following the addition of kerosene, whose conductivity is effectively zero and which should pool on the top of the saturated zone, we would expect to see an increase in resistivities wherever kerosene replaced water. This is the case; however, the profiles indicate the entire resistivity profile from the surface right down to the water table has changed. (Figure 4.5.5.1)

Following the final injection of kerosene, the resistivities at the top of the saturated zone increase from 100 ohm-m to 350 ohm-m. The resistivities continue to increase through the unsaturated zone to a maximum at the ground surface which has increased from 1300 ohm-m to 1900 ohm-m. As well as increased resistivities above the original zone of saturation, there are also increased resistivities in what was the original capillary fringe. The resistivities in this zone increased from 100 ohm-m to a maximum of 400 ohm-m. This may be explained by a combination of water displacement by the kerosene and by the reduction of the capillary fringe due to changes in interfacial tensions.

With each successive injection of kerosene, the resistivities above the water table increase. If "equilibrium" can be considered to be when there are no more changes which are discernible to a particular monitoring method then, following an injection, the test cell would reach "equilibrium" with respect to the DC resistivity system within a day. After more than one day following an injection, the resistivity profile was fairly stable.

For the DC resistivity surface surveys, Wenner array spacings of 20 cm show the near surface preinjection resistivities of about 1100 ohm-m while the deeper readings obtained with the 60 cm spacings gave an average apparent resistivity of 900 ohm-m. (Appendix E) That is, the resistivities decrease with increasing water content which increases with depth. As expected, the apparent resistivity values increase following successive injections. The average near surface apparent resistivity (using the 20 cm spacing) following injection #4 was 1600 ohm-m while the average at depth (using the 60 cm spacing) was 1350 ohm-m. (Appendix E)

By looking at individual data points rather than averages we can tell a bit about the lateral distribution of the resistivities. (Figure 4.5.5.2 to 4.5.5.5) In all of the figures we see that the largest changes in resistivities occurred after the injections of the largest volumes. At the 60 cm spacing, the resistivities appear to be constant across the test cell. On both lines, the end of the line closest to the injection point, as well as a region around the injection point (xy-grid location (23,21)), seem to have higher apparent resistivities. The resistivity data from the 20 cm spacings indicate that there is a region of high resistivities near the centre of the cell and low resistivities on the sides. This mounding in the centre of the cell seems in all cases to become more enhanced after each of the injections. Therefore it appears to be related to the introduction of kerosene.

Areas of high resistivities indicate areas which are depleted of water and could contain air, kerosene or a combination of the two. It is important to remember that the 20 cm spacing data is giving information from the very near surface where we would not expect to see the kerosene pool but which may be affected by the gravel filled injection point which extends down 30 cm. Also, although the kerosene is expected to pool at the top of the saturated zone, there will be residual kerosene in the area of the injection well as is verified by the coring results where kerosene was found as shallow as 10 cm from the surface.

A rough comparison of the borehole and surface resistivity results indicate that although giving similar readings near the surface, they differ greatly at depth. The resistivity borehole probe was located at xy-grid coordinates (-51.5, 50.0). Therefore, the borehole data were compared to the surface resistivities on line N2 at -51.5 cm and on line E2 at 50.0 cm. The near surface background resistivity which was obtained with surface electrode spacings of 20 cm was 1100 ohm-m and increased to 1650 ohm-m following injection #4. The corresponding borehole measurements from 20 cm were 950 ohm-m and 1500 ohm-m respectively. The resistivity readings at depth using the surface resistivity electrode spacing of 60 cm began at 900 ohm-m and increased to 1300 ohm-m after injection #4. However, the borehole data at 60 cm depth began at 350 ohm-m and increased to 700 ohm-m.

Following the end of the kerosene injections, only borehole resistivity measurements were taken. These resistivity profiles, again using the Wenner array 2.5 cm separations, show the results of the lowering and raising of the water table. (Figure 4.5.5.6) Day 89 (the background for this part of the experiment) is prior to the lowering of the water table, day 92 is with the water table at 1.4 m, and day 98 is after the water table has been reestablished at 1.1 m. When the water table was returned to 1.1 m, the resistivity profile was not the same as it was before lowering of the water table. There appears to be no change in the resistivity response below the top of the original saturated zone (i.e. 0.8 m) compared with that of background. However, above the top of the original saturated zone the resistivities decrease compared with background and these decreases become more enhanced towards the surface.

From theory, we expect that when the water table was lowered, the entire water content profile from the zone of residual saturation down to the top of the new saturated zone would have changed in response to the change in water table elevation. Upon returning the water table to its original level kerosene would be trapped within the saturated zone (as well as air if the water table was raised too quickly). This would result in increased resistivities from the lowest level of the top of the saturated zone to the initial top of the saturated zone. We would also expect the water content and the water content distribution above the top of the saturated zone table to have changed.

In the area between the lowest and the highest levels of the top of the saturated zone where we expected to see increased resistivities due to trapped kerosene, we see little change. The reason for this result may be due in part to the nature of trapped kerosene. Trapped kerosene is expected to be found in small blobs and ganglia which are not interconnected. Therefore, the distribution of trapped kerosene may not cause a significant change in the electrical flow within the medium. This is also evident from Archie's Law which shows that changes in saturation in a highly saturated medium have little effect on resistivity.

From the water table (1.1 m) to the top of the original saturated zone (0.80 m), there is no change. Since this is the zone in which the kerosene was expected to pool (and was later shown to have pooled), the water would have already been displaced. Therefore, lowering the water table would result in a the kerosene moving down in the profile and being replaced by air. The introduction of air into this region would have no effect on the resistivities.

In the zone from the top of the originally saturated zone (0.8 m) to surface, the resistivities decrease compared to background. These changes may be attributed to hysteresis. Hysteresis describes the change in the pressure saturation relationships between fluids dependent on whether the porous medium is undergoing drainage or imbibition (wetting). Since saturations during imbibition are lower than saturations during drainage at the same pressure, the saturations within the test cell should be lower after the water table is reestablished than before the drainage event. Lower saturations should result in an increase in resistivities rather than the observed decrease. Some possible mechanisms which could explain this phenomenon are: changes in fluid conductivities, temperature affects, or the imbibition geometry of the air-water interface as observed by Knight (1991).

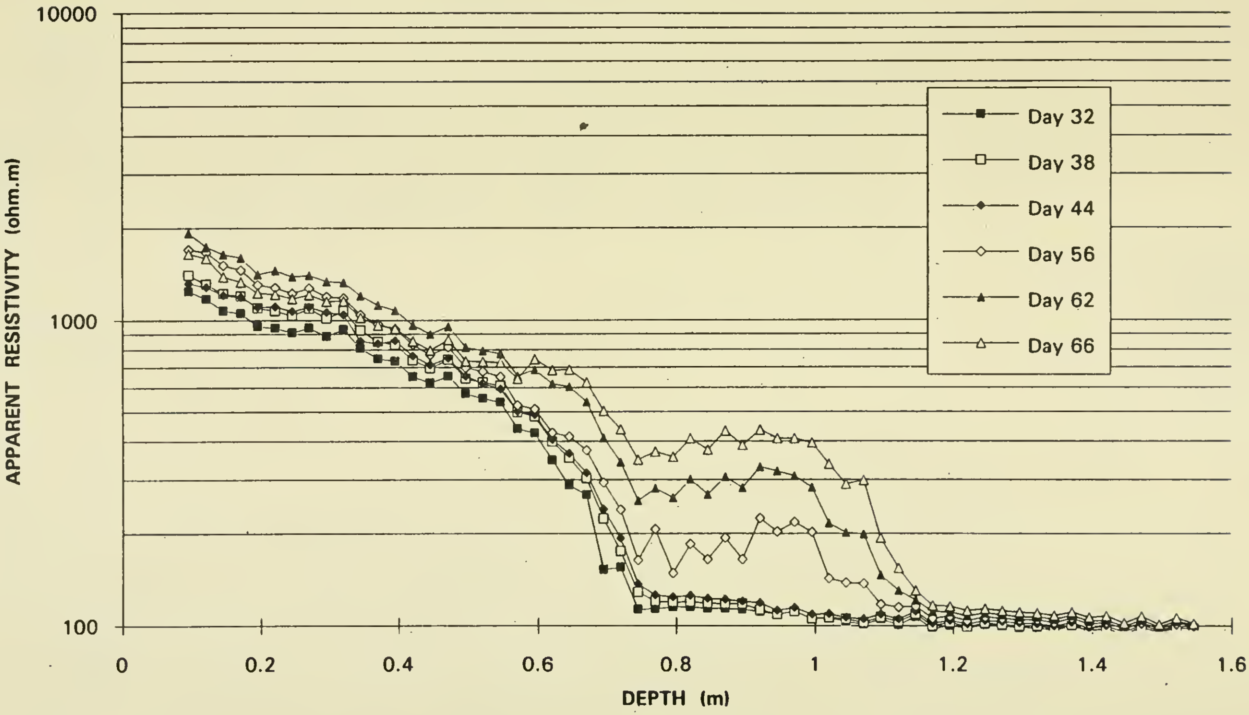

Figure 4.5.5.1 DC Resistivity insitu logging using a Wenner array with potential electrode spacing of 2.5 cm. Profiles show changing resistivities with time through the test cell. They include background readings and measurements following each injection.

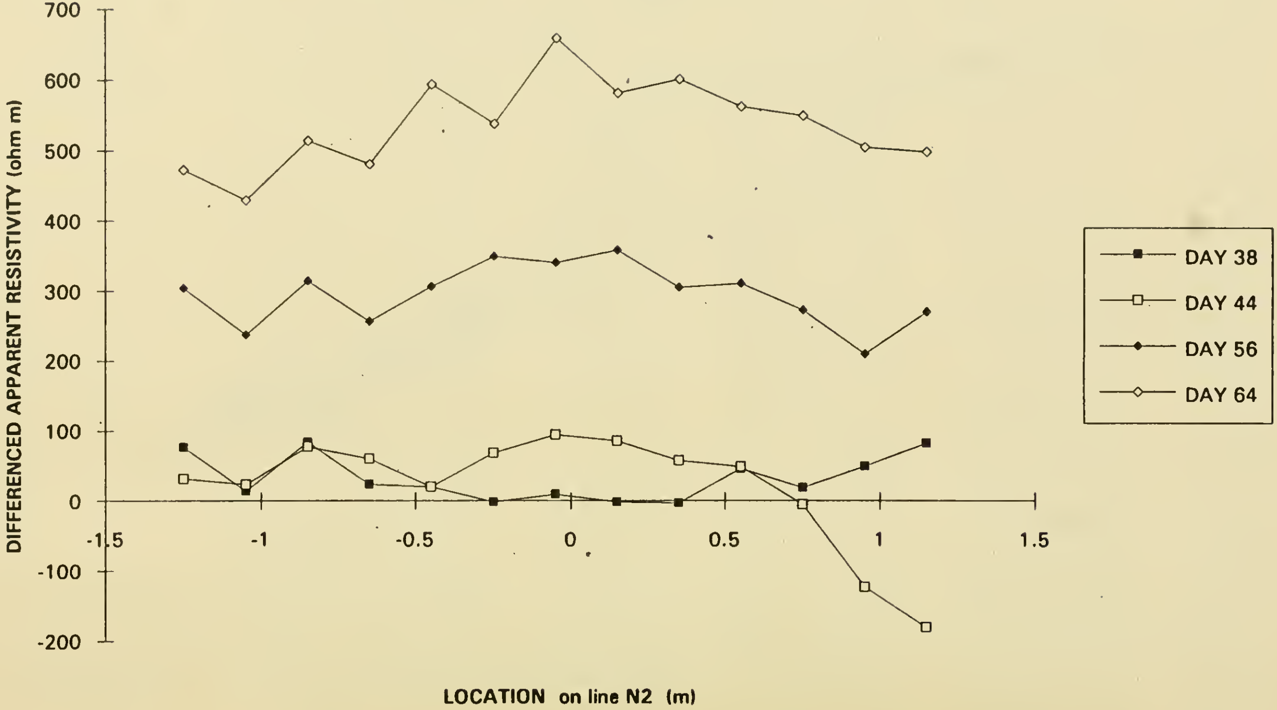

Figure 4.5.5.2 Differenced surface DC resistivity surveys using a Wenner array with potential electrode spacing of 20 cm. Profiles show changing apparent resistivities with time across the test cell along line N2. (The background resistivities have been subtracted.)

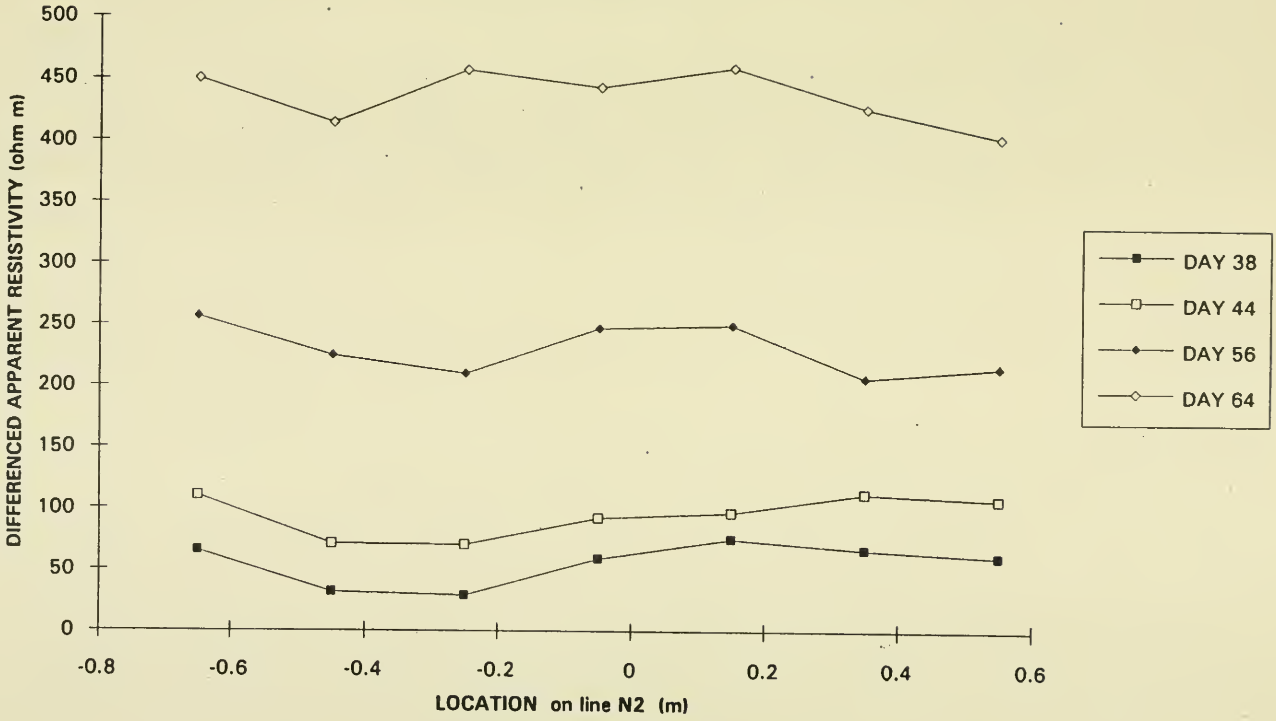

Figure 4.5.5.3 Differenced surface DC resistivity surveys using a Wenner array with potential electrode spacing of 60 cm. Profiles show changing apparent resistivities with time across the test cell along line N2. (The background resistivities have been subtracted.)

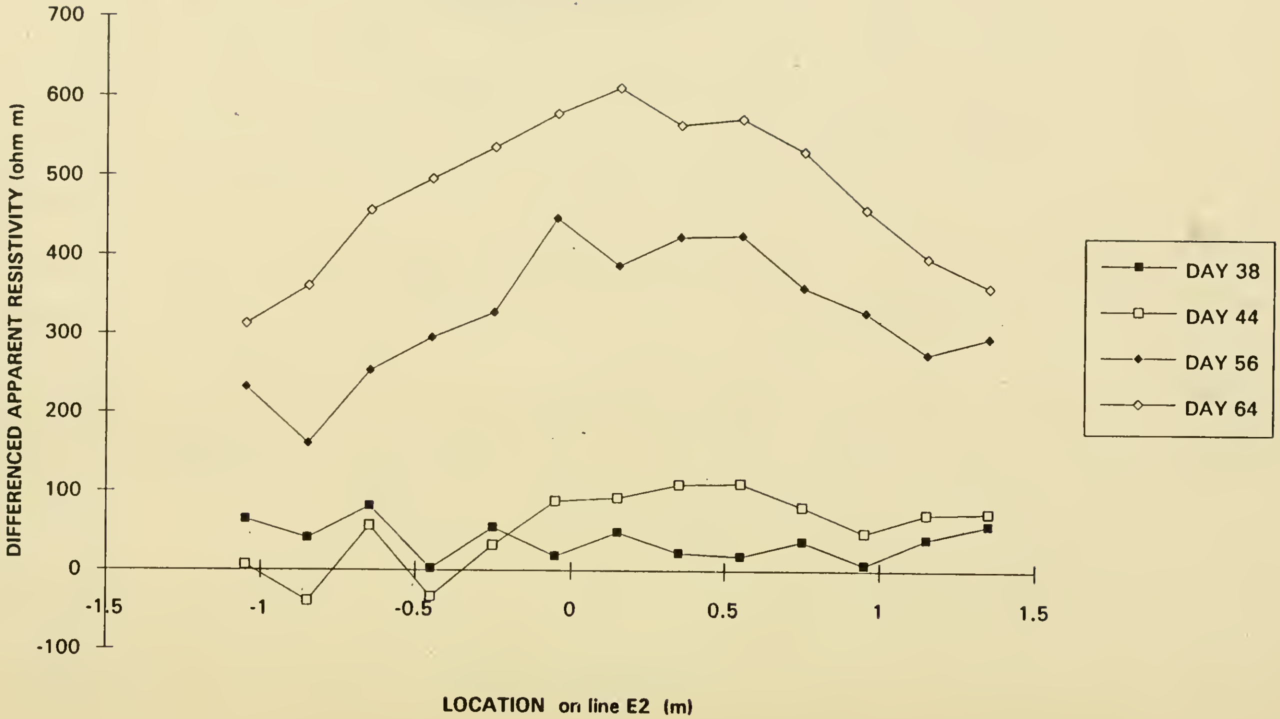

Figure 4.5.5.4 Differenced surface DC resistivity surveys using a Wenner array with potential electrode spacing of 20 cm. Profiles show changing apparent resistivities with time across the test cell along line E2. (The background resistivities have been subtracted.)

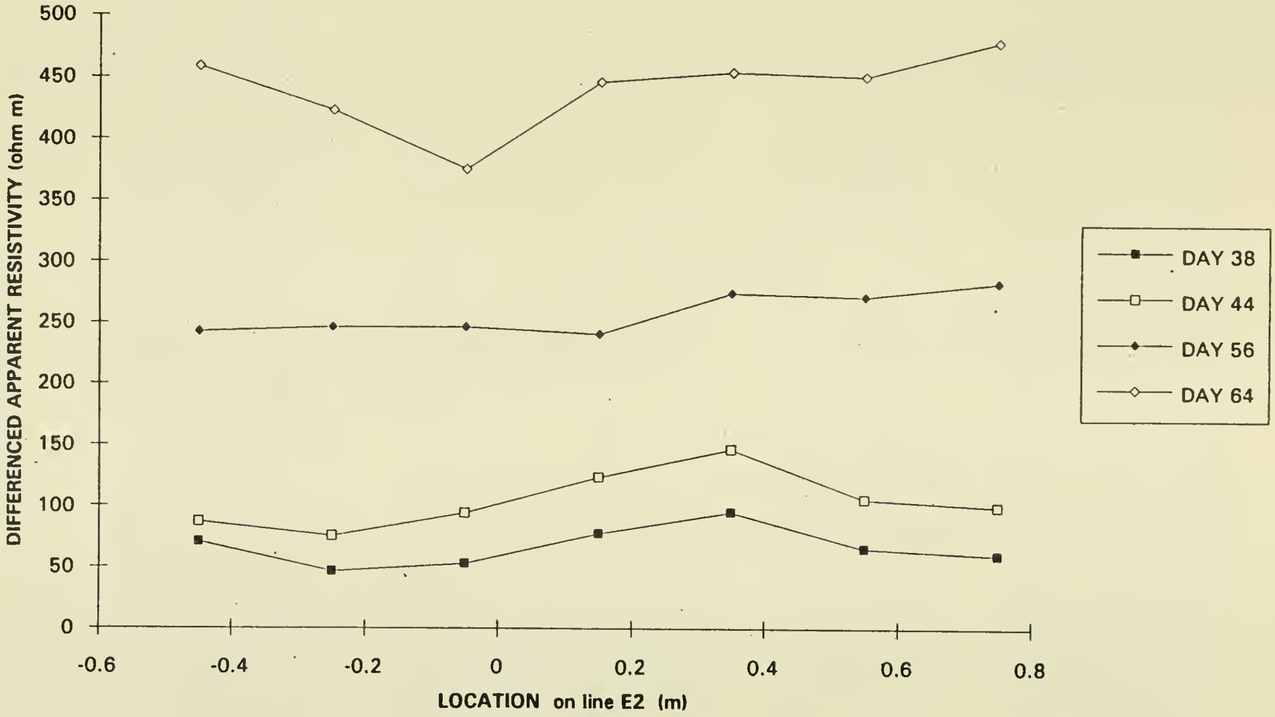

Figure 4.5.5.5 Differenced surface DC resistivity surveys using a Wenner array with potential electrode spacing of 60 cm. Profiles show changing apparent resistivities with time across the test cell along line E2. (The background resistivities have been subtracted.)

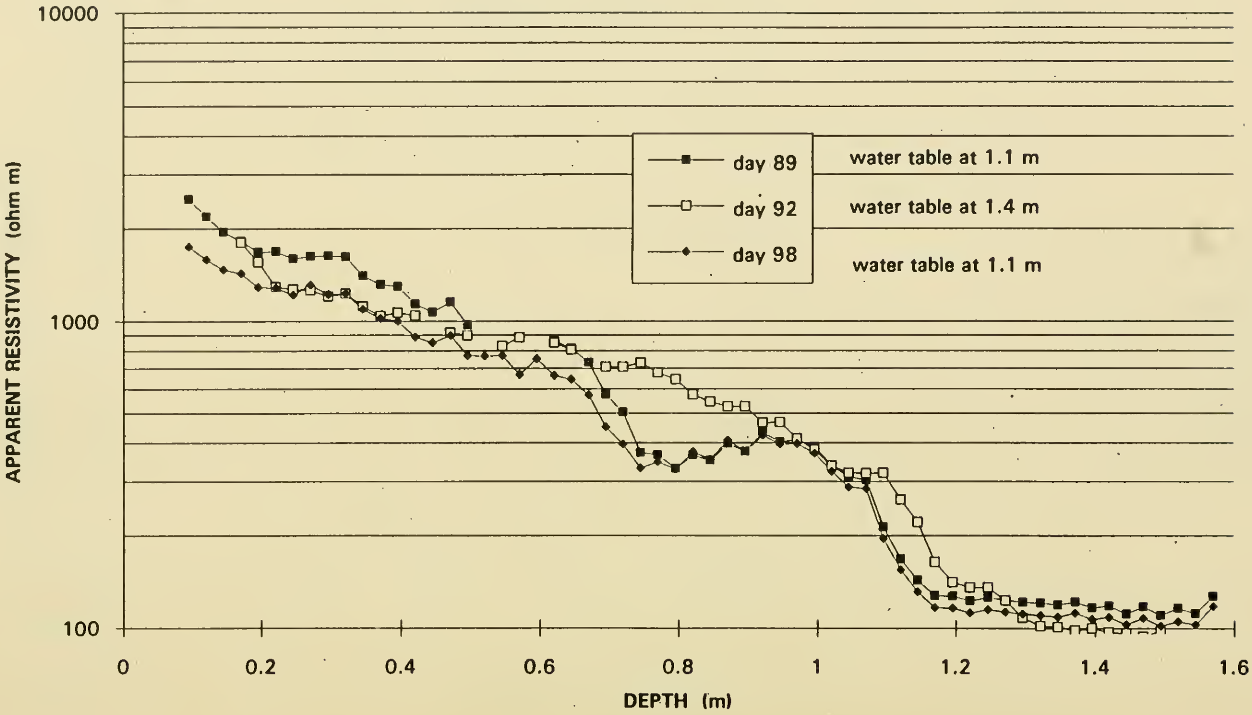

Figure 4.5.5.6 DC resistivity in situ logging with a potential electrode spacing of 2.5 cm. Three profiles: background (after final kerosene injection) with water table at 1.1 m, with the water table at 1.4 m, and finally with the water table returned to 1.1 m again.

4.5.6 Neutron Logging

The neutron logging results do not seem to give a great deal of information since they show little change throughout the experiment. This is due to the fact that the probe responds to total hydrogen content from both the water and the kerosene. Based on a chemical formula for kerosene of $C_{17}H_{36}$, as reported by Williams (1959), the ratio of hydrogen content by volume of kerosene to water is 1.090:1. Laboratory measurements of the weight percent hydrogen in the kerosene injected into the cell gave a ratio of 1.082:1. Since the hydrogen content in kerosene is only marginally higher than that in water, the replacement of water by kerosene would produce only a 10% change in the neutron response. In the case of kerosene and water, the neutron probe would be detecting total liquid content.

Although the individual depth measurements of the neutron probe are volume averages, they can still be very useful. For any one well, the radial distance of influence for a measurement is only affected by the liquid content since the sand pack, well and source detector assembly are not changing. The vertical zone of influence, along the axis of the well is approximately 15 cm centred on the source-detector assembly. (Appendix F, figures F.1 & F.2) However, although the probe samples a large volume, it is operated at 5 cm increments to allow for a detailed profile of the variations within the medium.

The background readings obtained from the seven glass wells show that the water content profile is constant within three standard deviations. (Figure 4.5.6.1) As the injections proceeded, the neutron profiles although increasing slightly where kerosene may have been replacing air in the capillary fringe, did not change a great deal. This indicates that kerosene must have been replacing water, which was removed via the well screen system. (Appendix F, figures F.3- F.6) Following the final injection however, the neutron count profile increases between 50 and 75 cm depth at glass well #4. (Figure 4.5.6.2) This may indicate that after the final injection, the kerosene pool incorporated a region which was above what had been previously saturated with water. The neutron probe shows changes in the neutron profiles after this injection in all of the wells but to varying degrees. (Figure 4.5.6.3) The neutron count profiles indicate that the kerosene pool is thicker in the middle and thinner on the sides which would agree with our schematic version of an LNAPL pool (figure 4.5.6.4) and the GPR results.

Following the lowering and raising of the water table we would expect kerosene, and possibly air, to have been trapped below the water table. The neutron profile would only be able to detect trapped air but assuming the water table was raised slowly enough and allowed to come to equilibrium, there should be no air trapped and therefore the total liquid in the profile should be the same. This however is not the case. Although the water injection rate was sufficiently slow, and equilibrium was established, hysteresis effects cause a substantial redistribution of water, kerosene and air throughout the sand profile. (Figure 4.5.6.5) (Appendix F, figure F.7)

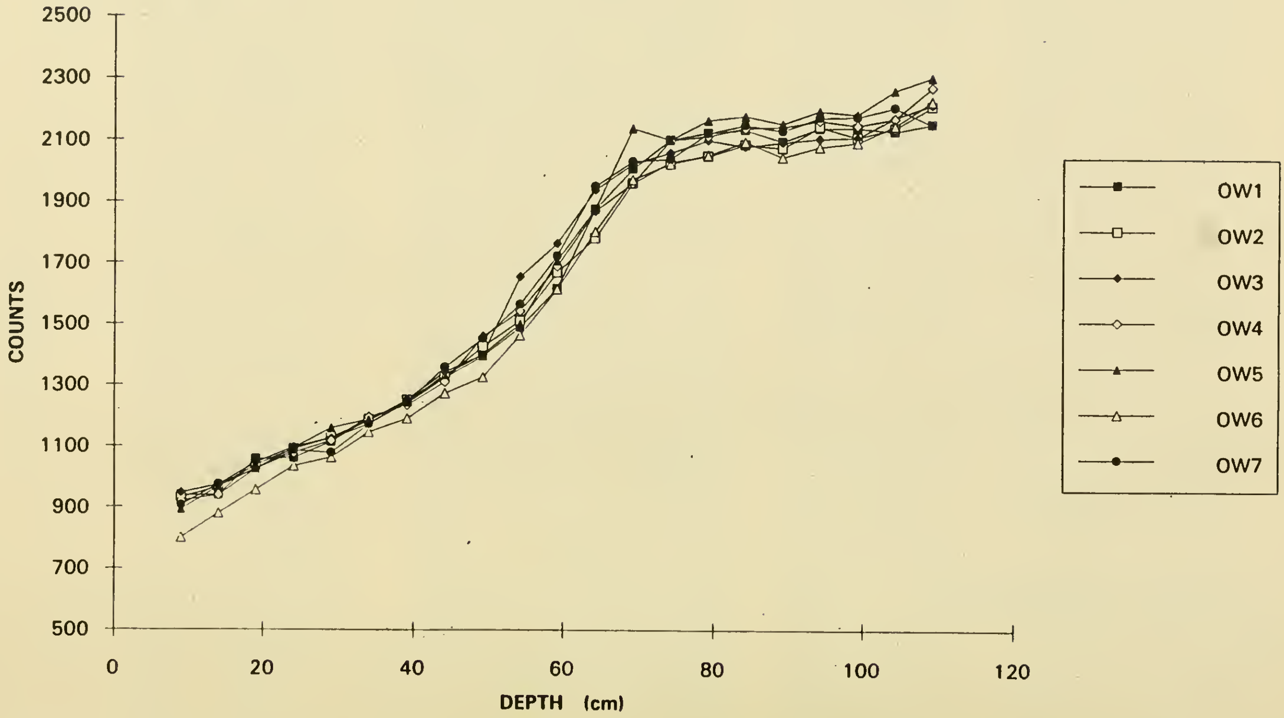

Figure 4.5.6.1 Neutron plobe logging in all glass wells with the water table at 1.1 m and before any kerosene has been injected.

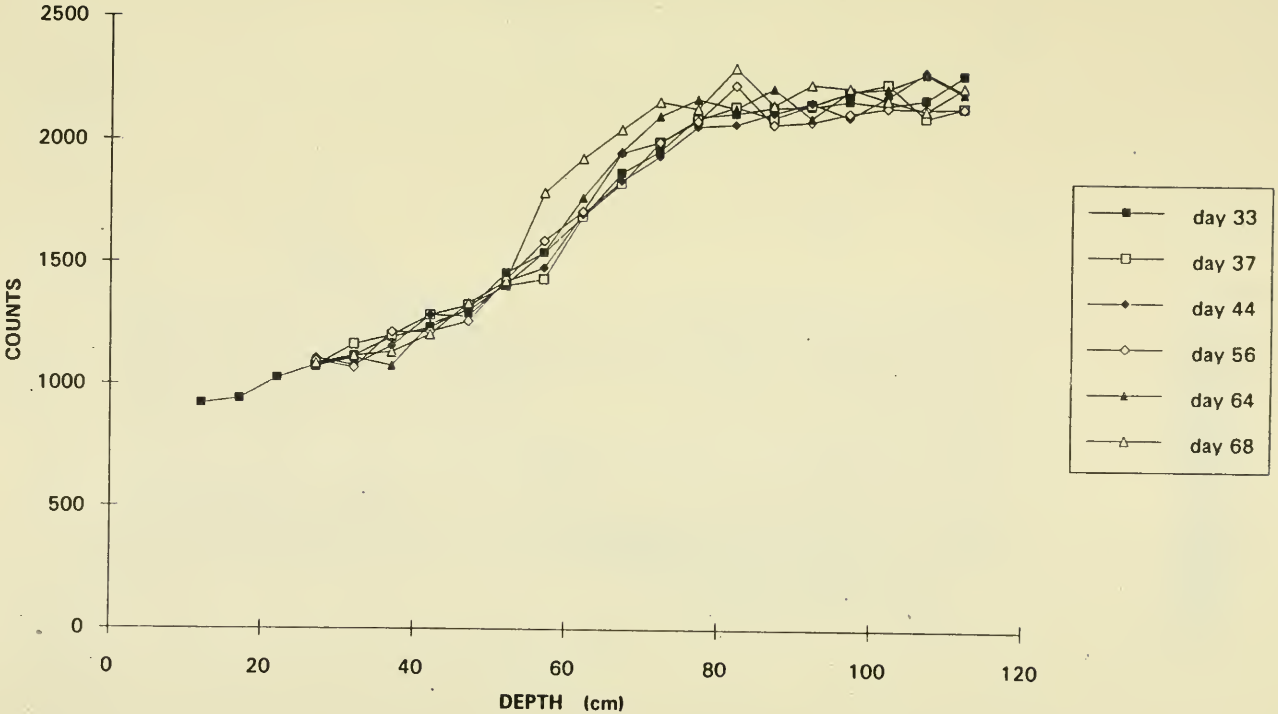

Figure 4.5.6.2 Neutron plobe logging in glass well #4 with the water table at 1.1 m.. Background profile and profiles following each kerosene injection.

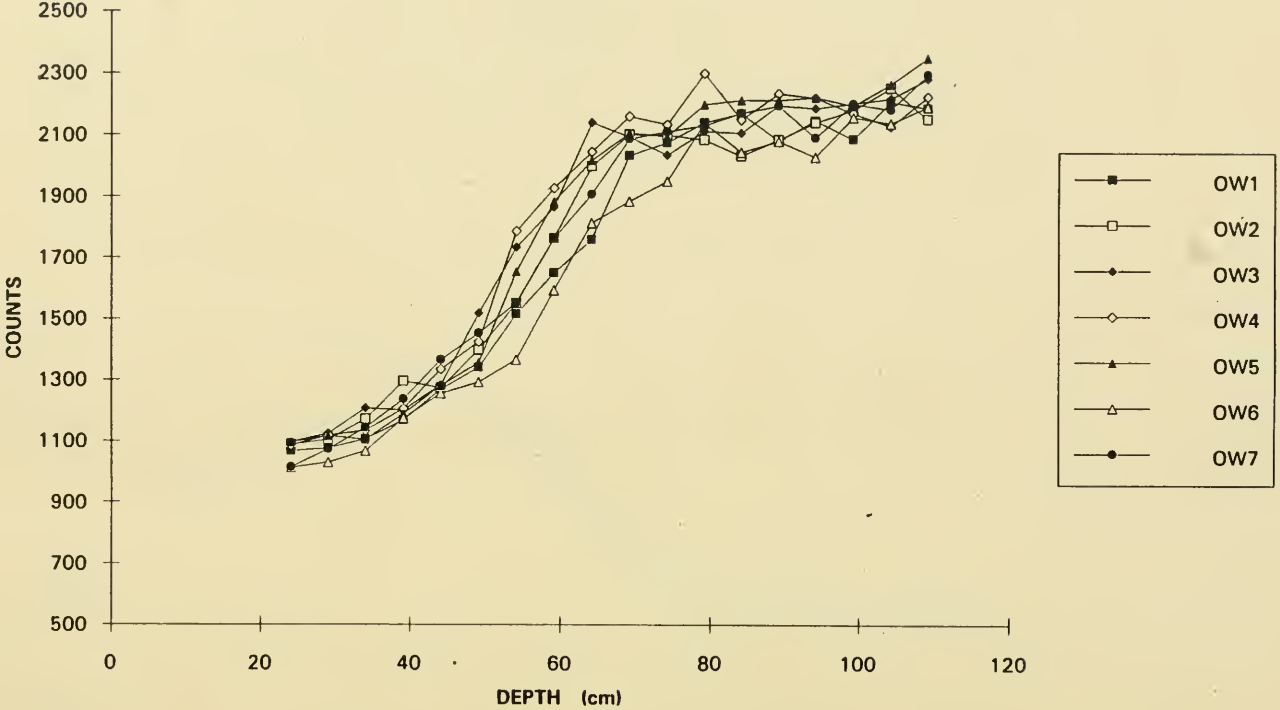

Figure 4.5.6.3 Neutron plobe logging in all glass wells with the water table at 1.1 m. All profiles are following the final kerosene injection.

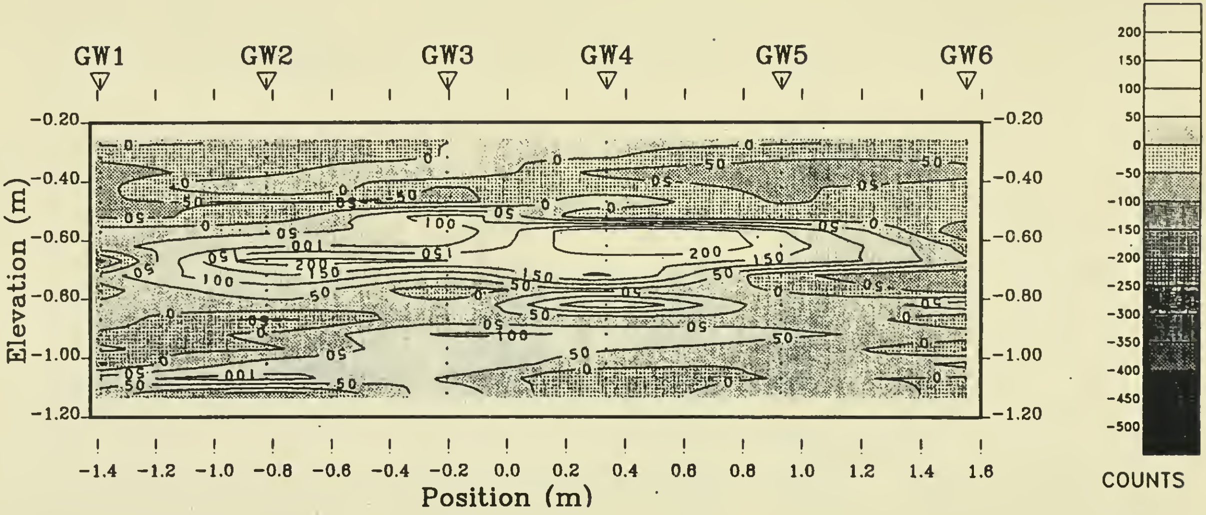

Figure 4.5.6.4 Cross section of neutron plobe logging results in all glass wells with the water table at 1.1 m. Neutron counts following the final kerosene injection differenced from background.

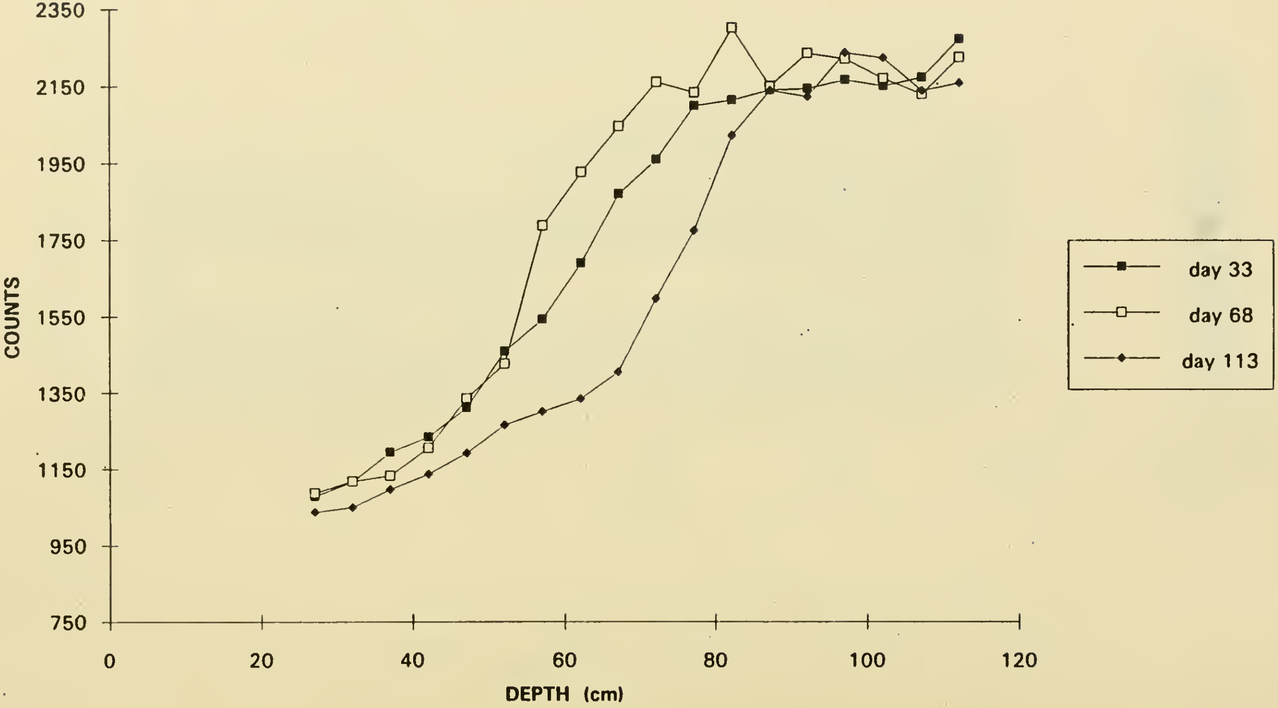

Figure 4.5.6.5 Neutron plobe logging results in glass well #4. Background (before injecting any kerosene) with the water table at 1.1 m, following final injection of kerosene, and after lowering and raising the water table to trap kerosene.

4.5.7 Radon Soil Gas

The radon concentrations in the soil gas extracted from the 14 access tubes within the test cell varied spatially and with time, due to inherent noise in the measurement process and to variations in pressure and temperature. To obtain an average response for the complete cell, the counts from all the soil gas access tubes were averaged. The counts per minute (cpm) before the first injection ranged from: 0-3 for ^{222} Rn(radon) and 3-7 for ^{220} Rn (thoron) (Figure 4.5.7.1). After the initial injection of 2 litres of kerosene, the ^{220} Rn counts increased to 25-30 cpm, which is well above levels recorded before the first injection. The increase in ^{222} Rn counts, however, was not above pre-injection levels. The next four injections resulted in a sustained increase in the ^{220} Rn, with the values always remaining at least 30 cpm above background. As with the 2 litre injection, the following injections did not increase the ^{222} Rn counts above pre-injection levels.

Radon soil gas consists of two isotopes. One isotope is ^{222} Rn (radon), with a half life of 3.8 days. It is within in the ^{238} U decay series and has as its parent ^{226} Ra . The other isotope is ^{220} Rn (thoron) with a much shorter half life of 55 seconds. It is in the ^{232} Th decay series and has as its parent ^{224}Ra.

Radon soil gas surveys have been performed commercially in an attempt to delineate LNAPL pools in the subsurface. In these surveys, the ^{222} Rn isotope has been used as the indicator of these pools since due to its much longer half life it can migrate further from its source. It has been estimated that the maximum migration distance of ^{222} Rn through dry soil, due to diffusion, is about 9 m but can in some cases, such as movement in fractures, it can move perhaps 100 m (Morse et al, 1982). Since ^{220} Rn has such a short half life, any enhancement in its concentration indicates only changes in the immediate environment from which it is sampled. ^{220} Rn would only be a useful indicator of deeper LNAPL pools if those pools altered the properties of the soil at the surface where the radon soil gas is collected (e.g. vapours migrating from the LNAPL source to the surface). The test cell with its thin unsaturated zone of 0.8 m, did not provide a suitable test of the enhancement in ^{220} Rn concentrations since we were essentially sampling the entire unsaturated zone.

We do not understand the process that resulted in the increased ^{220} Rn concentrations that we observed in our experiment. Laboratory measurements of the sandy soil used in the test cell have demonstrated that the source of the radon and thoron was within the soil grains. It has been shown that the fraction of radon atoms that escape from the soil grains (where the parent radium resides) into the soil gas is strongly controlled by moisture content (Strong and Levins, 1982). One possible explanation for the enhancement that we observed is that the pore scale water content distribution changed within the unsaturated zone due to kerosene vapours changing the thickness of water films on grains. The multilevel dielectric permittivity probe did not detect any change in water content within this zone; however, the resistivity probe did detect an increase in resistivity that could result from a redistribution water at the pore scale(e.g. fewer grain to grain connections through the pore water).

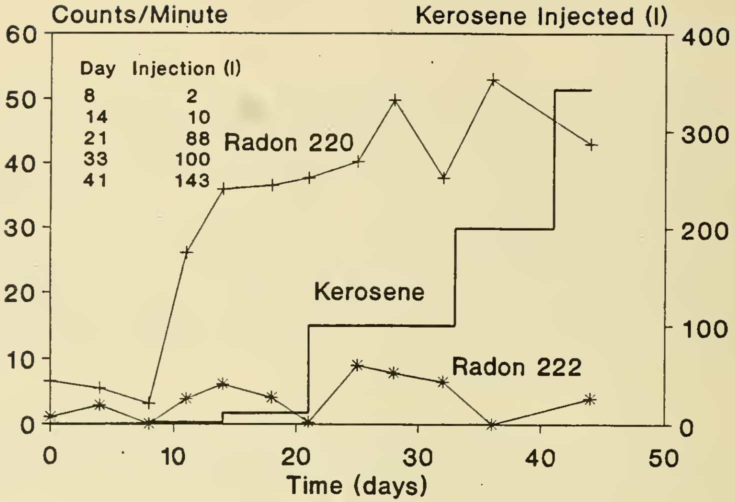

Figure 4.5.7.1 Radon monitoring results before and following kerosene injections in test cell. The alpha counts per minute from soil gas samples are shown for both isotopes ^{222} Rn (radon) and ^{220} Rn (thoron).

4.5.8 Borehole TV Camera

The borehole TV Camera did not deliver the results we had expected. The camera itself worked well and as a result there are video logs of the sand pack as seen from within the glass wells using white light. Unfortunately, the attempt to identify the dyed kerosene in ultraviolet light was unsuccessful.

During the first attempts, the "fluorescing blobs" which would identify the location of the kerosene, were not evident. It was impossible to determine if there was enough kerosene to make the fluorescent blobs discernible, if the kerosene pool had spread laterally enough to intersect the glass well, or if, due to the packing process, there was a low permeability sand layer surrounding each of the glass wells which the kerosene was avoiding. Although the other geophysical instruments were already seeing the affects of the kerosene, these affects were for the most part changes in water content.

With further kerosene injections, we did in fact view two "fluorescing blobs" of kerosene but these were only visible for a couple of days and then there were no further occurrences. A rod was pushed down beside one of the glass well to see if dyed kerosene would fill the void when the rod was removed but this too was unsuccessful. The geophysical equipment indicates that the kerosene pool did in fact at least reach the TDR probe which is further away from the injection point than some of the glass wells. Also, coring proved that there was a layer of the sand pack which was saturated with kerosene and which extended to at least one side of the test cell.

There are any number of explanations for the lack of success with this dye when it had proved successful at the OGI. The sand used at the OGI was coarser and contained some gravels. It may be that the use of Borden sand resulted in some kind of degradation of the dye with time or that the dye had sorbed to the sand. There is some physical evidence which indicates that the former is more probable since when the coring was done there was no dye visible on the sand or even in the kerosene itself.

4.5.9 Kerosene Saturation Stratigraphy from Soil Cores

After the last kerosene injection had reached equilibrium, four soil cores were collected from within the test cell at the locations shown in Figure 4.3.1. The cores were subsectioned into 5 cm lengths and the kerosene saturation in each of these soil samples was determined using a spectrophotometric technique. The core collection technique and kerosene saturation measurements are described in Appendix A.4.

The vertical profiles of kerosene saturation (fraction of pore space containing kerosene) show the development of a substantial pool (Figure 4.5.9.1) after a total of 343 litres was injected. The kerosene pool is centred at a depth of about 0.8 m with a maximum kerosene

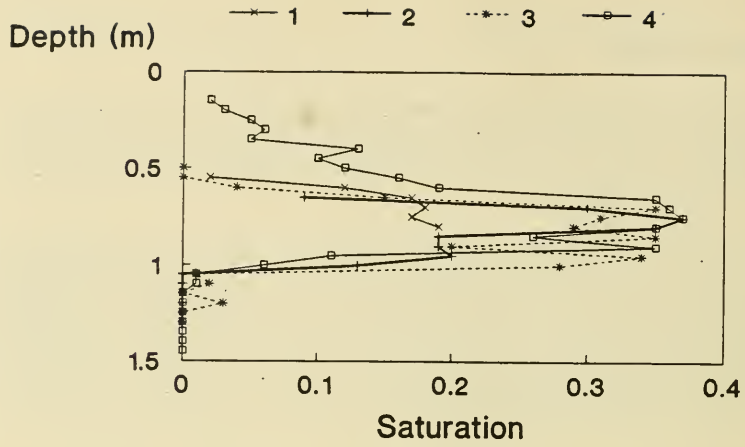

Figure 4.5.9.1: Kerosene saturation profiles measured on soil samples from core collected within the test cell after the last injection on day 77.

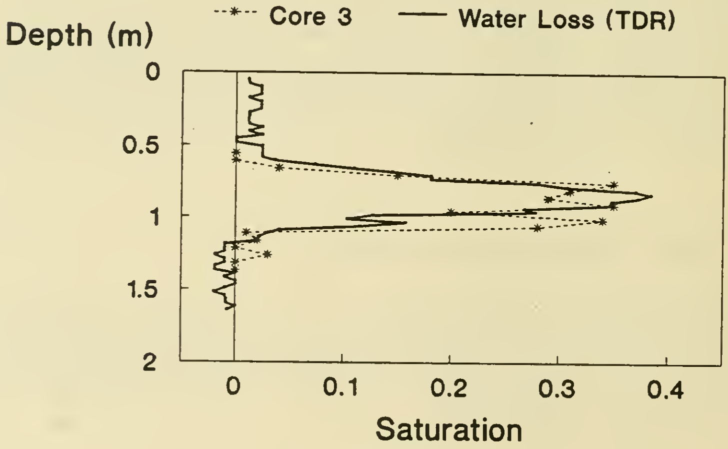

Figure 4.5.9.2: Water content loss compared with kerosene saturation profile from core 3, collected adjacent to the multilevel dielectric permittivity probe. The individual water loss measurements points were measured on the multilevel probe on day 77, just before coring.

saturation of between 35 and 40% . In all cores, kerosene saturation decreases significantly at a depth of approximately .9 m, and drops to near zero at 1.1 m, which is the depth of the water table. The kerosene saturation profile for core 4, which is near the injection point, shows that the kerosene extends up into the unsaturated zone and is actually above the injection depth of 0.3 m. Core 1 is near the edge of the tank and has substantially lower saturations. The total kerosene content in the pool appears to decrease the further one is from the injection point. This effect is also observed in the surface GPR data and in the neutron logging data.

The loss in water content, inferred from the in situ dielectric permittivity measurements (see section 4.5.4), is quite similar to the vertical profile of kerosene saturation from core 3 (Figure 4.5.9.2). Core 3 was collected 0.25 m from the multilevel dielectric permittivity probe. The dielectric permittivity measurements were taken just before the core was collected. This provides further support for the assumption that the water content loss is equivalent to the increase in kerosene saturation.

4.6 Discussion

The monitoring techniques described in the previous sections have given information about the LNAPL saturation and distribution within the test cell. This information has been inferred due to observed changes in the distribution of water caused by the LNAPL. The presence of the LNAPL has caused a reduction in the capillary fringe due to changing interfacial tensions and a depression of the water table due to the displacement of water by kerosene. In order to acquire more quantitative information about the LNAPL, it is necessary to combine the results obtained using all the geophysical methods.

By combining the information obtained from the TDR and the neutron probe it has been possible to determine the LNAPL saturation (DeRyck, 1994). Since the neutron data indicates total hydrogen content (from both the water and the kerosene) and the TDR indicates water content alone, a difference of the TDR data from that of the neutron data results in a kerosene content profile which can then be calibrated with coring results. Using the combined TDR and neutron data it was possible to obtain more accurate measurements of the kerosene saturation within the pooled zone than was possible using only the TDR data.

Although 450 L of water were removed from the test cell to lower the water table from 1.1 m to 1.4 m (bgs), only 230 L were required to return the water table to its original level. While some of this effect was due to trapped kerosene (and air) reducing the volume of water in the zone above the water table, it is hysteresis that has the greatest effect. Below about 0.8 m (the top of the original saturated zone), the neutron probe indicates at no time throughout the experiment did the total liquid content change by more than 10%. This indicates that below 0.80 m there is no significant change in the amount of trapped air. The TDR data shows changes in water content below 1.1 m only after the water table had been lowered and raised. Therefore the reduction in water content below this level was caused by trapped kerosene.

In this controlled environment, most of the geophysical techniques have been successful. The GPR, TDR, Neutron probe, DC resistivity and Radon Soil Gas methods appear to have been very successful, while the others have only been marginally successful. The geophysical techniques have given us information about the electrical property changes which occur when an LNAPL enters the subsurface as well as identifying some of the changes which occur in the physical properties of the soil. Although these techniques are not necessarily transferable to heterogeneous natural environments they may still provide useful information.

5. DISCUSSION

5.1 Implications for the Detection of LNAPLs

The mathematical modelling, laboratory measurements and the controlled spill experiment all demonstrated that in simple environments measurable changes would be observed with the following geophysical techniques: GPR, surface EM, DC resistivity, EM logging, neutron logging and radon. The ability of geophysics to delineate LNAPL contamination at a site where it has been accidentally spilled into the subsurface will depend on the specific characteristics of the site being investigated. The mathematical models and the results of the controlled spill presented in this report can be used to predict when these techniques have a reasonable chance of being successful. In our modelling and spill experiment we have also observed some characteristic responses from LNAPL pools at the water table that may be seen in data collected at these sites.

Ground Penetrating Radar

- An LNAPL contaminated water table will in some cases be a more gradational electrical interface than an uncontaminated water table. This effect would manifest itself in GPR sections as a reduction in the amplitude of the event from this interface.

- The reflection event from the water table would appear at later times in areas where a significant LNAPL pool exists.

- If a there is a stratigraphic horizon observed in a GPR section below the water table, then this horizon would appear earlier in time in the zone where the LNAPL pool exists. This was observed for the event from the bottom of the tank in GPR sections collected during the controlled spill.

Surface EM

- There would be a reduction in apparent conductivity over an LNAPL pool since the water saturated zone is deeper. The modelling suggests that this effect is quite small except in relatively conductive environments.

Borehole EM

- The increase in conductivity that occurs at the top of the saturated zone would appear at a greater depth in the region where an LNAPL pool exists. This effect may be difficult to distinguish from natural fluctuations in the water table.

DC Resistivity

- Over an LNAPL pool there would be an increase in apparent resistivity for appropriate electrode spacings due to the increased depth of the water table.

Neutron and Dielectric Permittivity Logging

- The soil moisture neutron logging device discussed in this report would be particularly useful in locating residual hydrocarbons in the unsaturated zone. The usefulness of the technique would be enhanced, in particular in the saturated and transition zone, if used in conjunction with a dielectric logging tool (DeRyck, 1994).

Radon Soil Gas

- We observed a large increase in ^{220}Rn (thoron), the short lived radon isotope. However, we do not believe that looking for anomalous concentrations of this isotope would be useful since most LNAPL pools generally occur at a greater depth than the zone from which the thoron is being sampled. Our observations do suggest that if there is also significant source of ^{222}Rn (radon) available in the soil, then its concentration in the soil gas could also be enhanced above LNAPL pools.

Other Comments

For the electrical methods (surface EM, borehole EM, and DC resistivity), our conclusions depend on the LNAPL decreasing the conductivity of the soil by displacing water. In some cases, the LNAPL may have associated inorganic contamination or may cause chemical alterations that give rise to increased inorganics in the groundwater. Both of these effects can increase the soil conductivity. If this is the case, the LNAPL may be located by its association with these enhanced inorganic species in the groundwater that may then be mapped with electrical methods.

All of the geophysical techniques, with the exception of the combined neutron and dielectric permittivity logging technique, are not directly detecting the LNAPL but are mapping changes in water content associated with the presence of the LNAPL For this reason, anomalous zones observed with the geophysical methods could also be attributed to other effects such as changes in water table elevation, infiltration from rainfall events, or changes in lithology (e.g. porosity) without other supporting evidence that rules out these effects.

It should be remembered that although geophysical methods can not in many cases delineate LNAPL pools in the subsurface, these techniques can still be very useful for: determining surficial geology, which could help in prediction of contaminant movement and location; and for monitoring the development of an LNAPL pool during and following a spill, or the reduction of a pool during a remediation procedure.

5.2 Recommendations for Future Research

- The combined neutron and dielectric permittivity logging technique (DeRyck, 1994) shows promise for delineating LNAPLs in the saturated and unsaturated zone and should be studied further.

- The geophysical techniques discussed in this report should also be applied at accidental spill sites. These sites are more likely to have a variable water table elevation, soil heterogeneities and a mix of LNAPLs that will complicate interpretation.

- The effect of LNAPLs on the induced polarization response of LNAPL contaminated soils should be studied further.

- Laboratory measurements of the electrical properties of LNAPL contaminated soils should be performed at GPR operating frequencies.

- The radon soil gas mapping technique should be studied further to understand the physical processes that can give rise to the observed enhancement in ^{220} Rn (thoron).

5.3 Publications Resulting from Funding

The following publications describe research partially or completely funded under project E561G by the Ontario Ministry of Environment and Energy:

1. DeRyck, S. M., Redman, J. D., and Annan, A. P., 1993. Geophysical monitoring of a controlled kerosene spill. Proceedings of the Symposium on the Application of Geophysics to Engineering and Environmental Problems, San Diego, California, pp. 5-19.

2. DeRyck, S.M., 1994. Monitoring a controlled LNAPL spill. MSc. Thesis, Dept. of Earth Science, University of Waterloo, Waterloo, Ontario, p. 232.

3. Endres, A.L., and J.D. Redman, 1993. Modelling the electrical properties of porous rocks and soils containing immiscible contaminants. Proceedings of the Symposium on the Application of Geophysics to Engineering and Environmental Problems, San Diego, California, pp. 21-38.

4. Redman, J.D., and DeRyck, S.M., 1994. Monitoring LNAPLs in the subsurface with multilevel TDR probes. Proceedings of Symposium on Time Domain Reflectometry in

Environmental, Infrastructure and Mining Applications, Northwestern University, Evanston Illinois, Sept. 1994.

5. Redman, J.D., DeRyck, S.M., and Annan, A.P., 1994. Detection of LNAPL pools with GPR: Theoretical modelling and surveys of a controlled spill. Proceedings of the Fifth International Conference on Ground Penetrating Radar, Kitchener, Ontario, June 1994, pp.1283-1294.

6. Schneider, G.W., S.M. DeRyck, and P.A. Ferre, 1993. The application of automated high resolution resistivity in monitoring hydrogeological field experiments. Proceedings of the Symposium on the Application of Geophysics to Engineering and Environmental Problems, San Diego, California, pp. 145-162.

7. Westbroek,H., 1993. The effect of relative kerosene saturation on the electrical conductivity of sand, B.Sc. Thesis, University of Waterloo, 43p.

ACKNOWLEDGMENTS

We would like to acknowledge the support of the Ministry of Environment and Energy for funding this research project. We would also like to thank Geonics, Hyd-Eng Geophysics, the Oregon Graduate Institute, Sensors and Software, and Scintrex for lending us their equipment.

6. REFERENCES

Annan, A.P., Cosway, S.W., and Redman, J.D., 1991. Water table detection with ground penetrating radar. Expanded Abstracts SEG 61st Annual Meeting, Nov. 1991, Houston, Texas.

Archie, G.E., 1942. The electrical resistivity log as an aid in determining some reservoir characteristics. Petroleum Technology, January Issue, pp. 54-62.

Armstrong, F.E. and R.J. Heemstra, 1973. Radiation halos and hydrocarbon reservoirs: A Review. U.S. Bureau of Mines Information Circular 8579.

Borner, F., Gruhne, M. and Schon, J., 1993. Contamination indications derived from electrical properties in the low frequency range. Geophysical Prospecting, V. 41, pp. 83-89.

Brewster, M.L., Redman, J.D. and Annan, A.P., 1992. Monitoring a controlled injection of perchloroethylene in a sandy aquifer with ground penetrating radar and time domain reflectometry. Proceedings of the Symposium on the Application of Geophysics to Engineering and Environmental Problems, Oakbrook, Illinois, pp. 611-618.

Campbell, M.J., and Ulrichs, J., 1969. Electrical properties of rocks and their significance for Lunar radar observations. J. Geophys. Res., V.74, p.5867-5881.

Daniels, J.J., Roberts, R. and Vendl, M, 1992. Site studies of ground penetrating radar for monitoring petroleum product contaminants. Proceedings of the Symposium on the Application of Geophysics to Engineering and Environmental Problems, Oakbrook, Illinois, pp. 597-609.

DeRyck, S. M., Redman, J. D., and Annan, A. P., 1993. Geophysical monitoring of a controlled kerosene spill. Proceedings of the Symposium on the Application of Geophysics to Engineering and Environmental Problems, San Diego, California, pp. 5-19.

DeRyck, S.M., 1994. Monitoring a controlled LNAPL spill. MSc. Thesis, Dept. of Earth Science, University of Waterloo, Waterloo, Ontario, p. 232.

Ellis, Darwin V., 1987, Well Logging for Earth Scientists, Elsevier Science Publishing Co., Inc..

Endres, Anthony L., 1993. Personal communication.

Endres, A. L. and Knight, R., 1991. The effects of pore-scale fluid distribution on the physical properties of partially saturated tight sandstones. J. Appl. Phys., v. 69, pp. 1091-1098.

Endres, A.L., and J.D. Redman, 1993. Modelling the electrical properties of porous rocks and soils containing immiscible contaminants. Proceedings of the Symposium on the Application of Geophysics to Engineering and Environmental Problems, San Diego, California, pp. 21-38.

Feng, S., and Sen, P. N., 1985. Geometrical model of conductive and dielectric properties of partially saturated rocks. J. Appl. Phys., v. 58, pp. 3236-3243.

Fuoss, R.M. and Hsia,K.L., 1967. Association of 1:1 salts in water. Proc. Natl. Acad. Sci., V. 57, pp.1550-1557.

Hasted, J.B., 1973. Aqueous Dielectrics. Chapman and Hall, London, p. 302.

Keech, D.A., 1988. Hydrocarbon thickness on groundwater by dielectric well logging. Proceedings of: Petroleum Hydrocarbons and Organic Chemicals in Ground Water: Prevention, Detection and Restoration, The Association of Ground Water Scientists and Engineers., pp. 275-289.

Knight, R., 1991. Hysteresis in the electrical resistivity of partially saturated sandstones. Geophysics, v. 56, pp. 2139-2147.

Lenhard, R. J., and Parker, J. C., 1990. Estimation of free hydrocarbon volume from fluid levels in monitoring wells. Groundwater, v. 28, pp. 57-67.

McNeill, J.D., 1980. Electromagnetic terrain conductivity measurement at low induction numbers. Geonics Technical Note 6.

McNeill, J.D., 1986. Geonics EM39 Borehole Conductivity Meter, Theory of Operation, Geonics Technical Note 20.

Morse, J.G., Rana,M.H., and Morse, L., 1982. Radon mapping as indicators of subsurface oil and gas. Oil and Gas Journal, v.80 n.19:227-246.

Musil, J. and Zacek, F., 1986. Microwave Measurements of Complex Permittivity by Free Space Methods and Their Applications. Elseveir, Amsterdam, p. 275.

Olhoeft G.R., 1981. Electrical properties of rocks and minerals. Short Course Notes, pp. 96.

Olhoeft, G.R., 1981. Electrical properties of rocks: in *Physical Properties of Rocks and Minerals V. II*, eds. Y.S. Touloukian, W.R. Judd,and R.F. Roy, McGraw-Hill, pp.257-329.

Olhoeft, G.R., 1986. Direct detection of hydrocarbon and organic chemicals with ground penetrating radar and complex resistivity. in Proc. of the NWWA/API Conf. on Petroleum Hydrocarbons and Organic Chemicals in Ground Water -- Prevention Detection and Restoration, Natl. Water Well Assoc., pp.284-305.

Pitchford, A.M., Mazzella, A.T., and Scarbrough, K.R., 1989. Soil-gas and geophysical techniques for detection of subsurface organic contamination. Environmental Monitoring Systems Laboratory, Technical Report , ESL-Tr-87-67, p.172.

Redman, J. D., 1992. Geophysics and the solvents-in-groundwater program. Proceedings of the Symposium on the Application of Geophysics to Engineering and Environmental Problems, Chicago, Illinois, pp. 375-382.

Schneider, G.W., S.M. DeRyck, and P.A. Ferre, 1993. The application of automated high resolution resistivity in monitoring hydrogeological field experiments. Proceedings of the Symposium on the Application of Geophysics to Engineering and Environmental Problems, San Diego, California, pp. 145-162.

Schneider, G. W., and Greenhouse, J. P., 1992, Geophysical detection of perchloroethylene in a sandy aquifer using resistivity and nuclear logging techniques, Proceedings, Symposium on the Application of Geophysics to Engineering and Environmental Problems, Chicago, Illinois, pp. 619-628.

Sen, P. N., Scala, C., and Cohen, M. H., 1981. A self-similar model for sedimentary rocks with application to the dielectric constant of fused glass beads. Geophysics, v. 46, pp. 781-795.

Shen, L.C., Savre, W.C., Price, J.M. and Athavale, K., 1985. Dielectric properties of reservoir rocks at ultra-high frequencies. Geophysics, v. 50, pp. 692-704.

Strong, K.P. and Levins, D.M., 1982. Effect of moisture content on radon emanation from uranium ore and tailings. Health Physics, V.42, p. 27-32.

Topp, G.C., J.L. Davis and A.P. Annan, 1980. Electromagnetic determination of soil water content: Measurement in coaxial transmission lines. Water Res. Res. 16:574-582.

Ucok, H., Olhoeft, G.R., and Ershaghi, I., 1979. Electrical resistivity of geothermal brines. SPE7878, pp.163-171, Symposium on Oilfield Chemistry and Geothermal Brines, Dallas:SPE.

Vanhala, H., Soininen, H., and Kukkonen, I., 1992. Detecting organic chemical contaminants by spectral-induced polarization method in glacial till environment, Geop., V.57, p.1014-1017.

van Genuchten, M. Th., and Nielsen, D. R., 1985. On describing and predicting the hydraulic properties of unsaturated soils. Annales Geophysicae, v. 3, pp. 615-628.

Von Hippel, A.R., 1961. Dielectric materials and applications. MIT Press, Cambridge, Mass., p. 438.

Voralek, J.W., 1991. Electrical conductivity of dense, non-aqueous phase liquid contaminants in a homogeneous porous media. B.Sc. Thesis, University of Waterloo, 58p.

Westbroek,H., 1993. The effect of relative kerosene saturation on the electrical conductivity of sand, B.Sc. Thesis, University of Waterloo, 43p.

Williams, W.H., 1959. Thermodynamic charts for the combustion products of nitric acid and kerosene. Reports and Memoranda No. 2982, R.A.E. Tech. Note R.P.D. 33, July 1950.

Wuenschel, P.C., 1960. Seismogram synthesis including multiples and transmission coefficients. Geophysics, Vol. 25, pp. 106-129.Annan, A.P., Cosway, S.W., and Redman, J.D., 1991. Water table detection with ground penetrating radar. Expanded Abstracts SEG 61st Annual Meeting, Nov. 1991, Houston, Texas.

Wygal, R.J., 1963. Construction of models that simulate oil reservoirs. Society of Petroleum Engineers Journal, December 1963, pp. 281-286.

TABLE of APPENDICES

Appendix A 102
General information on experimental set up and procedures.

Appendix A.1 102
Elevation corrected water table levels as measured in monitoring wells.

Appendix A.2 106
Temperature data. Thermistor measurements conversions to temperature.

Appendix A.3 108
Soil porosity measurements.

Figure A.3.1: Location within the test cell where samples for soil porosity analysis were taken.

Appendix A.4 110
Coring procedure, analyses, and results.

Figure A.4.1: Coring procedure, analyses, and results. (continued)
Calibration for kerosene in iso-octane.

Appendix A.5 113
Schedule of monitoring.

Appendix A.6 120
X-Y grid surface survey, location of probes and wells.

Figure A.6.1: X-Y grid surface survey, location of probes and wells. (continued)
Plan view of test cell.

Appendix A.7 122
Elevation survey in test cell.

Figure A.7.1: Elevation survey in test cell. Plan view of test cell. (continued)

Appendix B 126
EM38 data summary sheet and averages.

Appendix C 130

Ground Penetrating Radar

Figure C.1: GPR survey with 450 MHz antennae on day 32 along line N1. The water table is at 1.1 m and there is no kerosene in the test cell.

Figure C.2: GPR survey with 450 MHz antennae on day 32 along line N2. The water table is at 1.1 m and there is no kerosene in the test cell.

Figure C.3: GPR survey with 450 MHz antennae on day 32 along line N3. The water table is at 1.1 m and there is no kerosene in the test cell.

Figure C.4: GPR survey with 450 MHz antennae on day 32 along line E1. The water table is at 1.1 m and there is no kerosene in the test cell.

Figure C.5: GPR survey with 450 MHz antennae on day 32 along line E2. The water table is at 1.1 m and there is no kerosene in the test cell.

Figure C.6: GPR survey with 450 MHz antennae on day 32 along line E3. The water table is at 1.1 m and there is no kerosene in the test cell.

Figure C.7: GPR survey with 450 MHz antennae on day 71 along line N1. The water table is at 1.1 m. This is after the final injection therefore there are 343 L of kerosene in the test cell.

Figure C.8: GPR survey with 450 MHz antennae on day 71 along line N2. The water table is at 1.1 m. This is after the final injection therefore there are 343 L of kerosene in the test cell.

Figure C.9: GPR survey with 450 MHz antennae on day 71 along line N3. The water table is at 1.1 m. This is after the final injection therefore there are 343 L of kerosene in the test cell.

Figure C.10: GPR survey with 450 MHz antennae on day 71 along line E1. The water table is at 1.1 m. This is after the final injection therefore there are 343 L of kerosene in the test cell.

Figure C.11: GPR survey with 450 MHz antennae on day 71 along line E2. The water table is at 1.1 m. This is after the final injection therefore there are 343 L of kerosene in the test cell.

Figure C.12: GPR survey with 450 MHz antennae on day 71 along line E3. The water table is at 1.1 m. This is after the final injection therefore there are 343 L of kerosene in the test cell.

Appendix D (Note: There is no Appendix D)

Appendix E 142
Surface DC resistivity data.

Figure E.1: Surface DC resistivity along line N2, electrode spacing 20 cm. (Injections #1-4)

Figure E.2: Surface DC resistivity along line N2, electrode spacing 60 cm. (Injections #1-4)

Figure E.3: Surface DC resistivity along line E2, electrode spacing 20 cm. (Injections #1-4)

Figure E.4: Surface DC resistivity along line E2, electrode spacing 60 cm. (Injections #1-4)

Appendix F 148
Neutron probe

Figure F.1: Neutron measurements in vertical access tube with the test cell saturated to the surface. Determination of the vertical distance which is averaged in each measurement.

Figure F.2: Neutron measurements in vertical access tube with the test cell saturated to the surface. Determination of the vertical distance which is averaged in each measurement. Near surface readings only.

Figure F.3: Cross section of the test cell showing contoured Neutron logging measurements and profiles. Background readings only, that is, with the water table at 1.1 m and no kerosene injected.

Figure F.4: Cross section of the test cell showing contoured Neutron logging measurements differenced from background. The water table is at 1.1 m. The readings were made on day 56, after injection #3.

Figure F.5: Cross section of the test cell showing contoured Neutron logging measurements as difference from background. The water table is at 1.1 m. The readings were made on day 64, after injection #4.

Figure F.6: Cross section of the test cell showing contoured Neutron logging measurements as difference from background. The water table is at 1.1 m. The readings were made on day 113, after the lowering and raising of the water table in order to trap kerosene.

Appendix G 154
Dimensions of Radon Access Tube

CFB-LNAPL-1992/93				WATERTABLES			
			(values corrected for elevations)				
DAY	DATE	TIME	D1	D2	MW1	MW2	effluent
			(cm)	(cm)	(cm)	(cm)	(litres)
1	20-Aug		44.30	46.65	45.15	48.25	
5	24-Aug	10:00	47.70	51.25	48.95	53.25	
6	25-Aug	10:00	33.50	36.85	34.75	39.05	
7	26-Aug	7:00	27.90	31.25	29.75	34.25	
8	27-Aug		30.70	34.05	31.55	35.25	
13	1-Sep	am	52.00	54.75	53.15	57.65	
14	2-Sep	am	39.50	42.65	40.95	44.85	
15	3-Sep	9:00	1.70	5.20	4.75	4.20	
15	3-Sep	21:00	5.70	9.60	8.15	7.40	
16	4-Sep		50.10	pumping	52.55	50.40	
18	6-Sep	14:00	111.50	"	112.75	113.00	
18	6-Sep	16:00		"			
18	6-Sep	18:00	115.30	"	116.95	115.80	
19	7-Sep	10:30	116.50	"	117.75	117.00	
19	7-Sep	15:30	111.50	"	113.75	110.00	
20	8-Sep		111.00	"	111.70	110.65	
23	11-Sep		109.10	"	112.55	110.20	
24	12-Sep		110.40	"	109.20	109.65	
26	14-Sep		107.50	"	109.75	109.00	
30	18-Sep		103.50	"	106.75	105.00	
32	20-Sep		109.50	"	112.35	110.00	
33	21-Sep	9:00	108.50	"	117.75	111.00	0.00
34	22-Sep		111.70	"	112.75	112.00	17.00
35	23-Sep		111.70	"	113.75	112.80	10.50
37	25-Sep		111.30	"	113.05	112.00	0.00
38	26-Sep	am	111.50	"	111.95	111.20	2.50
39	27-Sep		110.50	"	112.35	111.80	21.25
41	29-Sep		110.90	"	111.95	113.00	0.00
42	30-Sep		111.90	"	113.15	111.40	0.00
44	2-Oct		108.90	"	110.75	110.20	0.00
45	3-Oct	am	110.50	"	111.75	110.40	0.00
46	4-Oct	pm	104.90	"	106.95	105.60	0.00
47	5-Oct		108.90	"	111.75	111.00	25.00
50	8-Oct		110.50	"	112.75	110.80	31.25
51	9-Oct		108.70	"	110.15	110.40	
52	10-Oct			"			
56	14-Oct		110.90	"	112.25	110.80	0.00
57	15-Oct	8:00	109.50	"	111.75	111.40	0.00
57	15-Oct	11:00		"			0.00
57	15-Oct	12:30		"			9.00
57	15-Oct	13:00		"			2.50
57	15-Oct	13:30		"			
57	15-Oct	18:00		"			16.25

Appendix A.1 Elevation corrected water table levels as measured in monitoring wells.

APPENDIX A

DAY	DATE	TIME	D1	D2	MW1	MW2	effluent
			(cm)	(cm)	(cm)	(cm)	(litres)
58	16-Oct		110.50	"	113.35	110.60	52.25
59	17-Oct		111.10	"	113.55	111.60	2.00
60	18-Oct		111.50	"	112.75	111.60	1.00
61	19-Oct		110.50	"	113.95	112.40	0.00
62	20-Oct		110.50	"	112.55	112.60	0.25
63	21-Oct		111.90	"	113.95	112.80	0.25
64	22-Oct		111.50	"	113.95	112.60	0.00
65	23-Oct	7:00	111.70	"	113.75	112.60	0.00
65	23-Oct	8:30	111.50	"	112.35	112.00	0.00
65	23-Oct	10:15	109.90	"	112.75	112.00	6.75
65	23-Oct	11:00	110.30	"	112.95	112.00	2.25
65	23-Oct	12:00	109.90	"	112.95	112.30	4.50
65	23-Oct	13:30	109.50	"	112.55	111.40	9.00
65	23-Oct	14:30	109.70	"	112.75	111.40	8.50
65	23-Oct	15:15	110.30	"	112.95	112.00	2.00
65	23-Oct	16:00	110.70	"	111.95	111.20	4.50
65	23-Oct	17:00	109.50	"	111.95	112.00	6.50
65	23-Oct	18:15	109.30	"	112.15	112.00	8.75
65	23-Oct	19:20	109.50	"	111.95	111.00	6.50
65	23-Oct	21:00	111.00	"	112.15	111.40	10.75
65	23-Oct	21:45		"			2.00
65	23-Oct	23:15	110.30	"	112.75	111.80	8.00
66	24-Oct	11:10	110.10	"	112.75	111.60	11.25
66	24-Oct	13:00		"			1.25
66	24-Oct	15:30	108.50	"	112.75	111.40	1.00
67	25-Oct	15:30	109.50	"	113.35	111.60	7.75
67	25-Oct	21:00		"			2.00
68	26-Oct	11:45	110.10	"	112.35	111.80	12.50
68	26-Oct	18:30		"			0.00
68	26-Oct	19:45		"			0.00
69	27-Oct	9:20	110.40	"	113.15	112.40	0.00
70	28-Oct	8:19	110.90	"	113.15	112.40	0.10
71	29-Oct	8:45	111.10	"	114.15	112.40	2.51
72	30-Oct	18:00	110.50	"	112.95	112.00	0.00
73	31-Oct	18:30	110.70	"	113.15	112.60	0.00
74	1-Nov	14:30	110.70	"	112.75	111.80	0.00
75	2-Nov	23:00	111.30	"	112.75	111.40	10.84
76	3-Nov	15:50	110.50	"	113.35	112.40	0.64
77	4-Nov	8:45	110.40	"	112.75	111.20	3.05
79	6-Nov	14:00	111.70	"	114.15	112.80	0.62
80	7-Nov	14:00	112.10	"	114.75	114.20	0.00
81	8-Nov	12:00	112.50	"	114.95	114.20	0.00
82	9-Nov	13:15	112.10	"	115.15	114.00	0.00
83	10-Nov	10:00	112.20	"	113.55	112.80	
84	11-Nov	13:30	111.30	"	112.75	112.80	
85	12-Nov	16:30	109.70	"	111.95	111.40	17.00

Appendix A.1 Elevation corrected water table levels as measured in monitoring wells. (continued)

APPENDIX A

DAY	DATE	TIME	D1	D2	MW1	MW2	effluent
			(cm)	(cm)	(cm)	(cm)	(litres)
86	13-Nov	10:00	110.90	"	114.55	114.40	11.23
87	14-Nov	10:00	113.30	"	116.75	113.40	0.00
88	15-Nov	20:45	113.50	"	114.75	114.50	0.00
89	16-Nov	12:00	111.30	"	114.55	113.90	0.00
89	16-Nov	22:00	131.50	"	135.35	133.20	150.00
90	17-Nov	1:00	136.30	"	138.75	137.00	67.50
90	17-Nov	8:10	136.70	"	139.25	139.40	102.50
90	17-Nov	20:00	137.10	"	139.15	138.00	65.00
91	18-Nov	10:00	139.70	"	140.55	141.80	35.00
92	19-Nov	8:30	136.10	"	138.55	138.00	
93	20-Nov	11:30	137.10	"	138.15	137.50	21.25
93	20-Nov	12:45	138.30	"	139.35	138.60	13.75
93	20-Nov	20:30	138.90	"	141.75	139.60	20.00
94	21-Nov	11:15	138.70	"	141.35	140.20	20.00
95	22-Nov	10:15	136.10	"	138.35	137.10	
96	23-Nov	11:30	135.30	"	137.05	135.40	
96	23-Nov	15:00	122.50	"	125.75	127.00	-17.50
96	23-Nov	17:40	115.00	"	117.25	117.40	-50.00
96	23-Nov	21:00	110.70	"	113.35	112.00	-70.00
97	24-Nov	8:30	115.10	"	116.75	118.60	0.00
97	24-Nov	15:15	109.90	"	111.75	112.00	-50.00
98	25-Nov	10:30	113.70	"	116.35	115.00	
98	25-Nov	12:30	109.90	"	111.15	110.00	-18.75
98	25-Nov	17:00	111.50	"	113.95	114.00	
98	25-Nov	18:00	109.50	"	111.95	111.00	-6.25
99	26-Nov	9:15	111.30	pump off	113.35	112.60	
104	1-Dec	12:55	114.50		116.75	116.00	
110	7-Dec	15:00	112.10		115.75	114.00	
113	10-Dec	15:30	113.50		116.75	114.00	
160	26-Jan		110.40				
195	2-Mar		138.00				
202	9-Mar		140.40			143.80	
204	11-Mar	11:17	139.90		139.75	142.00	
209	16-Mar		140.40				
216	23-Mar		141.80				
231	7-Apr		99.50				
314	29-Jun	14:00	60.50	62.00	61.75	62.00	

Appendix A.1 Elevation corrected water table levels as measured in monitoring wells. (continued)

CFB-LNAPL-1992/93 WATER LEVEL CORRECTIONS

A: the surveyed top of the PVC tubing

B: the calculated top of PVC tubing using elevation correction

DATUM = 0.7025 m *(which is the centre of the test cell)*

(ie: mid way between the third and fourth glass wells)

-- by convention, let survey measurements below the surface be negative)

-- therefore, CORRECTED ELEVATION = DATUM - (survey measurement)

C: the height of the PVC above the sand surface

-- note: this is the level to which all water levels are referenced to

D: elevation correted sand surface measurement wrt. the datum ie: D = B - C

E: conversion of "D" from (m) to (cm)

	A	B	C	D	E
	surveyed top (m)	actual top (m)	stick up (m)	sand surface (m)	sand surface (cm)
D1	0.5125	0.1900	0.1750	0.0150	1.50
D2	0.5350	0.1675	0.1775	-0.0100	-1.00
MW1	0.4325	0.2700	0.2675	0.0025	0.25
MW2	0.4550	0.2475	0.2875	-0.0400	-4.00

therefore, in order to correct the water level measurements

the following equations must be used

elevation corrected water level = water level reading - E

(since if the sand surface is above the datum, the depth to water will be increased)

D1: reading - 1.50 cm = elevation corrected water level

D2: reading + 1.00 cm = elevation corrected water level

MW1: reading - 0.25 cm = elevation corrected water level

MW2: reading + 4.00 cm = elevation corrected water level

Appendix A.1 Elevation corrected water table levels as measured in monitoring wells. (continued) (Actual water level correction calculations)

CFB-LNAPL-1992			TEMPERATURE							
	temperature is inversely proportional to resistivity									
	MW1, MW2, and D1 are monitoring wells (the measurements were made at the bottom of the wells)									
	GW1 is a glass well (the measurements were made at the bottom of the well)									
	E2-res10 and E2-res6 are resistivity electrode holes (the measurements were made near surface)									
		note:	DAY120 measurement E2-res10 is actually E2-res12							
			NA refers to measurements which were not available							
DAY	DATE	RESISTANCE (k-ohms)						AVERAGES		
			bottoms of wells			surface				
		MW1	MW2	D1	GW1	E2-res10	E2-res6	at depth	surface	
30	9/18/92	13.63	13.59	13.62		11.80	11.88	13.61	11.84	
38	9/26/92	13.89	13.82	13.69		14.80	14.78	13.80	14.79	
49	10/7/92	14.86	14.84		14.49	17.20	16.89	14.73	17.05	
57	10/15/92	14.91	15.05		14.79	19.15	19.18	14.92	19.17	
64	10/22/92	16.14	16.13		16.53	24.15	24.18	16.27	24.17	
86	11/13/92	18.99	19.11	18.61		23.29	23.40	18.90	23.35	
104	12/1/92	20.71	21.05	20.59		24.74	24.61	20.78	24.68	
120	12/17/92	22.12	22.49	22.16		28.15	27.59	22.26	27.87	
160	1/26/93		25.30	24.80		NA	NA	25.05		
195	3/2/93		26.50	26.40		NA	NA	26.45		
204	3/11/93	26.50	26.80	26.60		NA	NA	26.63		

Appendix A.2 Temperature data.
Thermistor measurements.

CFB-LNAPL-1992 **TEMPERATURE: conversions**

EQUIPMENT

THERMISTOR: YSI-4406

thermistor element part number 44006

accuracy ± 0.2 °C

TEMPERATURE CONVERSION *where R = resistance measurement from thermistor*

temperature (°C) = d0 + d1 * ln(R) + d2 * [ln(R)]^2 + d3 * [ln(R)]^3

d0 = 523.0119396

d1 = -97.4282453

d2 = 6.2323996

d3 = -0.1655577

DAY	RESISTANCE (averages)		DAY	RESISTANCE (averages)		DAY	TEMPERATURE		DAY	TEMPERATURE	
	at depth (K-ohms)	surface (K-ohms)		at depth (ohms)	surface (ohms)		at depth (°C)	surface (°C)		at depth (°C)	surface (°C)
30	13.61	11.84	30	13613	11840	30	17.52491	20.87364	30	17.52	20.87
38	13.80	14.79	38	13800	14790	38	17.20133	15.56371	38	17.20	15.56
49	14.73	17.05	49	14730	17045	49	15.65940	12.25302	49	15.66	12.25
57	14.92	19.17	57	14917	19165	57	15.36311	9.560484	57	15.36	9.56
64	16.14	24.17	64	16135	24165	64	13.52625	4.342478	64	13.53	4.34
86	18.90	23.35	86	18903	23345	86	9.874307	5.110933	86	9.87	5.11
104	20.78	24.68	104	20783	24675	104	7.720104	3.878994	104	7.72	3.88
120	22.26	27.87	120	22257	27870	120	6.178499	1.197619	120	6.18	1.20
160	25.05		160	25050		160	3.544925		160	3.54	
195	26.45		195	26450		195	2.344962		195	2.34	
204	26.63		204	26633		204	2.193049		204	2.19	
									average	10.10	9.10
						average for main experiment (Day 1-104)				13.84	8.95

Appendix A.2 Temperature data. (continued)
Thermistor measurements conversions to temperature.

APPENDIX A

GRAIN DENSITY DETERMINATION

DATE Sept 9/92

LNAPL Spill Site -- Borden Sand -- Sue DeRyck

	TRY 1	TRY 2	TRY 3	TRY 4	TRY 5	AVG	UNITS	COR VAL	DIF VAL	
STANDARDIZE ON EMPTY CUP	999.30	999.25	999.25			999.27	(g/cc)	0	0.7333	
READING ON SMALL BALL	7.80	7.76	7.77			7.78		8.58	0.8033	0.0082
READING ON LARGE BALL	28.16	28.18	28.21			28.18		28.96	0.7767	0.0015

~~~~~~~~~~~~~~

AVG= 0.0048

SPECIMEN	WT CUP (g)	CUP + SPECIMEN	WT SPEC (g)	MEASURED VOLUME (CC) V1	V2	V3	MEAN VOL V	CORR'T VOLUME	DENSITY
SD 1	102.367	148.846	46.479	16.32	16.34	16.33	16.33	17.15	2.71
SD 2	102.367	149.045	46.678	16.42	16.43	16.44	16.43	17.25	2.71
SD 3	102.367	148.483	46.116	16.32	16.33	16.33	16.33	17.14	2.69
SD 4	102.367	149.110	46.743	16.68	16.67	16.67	16.67	17.49	2.67

CALCULATION OF SAMPLE POROSITIES
FROM LNAPL SPILL SITE AT BORDEN
SEPT 9/92

BULK VOLUME = PI*RADIUS*RADIUS*LENGTH

RADIUS = 1.75 cm

LENGTH = 3.0 cm

SPECIMEN	BULK VOLUME (ml)	DRY WEIGHT (g)	GRAIN DENSITY (g/cc)	PORE VOLUME (ml)	POROSITY (pore/bulk volume)
SD 1	28.86	46.479	2.71	11.71	0.41
SD 2	28.86	46.678	2.71	11.64	0.40
SD 3	28.86	46.116	2.69	11.72	0.41
SD 4	28.86	47.044	2.67	11.24	0.39

Appendix A.3 Soil porosity measurements.
~~~~~~~~~~~~~~

PLAN VIEW

SOIL DENITIY MEASUREMENTS

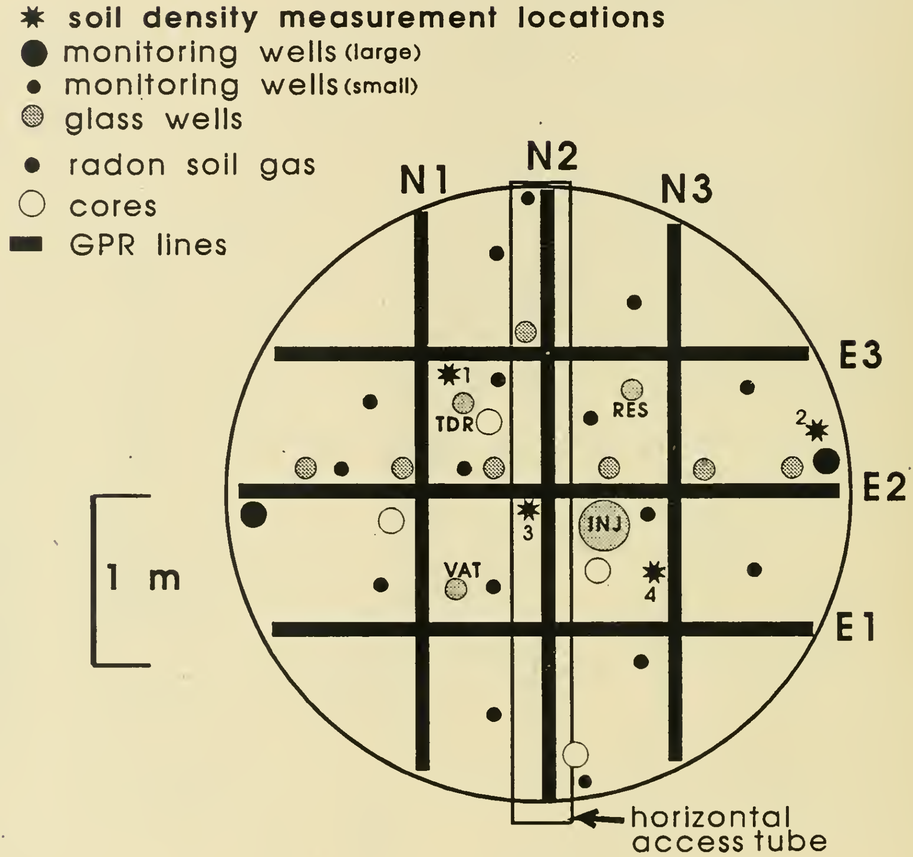

TDR : dielectric permittivity probe (time domain reflectometry)
RES : resistivity probe
VAT : vertical access tube
INJ : injection point

Figure A.3.1 Location within the test cell where samples for soil porosity analysis were taken.

Appendix A.4: KEROSENE SATURATION MEASUREMENTS OF CORE

This section describes the procedure used to collect and to determine the kerosene saturation in soil cores taken from within the LNAPL test cell. Four soil cores were collected at the locations shown in Figure 4.3.1, after the final kerosene injection had reached equilibrium.

A.4.1 Core Collection Procedure

Each of the four cores was taken in three sections. The first section sampled the unsaturated zone (0.0 -50 cm), the second sampled the tension saturated zone (50 - 90 cm), and the third section sampled the bottom of the tension saturated zone, and the top of the water table (90 - 140 cm).

The core sections were collected by driving 5 cm diameter aluminum core tube into the sand to the desired depth. The core tube was then pulled out, checked to ensure full recovery of sand and then immediately capped, taped, and labelled. To collect the next section the core tube was put back into the hole from which the core had been previously retreived (the hole remained open within the unsaturated zone). For the last section, which extended below the water table, a core catcher was attached to the end of the core tube before driving into the sand.

Using this procedure, four cores were collected at the locations shown in Figure 4.4.1. Core #1 was the test core which was used to determine the optimum core length and procedure to obtain the best recovery. This core was therefore not as successful as the other three cores. The final section of core #4 was longer (60cm) than for the other cores to ensure that the zone below the kerosene pool was sampled.

A.4.2 Measurement of Kerosene Saturation

The four cores, each consisting of three sections, were transported from the LNAPL site at CFB Borden in an upright position to prevent redistribution of the kerosene in the soil. In the lab, these cores were further subdivided into 5cm segments. The segments which had a kerosene aroma were subsampled twice using a 2cc core sampler (to give a 4 cc sample), immersed into 120ml of iso-octane, and shaken vigorously.

When the soil sample is added to the iso-octane, since water and iso-octane are immisible they form separate liquid phases. Since the kerosene in the sample is immisicible with water but misicible with iso-octane, it is extracted into the iso-octane phase. The kerosene content in the iso-octane was determined by measuring the absorbance of an subsample of the iso-octane (containing the dissolved kerosene) at 270 nm using an ultraviolet-visible spectrophotometer. The measusements were performed in the ultraviolet at 270nm, since this is the wavelength of maximum absorbance for kerosene.

The spectrophotometer was calibrated by using a range of kerosene concentrations in iso-octane. The kerosene used in these calibrations was dyed with Kodak fluorescent dye Courmarin No. 7 at a concentration of 12mg/litre (as was used for the injection in the LNAPL cell). To perform the calibration, five standards of the following concentrations of kerosene in iso-octane were used:

(a) Std. 0.0005 created from 50ul kerosene in 100ml iso-octane.
(b) Std. 0.0010 created from 100ul kerosene in 100ml iso-octane.
(c) Std. 0.0010 created from 150ul kerosene in 100ml iso-octane.
(d) Std. 0.0020 created from 200ul kerosene in 100ml iso-octane.
(e) Std. 0.0025 created from 250ul kerosene in 100ml iso-octane.

The absorbance of each kerosene standard was measured at 270nm and plotted versus concentration of kerosene in iso-octane (Figure A.4.1). The data were fitted with a second order polynomial of the form: $y = ax^2 + bx + c$ with $a = 0.000389$, $b = 0.000681$, $c = 0.000045$. Using this relationship the kerosene saturation was determined for each soil sample taken from the cores (Figures 4.5.9.1).

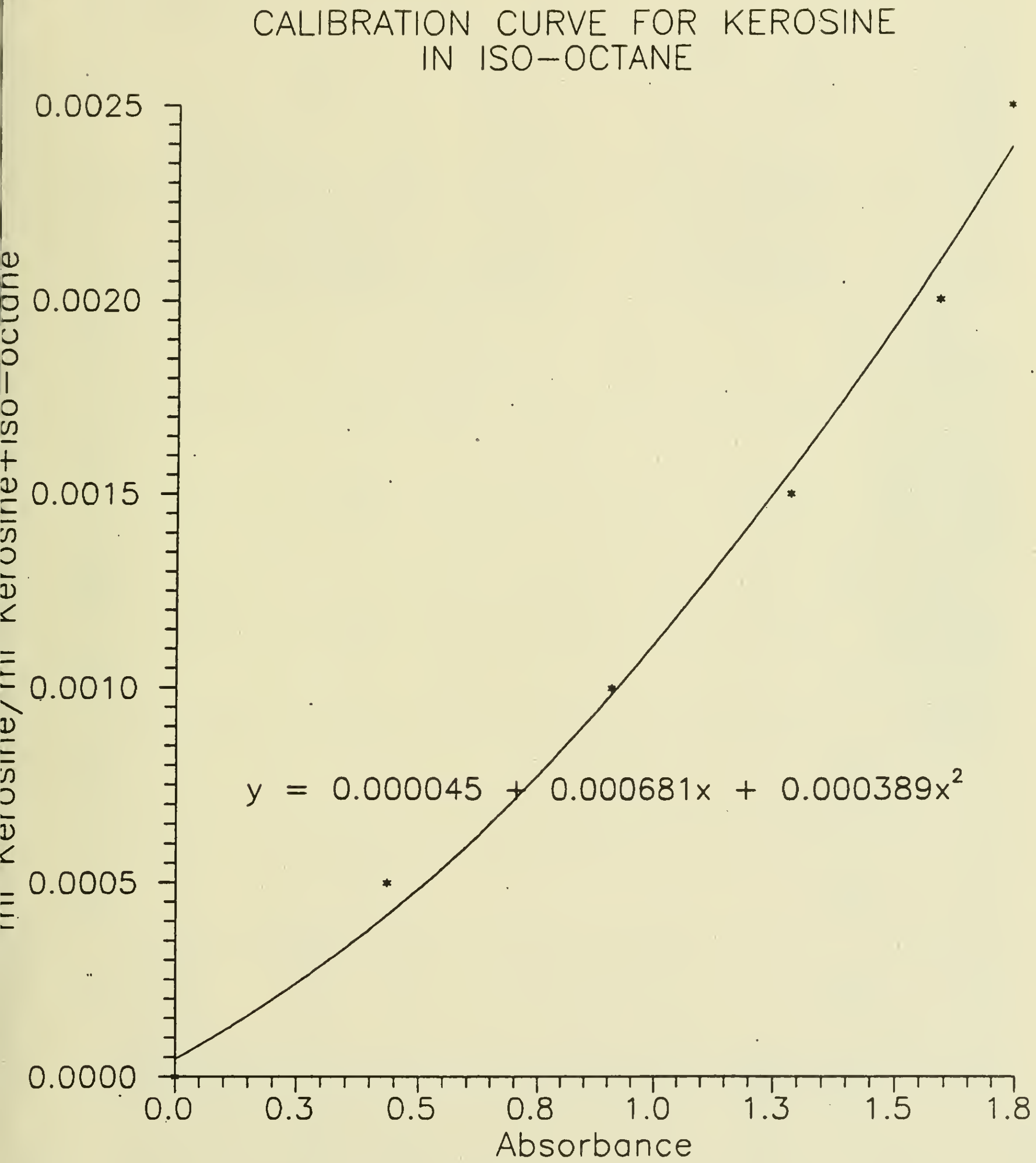

Figure A.4.1 Coring procedure, analyses, and results. (continued)
Calibration for kerosene in iso-octane.

LNAPL					CFB BORDEN (UNSATURATED ZONE)					Susan DeRyck	
				UNIVERSITY OF WATERLOO: (EARTH SCIENCES)							
				WATERLOO CENTRE for GROUNDWATER RESEARCH							
					CONTROLLED LNAPL SPILL 1992						
DAY	DATE	TDR	GPR	CPN	RES	RADON	TV	TEMP			
	mm/dd/yy	file: LNPL__	disk								
									Water Table measured daily		
0	08/19/92								finish packing tank		
1	08/20/92	0071-0134				*******			--soil density measurement		
2	08/21/92										
3	08/22/92										
4	08/23/92										
5	08/24/92	0135-0198		*******							
6	08/25/92			*******							
7	08/26/92										
8	08/27/92	0199-0262	1						water table approx. saturated		
9	08/28/92										
10	08/29/92										
11	08/30/92										
12	08/31/92										
13	09/01/92		1, 2						adding water		
14	09/02/92		2						SATURATED		
15	09/03/92	0301-0364							after TDR, lower watertable		
16	09/04/92								lower water table		
17	09/05/92								lower water table		
18	09/06/92								lower water table		
19	09/07/92								WATER TABLE @ 1.1 m		
20	09/08/92	0365-0428		*******							
21	09/09/92										

Appendix A.5 Schedule of monitoring.

DAY	DATE	TDR	GPR	CPN	RES	RADON	TV	TEMP			
	mm/dd/yy	file: LNPL__	disk								
22	09/10/92										
23	09/11/92	0429-0492	2, 3								
24	09/12/92					•••••••					
25	09/13/92			•••••••							
26	09/14/92										
27	09/15/92	0493-0556	3								
28	09/16/92		3		•••••••	•••••••					
29	09/17/92										
30	09/18/92	0557-0620	set up					•••••••	put in injection point		
31	09/19/92										
32	09/20/92		J		•••••••			•••••••			
33	09/21/92	0621-0684		•••••••		•••••••			(day 33 readings finished B4 06:30)		
33	09/21/92								INJ. #1	2.2 L	@06:30
34	09/22/92			•••••••							
35	09/23/92	0685-0748			•••••••	•••••••					
36	09/24/92										
37	09/25/92		4	•••••••							
38	09/26/92	0749-0805			•••••••	•••••••	•••••••		(day 38 readings finished B4 17:30)		
38	09/26/92								INJ. #2	10 L	@17:30
39	09/27/92						•••••••				
40	09/28/92										
41	09/29/92			•••••••	•••••••						
42	09/30/92	0813-0875				•••••••					
43	10/01/92										
44	10/02/92	0877-0940	5	•••••••	•••••••		•••••••				
45	10/03/92		4, 5, 10			•••••••			(day 45 readings finished B4 14:30)		
45	10/03/92								INJ. #3	88 L@14:30-20:30	
45	10/03/92	0941-1004	5				•••••••		(day 45 readings starting after 20:30)		

Appendix A.5 Schedule of monitoring. (continued)

DAY	DATE	TDR	GPR	CPN	RES	RADON	TV	TEMP			
	mm/dd/yy	file: LNPL__	disk								
46	10/04/92	1005-1068	12	*******	*******		*******		@15:00 pump wasn't working		
47	10/05/92				*******						
48	10/06/92	1069-1132			*******						
49	10/07/92		12		*******	*******	*******				
50	10/08/92		12	*******	*******						
51	10/09/92				*******						
52	10/10/92	1133-1196	11		*******	*******					
53	10/11/92	1197-1260			*******						
54	10/12/92	1261-1324			*******						
55	10/13/92										
56	10/14/92	1325-1388	11	*******	*******	*******	*******				
57	10/15/92	1389-1452							(day 57 readings finished B4 08:30)		
57	10/15/92		10, during						INJ. #4	100L@08:40-19:00	
57	10/15/92	1453-1466					*******	*******			
58	10/16/92	???????	10		*******				-GPR malfunctioning		
59	10/17/92	1517-1581			*******				-GPR malfunctioning		
60	10/18/92				*******	*******	*******				
61	10/19/92			*******							
62	10/20/92	1582-1645									
63	10/21/92	1646-1709	9	*******	*******						
64	10/22/92	1710-1773		*******	*******						
65	10/23/92								INJ. #5	150L@07:00-21:00	
65	10/23/92	1774-1837	7		*******				(day 65 readings during inj.#5)		
65	10/23/92	1838-1901	6, 7		*******				(day 65 readings during inj.#5)		
65	10/23/92	1902-1965	7		*******				(day 65 readings during inj.#5)		
65	10/23/92	1966-2029	6, 7		*******				(day 65 readings starting after 21:00)		
66	10/24/92	2030-2093	9, 10								
67	10/25/92	2094-2157	too cold						(too cold for GPR)		

Appendix A.5 Schedule of monitoring. (continued)

APPENDIX A

DAY	DATE	TDR	GPR	CPN	RES	RADON	TV	TEMP			
	mm/dd/yy	file: LNPL__	disk								
68	10/26/92	2158-2221	8	•••••••		•••••••					
69	10/27/92	2222-2285	•••••••		•••••••		•••••••				
70	10/28/92	2286-2349	•••••••	•••••••							
71	10/29/92	2350-2413	•••••••		•••••••		•••••••				
72	10/30/92				•••••••		•••••••				
73	10/31/92				•••••••						
74	11/01/92	2414-2477		•••••••	•••••••						
75	11/02/92				•••••••				GPR not working		
76	11/03/92										
77	11/04/92	2478-2541			•••••••						
77	11/04/92								CORING		
78	11/05/92				•••••••						
79	11/06/92				•••••••						
80	11/07/92				•••••••						
81	11/08/92				•••••••						
82	11/09/92	2542-2605			•••••••						
83	11/10/92				•••••••						
84	11/11/92				•••••••						
85	11/12/92				•••••••						
86	11/13/92	push-in			•••••••				TDR push-in probes (0001...0085)		
87	11/14/92				•••••••						
88	11/15/92				•••••••						
89	11/16/92	2606-2669			•••••••				(day 89 readings finished B4 pumping)		
89	11/16/92								LOWER WATER TABLE		
90	11/17/92				•••••••				lowering water table		
91	11/18/92				•••••••				lowering water table		
92	11/19/92				•••••••				lowering water table		

Appendix A.5 Schedule of monitoring. (continued)

DAY	DATE	TDR	GPR	CPN	RES	RADON	TV	TEMP			
	mm/dd/yy	file: LNPL__	disk								
92	11/19/92								pump froze, stop pumping		
93	11/20/92				•••••••						
93	11/20/92								resume pumping		
94	11/21/92				•••••••				lowering water table		
94	11/21/92								stop pumping		
95	11/22/92				•••••••						
96	11/23/92	2670-2733			•••••••				(day 96 readings finished B4 raising)		
96	11/23/92								RAISING WATER TABLE		
97	11/24/92	2734-2797			•••••••				raising water table		
98	11/25/92				•••••••				raising water table		
98	11/25/92								stop pumping		
99	11/26/92				•••••••						
100	11/27/92										
101	11/28/92										
102	11/29/92										
103	11/30/92										
104	12/01/92	2798-2861							on/off pumping		
105	12/02/92										
106	12/03/92										
107	12/04/92										
108	12/05/92										
109	12/06/92										
110	12/07/92										
111	12/08/92										
112	12/09/92										
113	12/10/92	2872-2935		•••••••	•••••••						

Appendix A.5 Schedule of monitoring. (continued)

DAY	DATE	TDR	GPR	CPN	RES	RADON	TV	TEMP			
	mm/dd/yy	file: LNPL__	disk								
114	12/11/92										
115	12/12/92										
116	12/13/92										
117	12/14/92										
118	12/15/92										
119	12/16/92	2936-2999	*******	*******	*******				new GPR system		
120	12/17/92		*******						new GPR system		
121	12/18/92										
122	12/19/92										
123	12/20/92										
124	12/21/92										
125	12/22/92										
126	12/23/92										
!!!!!!!!!!!!!	!!!!!!!!!!!!!	!!!!!!!!!!!!!	!!!!!!!!!!!!!	!!!!!!!!!!!!!	!!!!!!!!!!!!!	!!!!!!!!!!!!!	!!!!!!!!!!!!!	!!!!!!!!!!!!!	!!!!!!!!!!!!!	!!!!!!!!!!!!!	!!!!!!!!!!!!!
	End of formal experiment, until spring 1993 (occasional water levels taken)										
!!!!!!!!!!!!!	!!!!!!!!!!!!!	!!!!!!!!!!!!!	!!!!!!!!!!!!!	!!!!!!!!!!!!!	!!!!!!!!!!!!!	!!!!!!!!!!!!!	!!!!!!!!!!!!!	!!!!!!!!!!!!!	!!!!!!!!!!!!!	!!!!!!!!!!!!!	!!!!!!!!!!!!!
DAY	DATE	TDR	GPR	CPN	RES	RADON	TV	TEMP			
160	01/26/93								water table okay		
195	3/2/93								water table dropping		
202	3/9/93								water table dropping		
204	3/11/93	3000-3063		*******					water table dropping		
209	3/16/93								water table dropping		

Appendix A.5 Schedule of monitoring. (continued)

DAY	DATE	TDR	GPR	CPN	RES	RADON	TV	TEMP			
	mm/dd/yy	file: LNPL__	disk								
216	3/23/93								water table dropping		
231	4/7/93								water table back to normal		
314	6/29/93	3064-3127	P	*******					water table high (ie: 0.60m)		

Appendix A.5 Schedule of monitoring. (continued)

CFB-LNAPL-1992 **X-Y GRID SURVEY**

NAMING CONVENTIONS

RES = borehole resistivity probe
TDR = dielectic permittivity probe (time domain reflectometry)
VAT = vertical access tube
INJ = injection point
GW# = glass wells
D# = large diameter monitoring well attached to well screen
MW# = small diameter monitoring well
RG# = radon soil gas access tubes

The centre of the X-Y grid is considered to be the intersection of the two perpendicular Ground Penetreting Radar (GPR) lines N2 & E2.

– N2 represents the X-axis with negative values towards the west.

– E2 represents the Y-axis with negative values towards the south.

	X (cm)	Y (cm)		X (cm)	Y (cm)
RES	-51.5	50.0			
TDR (A)	-60.0	-33.0	**TDR (B)**	-45	-47.5
VAT	48.0	-42.0			
INJ	23.0	21.0			
GW1	-15.5	-139.0			
GW2	-21.5	-82.0			
GW3	-21.0	-20.5			
GW4	-21.5	33.5			
GW5	-21.5	93.0			
GW6	-21.5	155.0			
GW7	-98.0	-10.0			
D1	7.0	-159.0			
D2	-28.0	167.5			
MW1	-182.5	-14.0			
MW2	150.5	22.5			
RG1	-19.5	-108.0			
RG2	-65.0	-84.0			
RG3	31.0	-86.0			
RG4	-121.5	-25.0			
RG5	-64.0	-21.0			
RG6	-19.5	-30.5			
RG7	51.0	-21.5			
RG8	106.5	-28.5			
RG9	-101.0	43.0			
RG10	-45.5	36.0			
RG11	16.0	49.5			
RG12	83.5	45.0			
RG13	-66.0	108.5			
RG14	22.0	104.5			

	GPR GRID	
intersection	X (cm)	Y (cm)
[N1/E1]	-90	-65
[N1/E2]	0	-65
[N1/E3]	66	-65
[N2/E1]	-90	0
[N2/E2]	0	0
[N2/E3]	66	0
[N3/E1]	-90	66
[N3/E2]	0	65
[N3/E3]	66	65

Appendix A.6 X-Y grid surface survey, location of probes and wells.

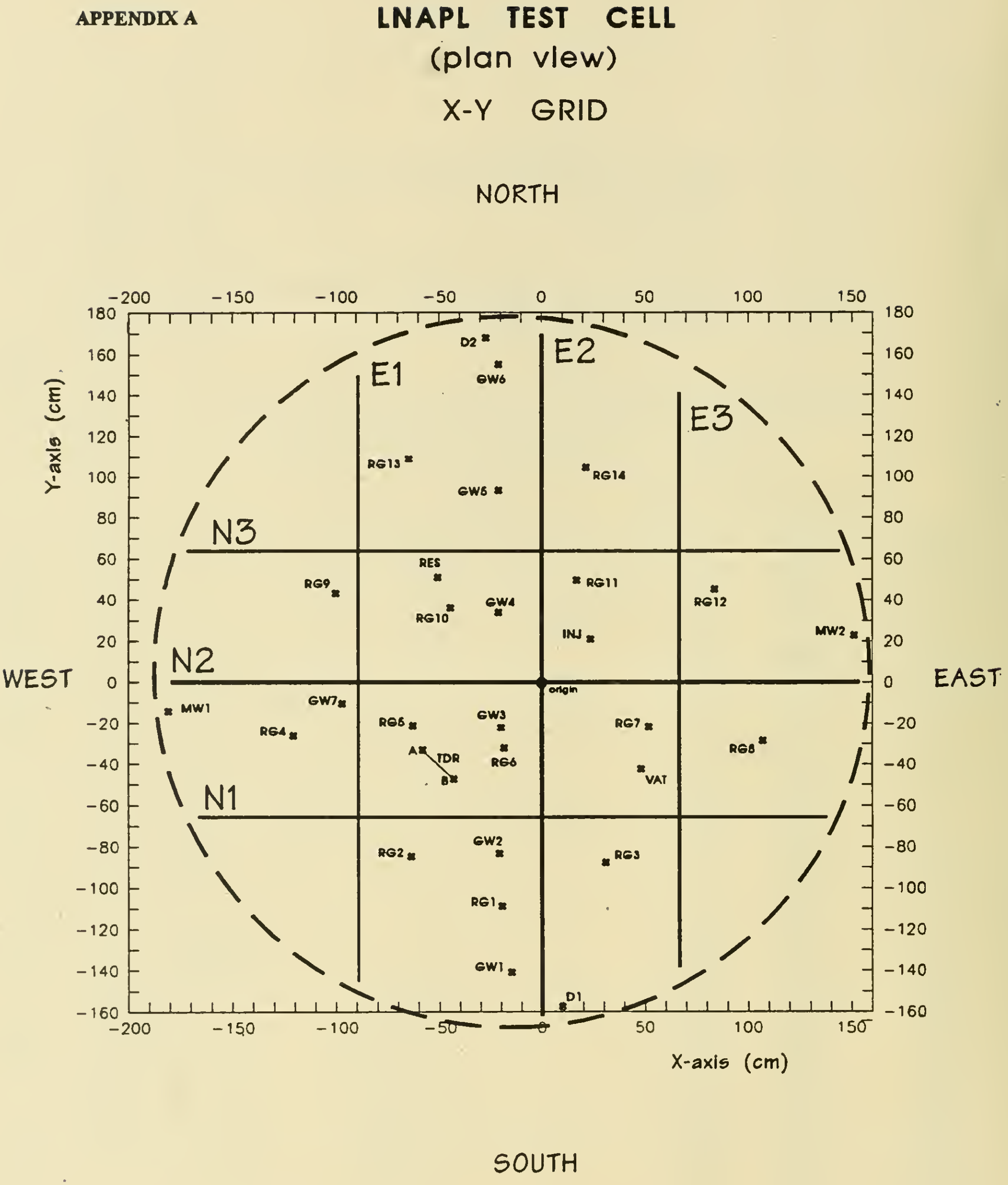

Figure A.6.1 X-Y grid surface survey, location of probes and wells. (continued) Plan view of test cell.

CFB-LNAPL-1992 **ELEVATION SURVEY**

NAMING CONVENTIONS

BM = bench mark
DATUM = top of sand surface in centre of test cell
HAT(W) = top of horizontal access tube (at the sealed end of the tube on the west side of the tank)
HAT(E) = top of horizontal access tube (at the open end of the tube on the east side of the tank)
RES = top of borehole resistivity probe
TDR = top of dielectic permittivity probe (time domain reflectometry)
VAT = top of vertical access tube
D# = top of large diameter monitoring well attached to well screen
MW# = top of small diameter monitoring well
GW# = top of glass wells

T (?) = reference to top of tank edge in the vicinity of (?)
S (?) = reference to sand surface in the vicinity of (?)

The bench mark (BM) is located along the rail in the railway track which is closest to the LNAPL test site.
The stadia rod was placed on the third join in the rail when travelling towards the LNAPL site from the road.
(The referenced road is the one which passes by the front entrance gate of the site.)

CONVERSIONS

column
A : SURVEY: actual survey measurement (m)
B : ELEV.: calculated elevation with respect to the datum (m)

- let the datum be zero elevation
- let elevations below the datum (ie: below the sand surface) be negative by convention
- let elevations above the datum (ie: above the sand surface) be positive by convention

ELEVATION = DATUM - SURVEY READINGS
= 0.7025 - survey readings (m)

Appendix A.7 Elevation survey in test cell.

CFB-LNAPL-1992	ELEVATION SURVEY DATA		
	A SURVEY (m)	B ELEV. (m)	ELEV. (cm)
BM	2.9550	-2.2525	-225.25
HAT(W)	2.4672	-1.7647	-176.47
HAT(E)	2.6150	-1.9125	-191.25
RES	0.6200	0.0825	8.25
TDR	0.4025	0.3000	30.00
VAT	0.6125	0.0900	9.00
D1	0.5125	0.1900	19.00
D2	0.5350	0.1675	16.75
MW1	0.4325	0.2700	27.00
MW2	0.4550	0.2475	24.75
GW1	0.5600	0.1425	14.25
GW2	0.5550	0.1475	14.75
GW3	0.5625	0.1400	14.00
GW4	0.5475	0.1550	15.50
GW5	0.5575	0.1450	14.50
GW6	0.5475	0.1550	15.50
GW7	0.5525	0.1500	15.00
T (N1)	0.5700	0.1325	13.25
T (N2)	0.6000	0.1025	10.25
T (E1)	0.5700	0.1325	13.25
T (E2)	0.5900	0.1125	11.25
S (N1)	0.6875	0.0150	1.50
S (N2)	0.7200	-0.0175	-1.75
S (E1)	0.7000	0.0025	0.25
S (E2)	0.7425	-0.0400	-4.00
S (RES)	0.7000	0.0025	0.25
S (TDR)	0.6850	0.0175	1.75
S (VAT)	0.7075	-0.0050	-0.50
DATUM	0.7025	0.0000	0.00

Appendix A.7 Elevation survey in test cell. (continued)

CFB-LNAPL-1992			ELEVATION SURVEY STATISTICS					
				CPN				
		ELEV.		stick-up				
		(cm)		(cm)				
	GW1	14.25		13				
	GW2	14.75		12				
	GW3	14.00		13				
	GW4	15.50		14				
	GW5	14.50		15				
	GW6	15.50		17				
	GW7	15.00		13				
	average	14.79		13.86				
	std. dev	0.585		1.676				
	T (N1)	13.25						
	T (N2)	10.25						
	T (E1)	13.25						
	T (E2)	11.25						
	average	12.00						
	std. dev	1.5						
	S (N1)	1.50						
	S (N2)	-1.75						
	S (E1)	0.25						
	S (E2)	-4.00						
	S (RES)	0.25						
	S (TDR)	1.75						
	S (VAT)	-0.50						
	DATUM	0.00						
	average	-0.31						
	std. dev	1.850						

Appendix A.7 Elevation survey in test cell. (continued)

PLAN VIEW of TEST CELL
ELEVATIONS

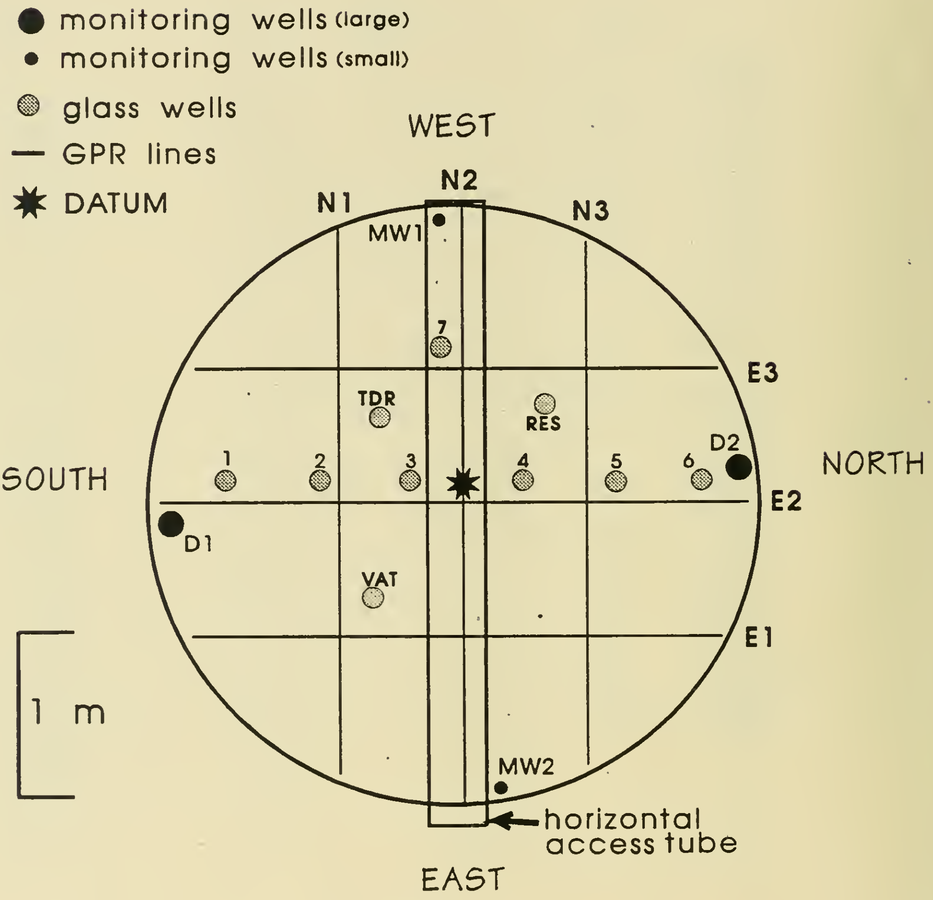

TDR : dielectric permittivity probe (time domain reflectometry)
RES : resistivity probe
VAT : vertical access tube
INJ : injection point

Figure A.7.1 Elevation survey in test cell. Plan view of test cell. (continued)

CFB-LNAPL-92 EM38

DATA SUMMARY SHEET

The data summary divides data into day, dipole mode and direction.

On a particular day for a particular dipole mode, all data on lines in the same direction are combined,

except for stations 1 & 7 which were close to the edges of the tank.

DAY 14 vertical north (mS/m)	DAY 14 vertical east (mS/m)	DAY 14 horizontal north (mS/m)	DAY 14 horizontal east (mS/m)	DAY 29 vertical north (mS/m)	DAY 29 vertical east (mS/m)	DAY 29 horizontal north (mS/m)	DAY 29 horizontal east (mS/m)	DAY 76 vertical north (mS/m)	DAY 76 vertical east (mS/m)	DAY 76 horizontal north (mS/m)	DAY 76 horizontal east (mS/m)
5.2	5.8	7.4	6.8	4.4	3.7	2.3	1.0	1.9	2.9	2.7	2.7
6.0	6.2	8.0	6.7	3.9	3.5	2.1	0.9	2.3	2.9	2.6	2.5
6.2	6.8	8.5	7.1	4.8	4.3	2.5	1.2	2.2	2.6	2.6	2.6
5.7	6.8	8.2	8.1	3.8	3.6	2.6	1.3	2.2	2.5	3.1	2.9
4.8	6.7	8.5	8.3	4.2	3.9	3.0	2.5	2.4	2.6	3.5	3.1
6.3	6.1	8.0	7.3	4.5	5.0	2.3	1.7	2.0	2.9	2.7	3.2
7.0	6.8	8.2	7.7	4.3	4.5	1.9	1.3	2.5	3.4	2.8	3.1
7.0	6.7	8.4	7.9	4.8	4.0	2.3	1.3	3.0	3.4	3.5	3.0
7.1	6.4	8.2	7.7	4.8	3.7	2.1	1.5	2.7	2.8	3.5	3.0
7.0	6.3	8.8	7.9	4.2	4.5	2.6	2.6	2.6	3.3	3.6	2.9
6.8	5.4	8.8	8.0	4.3	4.5	2.5	2.1	2.4	3.0	2.7	3.5
6.3	5.8	9.0	8.4	3.8	4.2	1.9	2.2	2.4	3.2	3.0	3.4
6.7	5.8	8.7	8.1	3.8	3.5	1.9	1.5	2.8	3.0	3.6	3.3
6.3	5.8	9.0	8.2	4.2	3.3	2.8	0.9	2.5	3.2	3.7	3.3
5.8	5.8	8.8	8.2	3.8	3.8	2.1	2.0	2.7	3.5	4.0	3.6
averages											
5.5	5.8	8.1	7.5	4.1	3.8	2.2	1.5	2.3	3.2	3.4	3.2
	5.65		7.80		3.93		1.85		2.75		3.25

Appendix B EM38 data summary sheet and averages.

CFB-LNAPL-92		EM38						
	100 ms/m							
DAY 14								
9/2/92					9/2/92			
vertical dipole mode					*vertical dipole mode*			
LINE	N1	N2	N3		E1	E2	E3	
STATION	(mS/m)	(mS/m)	(mS/m)		(mS/m)	(mS/m)	(mS/m)	
1	4.5	4.8	6.0		8.8	4.8	5.0	
2	5.2	6.3	6.8	@ E1	5.8	6.1	5.4	@ N1
3	6.0	7.0	6.3		6.2	6.8	5.8	
4	6.2	7.0	6.7	@ E2	6.8	6.7	5.8	@ N2
5	5.7	7.1	6.3		6.8	6.4	5.8	
6	4.8	7.0	5.8	@ E3	6.7	6.3	5.8	@ N3
7	4.8	4.8	5.1	against edge	6.0	4.6	4.9	against edge
DAY 14								
9/2/92					9/2/92			
horizontal dipole mode					*horizontal dipole mode*			
LINE	N1	N2	N3		E1	E2	E3	
STATION	(mS/m)	(mS/m)	(mS/m)		(mS/m)	(mS/m)	(mS/m)	
1	7.2	7.5	10.5		8.8	6.8	7.1	
2	7.4	8.0	8.8	@ E1	6.8	7.3	8.0	@ N1
3	8.0	8.2	9.0		6.7	7.7	8.4	
4	8.5	8.4	8.7	@ E2	7.1	7.9	8.1	@ N2
5	8.2	8.2	9.0		8.1	7.7	8.2	
6	8.5	8.8	8.8	@ E3	8.3	7.9	8.2	@ N3
7	8.7	9.0	8.7	against edge	8.0	7.0	7.7	against edge

DAY 29								
9/17/92					9/17/92			
vertical dipole mode					*vertical dipole mode*			
LINE	N1	N2	N3		E1	E2	E3	
STATION	(mS/m)	(mS/m)	(mS/m)		(mS/m)	(mS/m)	(mS/m)	
1	4.5	4.5	4.0		8.5	4.0	4.7	
2	4.4	4.5	4.3	@ E1	3.7	5.0	4.5	@ N1
3	3.9	4.3	3.8		3.5	4.5	4.2	
4	4.8	4.8	3.8	@ E2	4.3	4.0	3.5	@ N2
5	3.8	4.8	4.2		3.6	3.7	3.3	
6	4.2	4.2	3.8	@ E3	3.9	4.5	3.8	@ N3
7	4.2	3.2	2.4	against edge	4.4	6.0	3.5	against edge

Figure B EM38 data summary sheet and averages. (continued)

DAY 29					DAY 29			
9/17/92					9/17/92			
horizontal dipole mode					*horizontal dipole mode*			
LINE	N1	N2	N3		E1	E2	E3	
STATION	(mS/m)	(mS/m)	(mS/m)		(mS/m)	(mS/m)	(mS/m)	
1	2.2	2.1	4.2		4.5	1.3	1.0	
2	2.3	2.3	2.5	@ E1	1.0	1.7	2.1	@ N1
3	2.1	1.9	1.9		0.9	1.3	2.2	
4	2.5	2.3	1.9	@ E2	1.2	1.3	1.5	@ N2
5	2.6	2.1	2.8		1.3	1.5	0.9	
6	3.0	2.6	2.1	@ E3	2.5	2.6	2.0	@ N3
7	3.0	2.6	2.2	against edge	2.3	0.0	1.9	against edge

DAY 76								
11/3/92					11/3/92			
vertical dipole mode					*vertical dipole mode*			
LINE	N1	N2	N3		E1	E2	E3	
STATION	(mS/m)	(mS/m)	(mS/m)		(mS/m)	(mS/m)	(mS/m)	
1	2.5	2.2	2.6		7.9	3.3	3.5	
2	1.9	2.0	2.4	@ E1	2.9	2.9	3.0	@ N1
3	2.3	2.5	2.4		2.9	3.4	3.2	
4	2.2	3.0	2.8	@ E2	2.6	3.4	3.0	@ N2
5	2.2	2.7	2.5		2.5	2.8	3.2	
6	2.4	2.6	2.7	@ E3	2.6	3.3	3.5	@ N3
7	2.5	2.3	3.0	against edge	2.6	4.6	3.5	against edge

DAY 76								
11/3/92					11/3/92			
horizontal dipole mode					*horizontal dipole mode*			
LINE	N1	N2	N3		E1	E2	E3	
STATION	(mS/m)	(mS/m)	(mS/m)		(mS/m)	(mS/m)	(mS/m)	
1	1.8	2.7	2.8		5.6	3.2	2.8	
2	2.7	2.7	2.7	@ E1	2.7	3.2	3.5	@ N1
3	2.6	2.8	3.0		2.5	3.1	3.4	
4	2.6	3.5	3.6	@ E2	2.6	3.0	3.3	@ N2
5	3.1	3.5	3.7		2.9	3.0	3.3	
6	3.5	3.6	4.0	@ E3	3.1	2.9	3.6	@ N3
7	3.6	4.0	4.3	against edge	3.0	1.3	3.1	against edge

Figure B EM38 data summary sheet and averages. (continued)

CFB-LNAPL-92		EM38						
	apparent conductivity (mS/m)							
	vertical dipole mode							
		stn.#1	stn.#2	stn.#3	stn.#4	stn.#5	stn.#6	stn.#7
	day14(N2)	4.8	6.3	7	7	7.1	7	4.8
	day14(E2)	4.8	6.1	6.8	6.7	6.4	6.3	4.6
	day29(N2)	4.5	4.5	4.3	4.8	4.8	4.2	3.2
	day29(E2)	4	5	4.5	4	3.7	4.5	6
	day76(N2)	2.2	2	2.5	3	2.7	2.6	2.3
	day76(E2)	3.3	2.9	3.4	3.4	2.8	3.3	4.6
	horizontal dipole mode							
		stn.#1	stn.#2	stn.#3	stn.#4	stn.#5	stn.#6	stn.#7
	day14(N2)	7.5	8	8.2	8.4	8.2	8.8	9
	day14(E2)	6.8	7.3	7.7	7.9	7.7	7.9	7
	day29(N2)	2.1	2.3	1.9	2.3	2.1	2.6	2.6
	day29(E2)	1.3	1.7	1.3	1.3	1.5	2.6	0
	day76(N2)	2.7	2.7	2.8	3.5	3.5	3.6	4
	day76(E2)	3.2	3.2	3.1	3	3	2.9	1.3

Figure B EM38 data summary sheet and averages. Plot data (continued)

APPENDIX C

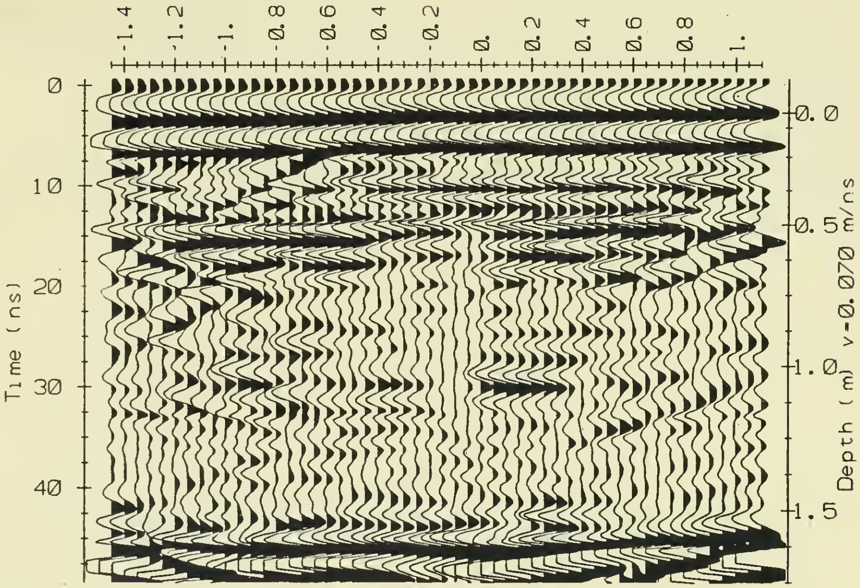

Figure C.1 GPR survey with 450 MHz antennae on day 32 along line N1. The water table is at 1.1 m and there is no kerosene in the test cell.

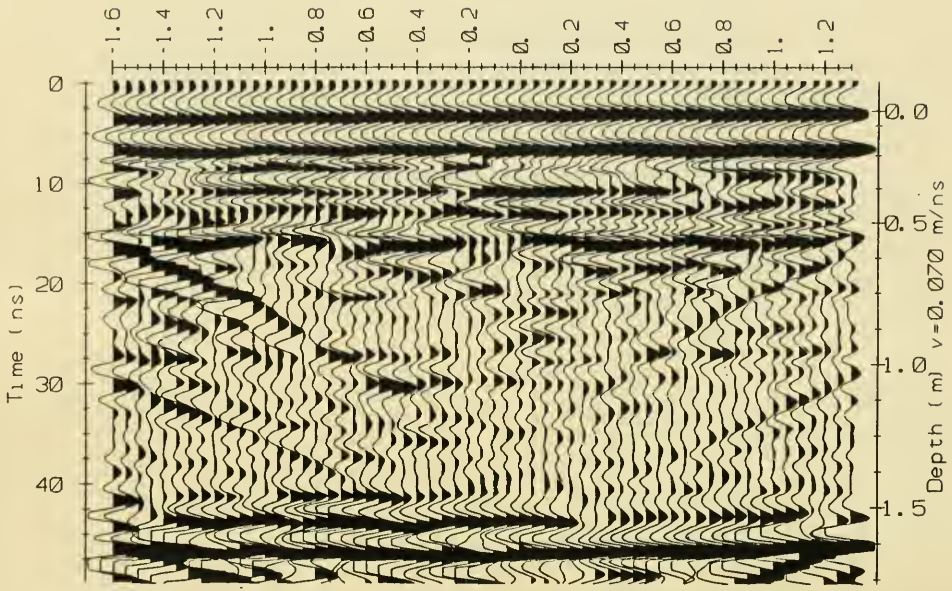

Figure C.2 GPR survey with 450 MHz antennae on day 32 along line N2. The water table is at 1.1 m and there is no kerosene in the test cell.

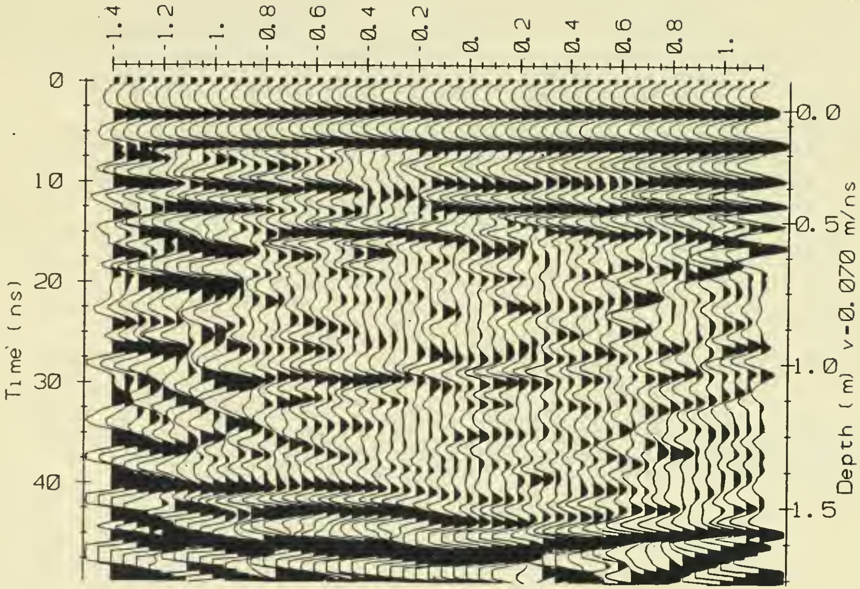

Figure C.3 GPR survey with 450 MHz antennae on day 32 along line N3. The water table is at 1.1 m and there is no kerosene in the test cell.

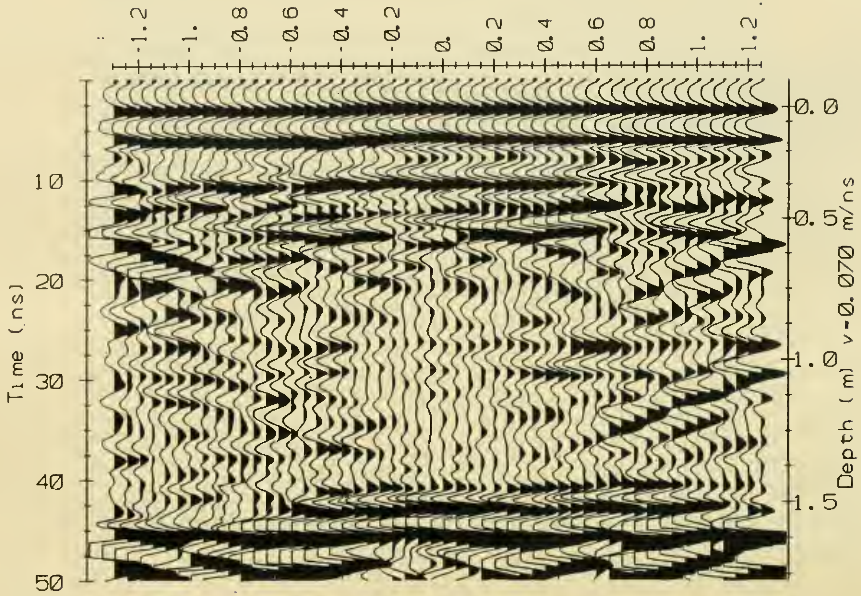

Figure C.4 GPR survey with 450 MHz antennae on day 32 along line E1. The water table is at 1.1 m and there is no kerosene in the test cell.

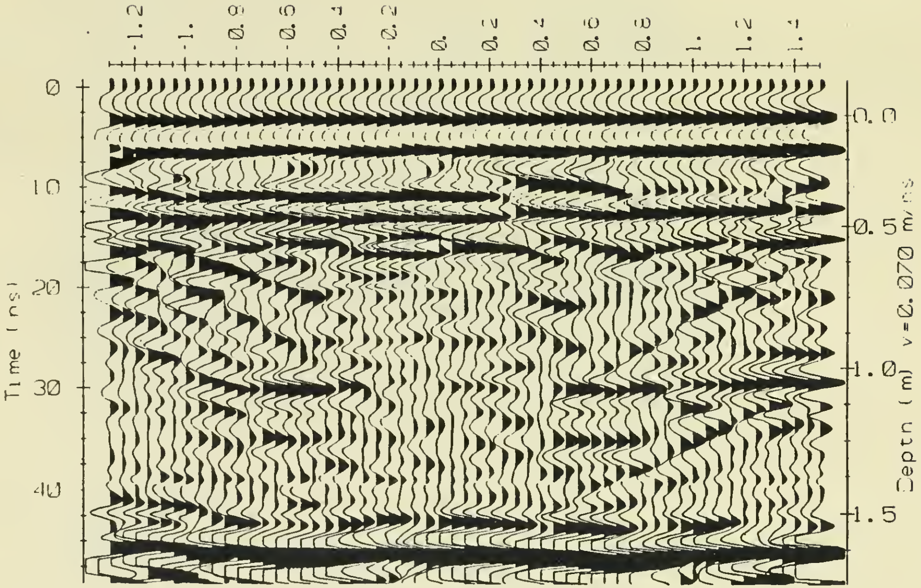

Figure C.5 GPR survey with 450 MHz antennae on day 32 along line E2. The water table is at 1.1 m and there is no kerosene in the test cell.

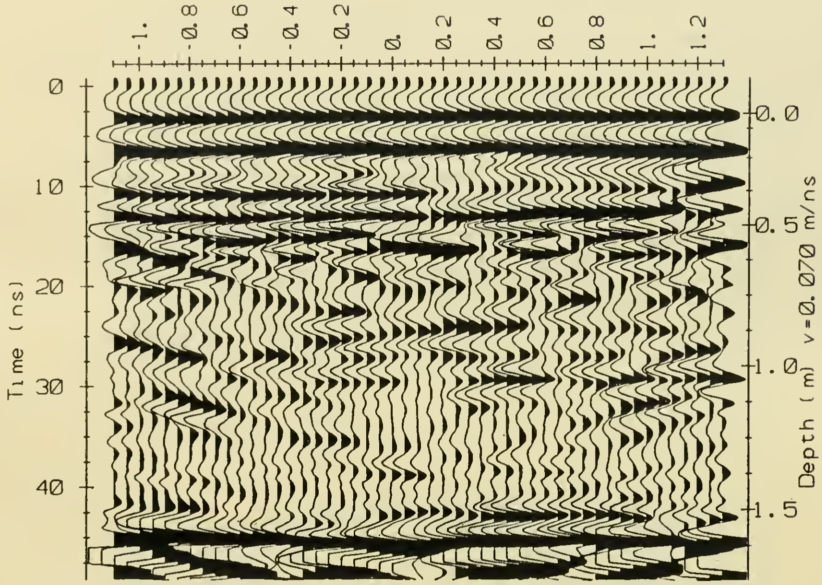

Figure C.6 GPR survey with 450 MHz antennae on day 32 along line E3. The water table is at 1.1 m and there is no kerosene in the test cell.

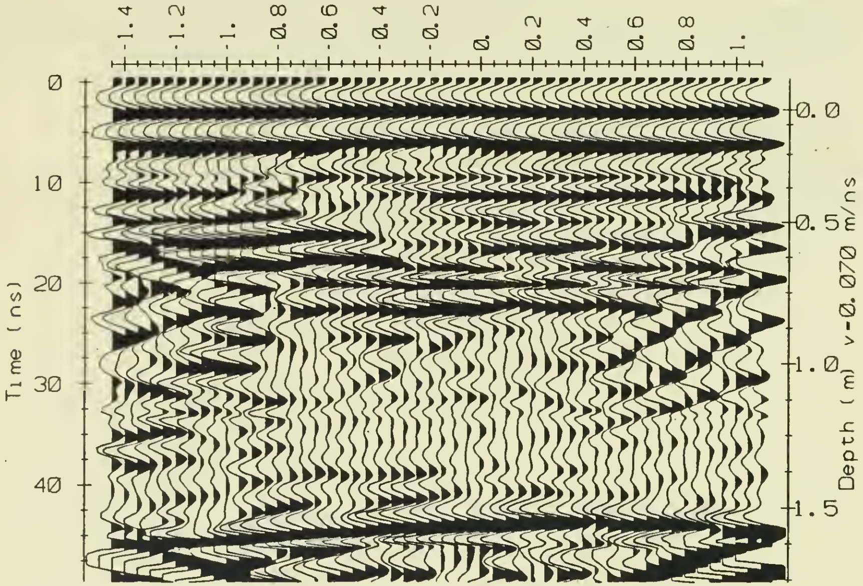

Figure C.7 GPR survey with 450 MHz antennae on day 71 along line N1. The water table is at 1.1 m. This is after the final injection therefore there are 343 L of kerosene in the test cell.

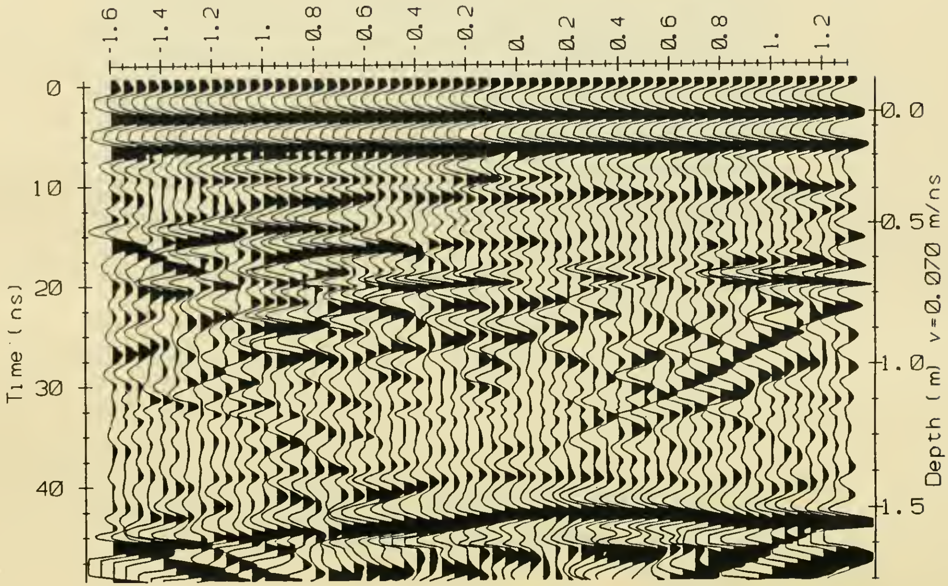

Figure C.8 GPR survey with 450 MHz antennae on day 71 along line N2. The water table is at 1.1 m. This is after the final injection therefore there are 343 L of kerosene in the test cell.

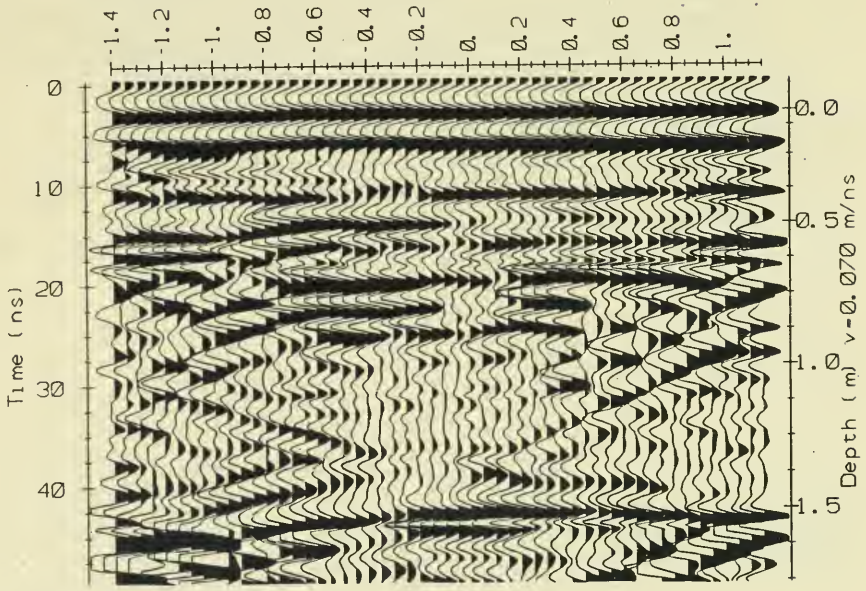

Figure C.9 GPR survey with 450 MHz antennae on day 71 along line N3. The water table is at 1.1 m. This is after the final injection therefore there are 343 L of kerosene in the test cell.

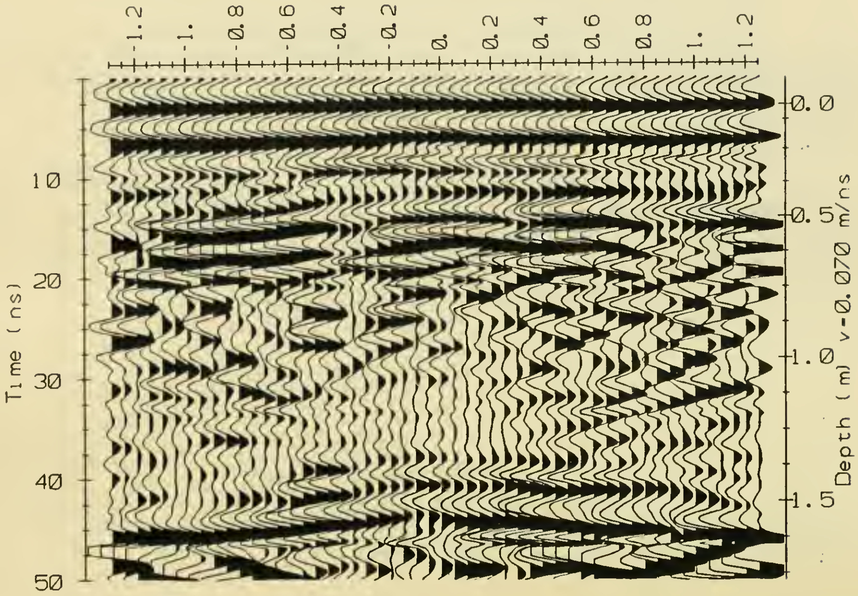

Figure C.10 GPR survey with 450 MHz antennae on day 71 along line E1. The water table is at 1.1 m. This is after the final injection therefore there are 343 L of kerosene in the test cell.

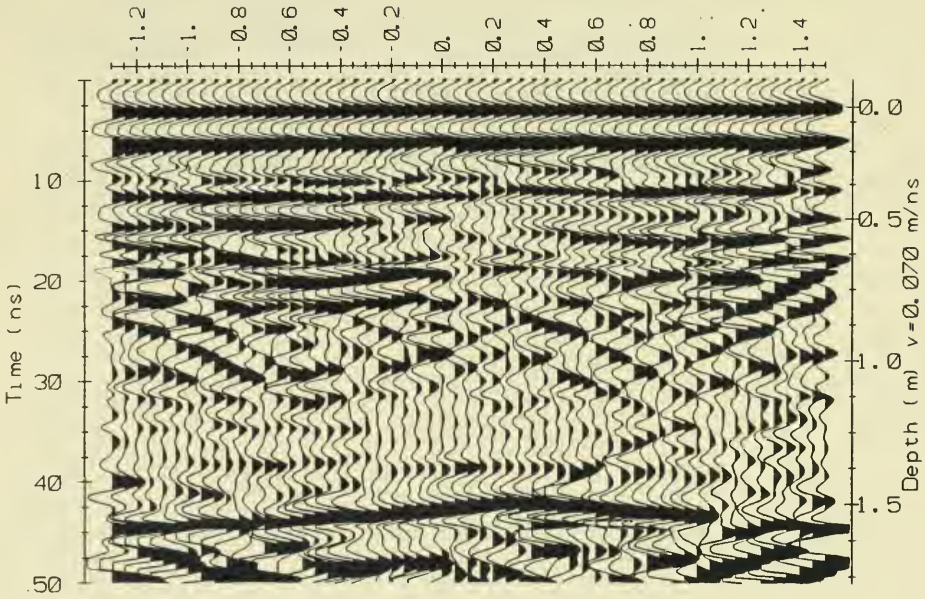

Figure C.11 GPR survey with 450 MHz antennae on day 71 along line E2. The water table is at 1.1 m. This is after the final injection therefore there are 343 L of kerosene in the test cell.

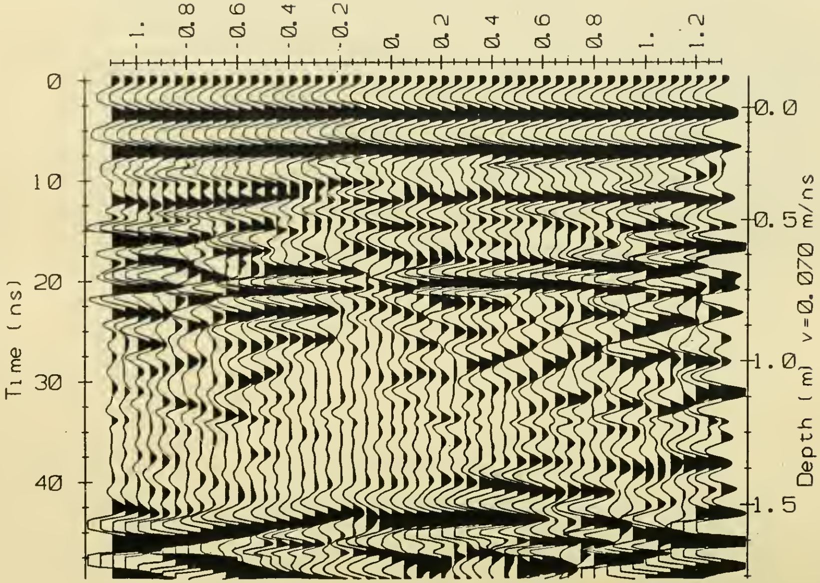

Figure C.12 GPR survey with 450 MHz antennae on day 71 along line E3. The water table is at 1.1 m.

SURFACE RESISTIVITY line E2 depth 20 cm

location	DAY 32	DAY 38	DAY 44	DAY 56	DAY 64
1.35	1098.82	1156.14	1171.73	1393.5	1457.86
1.15	1040.93	1080.81	1112.02	1315.23	1437.19
0.95	1054.5	1061.72	1102.21	1381.54	1512.65
0.75	1019.27	1056.1	1099.85	1377.6	1550.58
0.55	1071.73	1089.49	1181.97	1496.22	1643.87
0.35	1105.29	1127.8	1214.2	1527.97	1669.78
0.15	1080.2	1128.7	1171.95	1466.29	1691.18
-0.05	1093.26	1111.43	1181.1	1539.67	1671.71
-0.25	1089.93	1144.42	1121.95	1416.85	1625.72
-0.45	1048.23	1050.44	1015.02	1343.03	1544.07
-0.65	1024.44	1105.76	1080.33	1277.18	1480.4
-0.85	1090.82	1131.41	1051.5	1251.25	1451.37
-1.05	999.7	1063.98	1006.18	1231.39	1312.27
average	1062.86	1100.63	1116.15	1385.98	1542.20

SURFACE RESISTIVITY line E2 depth 60 cm

location	DAY 32	DAY 38	DAY 44	DAY 56	DAY 64
0.75	982.6	1042.19	1081.65	1264.37	1460.65
0.55	893.96	959.06	999.09	1164.33	1344.21
0.35	856.8	951.63	1002.73	1130.6	1310.67
0.15	880.5	957.78	1003.66	1120.67	1326.22
-0.05	880.4	933.17	974.18	1126.56	1255.16
-0.25	866.32	912.86	941.52	1112.2	1288.9
-0.45	895.44	965.85	982.21	1138.02	1354.02
average	893.72	960.36	997.86	1150.96	1334.26

****

AVERAGE surface resistivity at 20 cm Wenner array electrode spacing (line N2 & E2)

		DAY 32	DAY 38	DAY 44	DAY 56	DAY 64
N2	averages	1094.42	1126.41	1114.37	1389.26	1631.78
E2	averages	1062.86	1100.63	1116.15	1385.98	1542.20
	average	1078.64	1113.52	1115.26	1387.62	1586.99

AVERAGE surface resistivity at 60 cm Wenner array electrode spacing (line N2 & E2)

		DAY 32	DAY 38	DAY 44	DAY 56	DAY 64
N2	averages	902.51	957.73	996.43	1132.16	1338.14
E2	averages	893.72	960.36	997.86	1150.96	1334.26
	average	898.11	959.05	997.15	1141.56	1336.20

Appendix E Surface DC Resistivity data.

SURFACE RESISTIVITY line N2 depth 20 cm

location	DAY 32	DAY 38	DAY 44	DAY 56	DAY 64
1.15	1053.36	1135.19	873.81	1322.7	1551.35
0.95	966.93	1016.06	844.57	1176.7	1471.64
0.75	940.88	959.65	935.65	1213.17	1490.37
0.55	1025.32	1071.63	1074.08	1335.37	1587.5
0.35	1025.75	1022.59	1083.34	1330.56	1627.01
0.15	1123.31	1121.67	1208.68	1481.04	1705
-0.05	1087.21	1096.31	1181.58	1427.38	1746.69
-0.25	1083.37	1081.7	1151.63	1432.74	1621.15
-0.45	1073.44	1093.47	1093.13	1379.84	1667.15
-0.65	1174.94	1198.11	1234.95	1431.72	1655.97
-0.85	1139.31	1223.33	1216.83	1453.53	1653.09
-1.05	1250.34	1263.88	1273.93	1487.8	1680.22
-1.25	1283.28	1359.73	1314.67	1587.82	1755.96
average	1094.42	1126.41	1114.37	1389.26	1631.78

SURFACE RESISTIVITY line N2 depth 60 cm

location	DAY 32	DAY 38	DAY 44	DAY 56	DAY 64
-0.65	948.56	1013.93	1058.7	1204.97	1398.34
-0.45	883.78	915.36	954.66	1108.53	1297.84
-0.25	855.2	884.19	925.18	1065.2	1312
-0.05	906.59	965.51	998.38	1153.35	1349.46
0.15	883.57	958.34	979.78	1132.81	1342.23
0.35	906.61	973.06	1018.34	1112.65	1332.22
0.55	933.23	993.7	1039.98	1147.58	1334.89
average	902.51	957.73	996.43	1132.16	1338.14

Appendix E Surface DC Resistivity data. (continued)

APPENDIX E

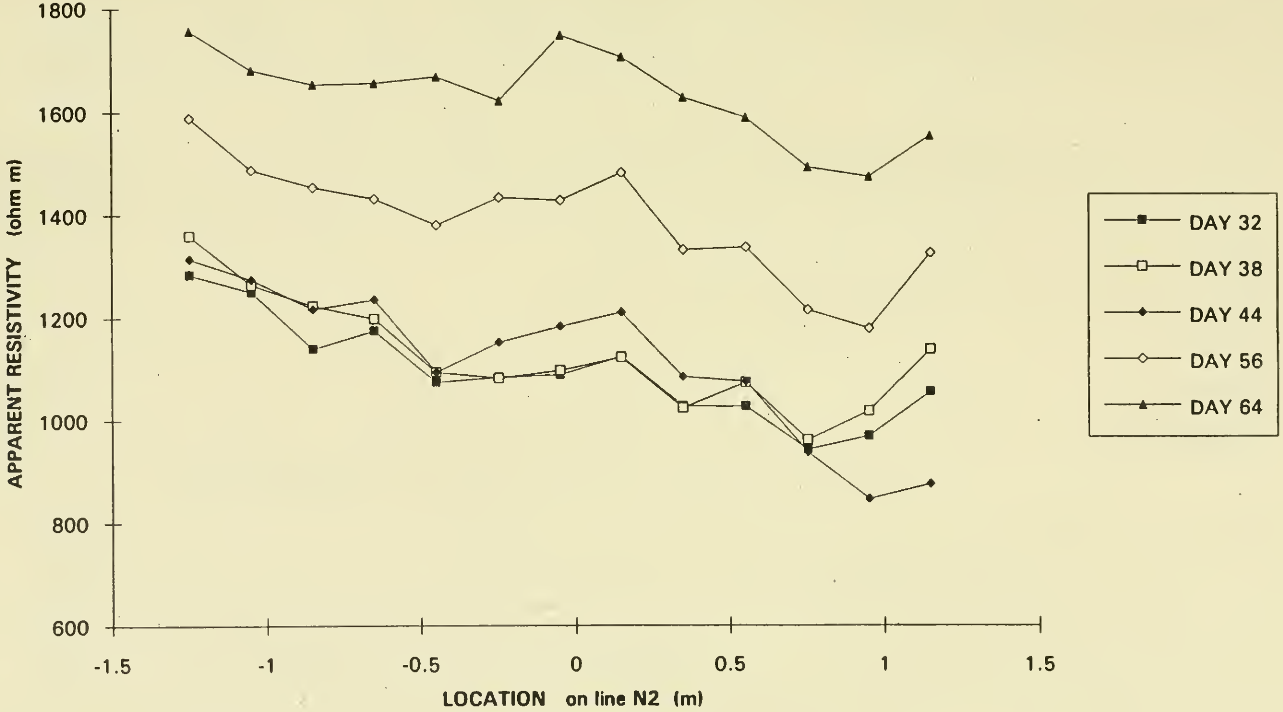

Figure E.1 Surface DC resistivity surveys using a Wenner array with potential electrode spacing of 20 cm. Profiles show changing apparent resistivities with time across the test cell along line N2.

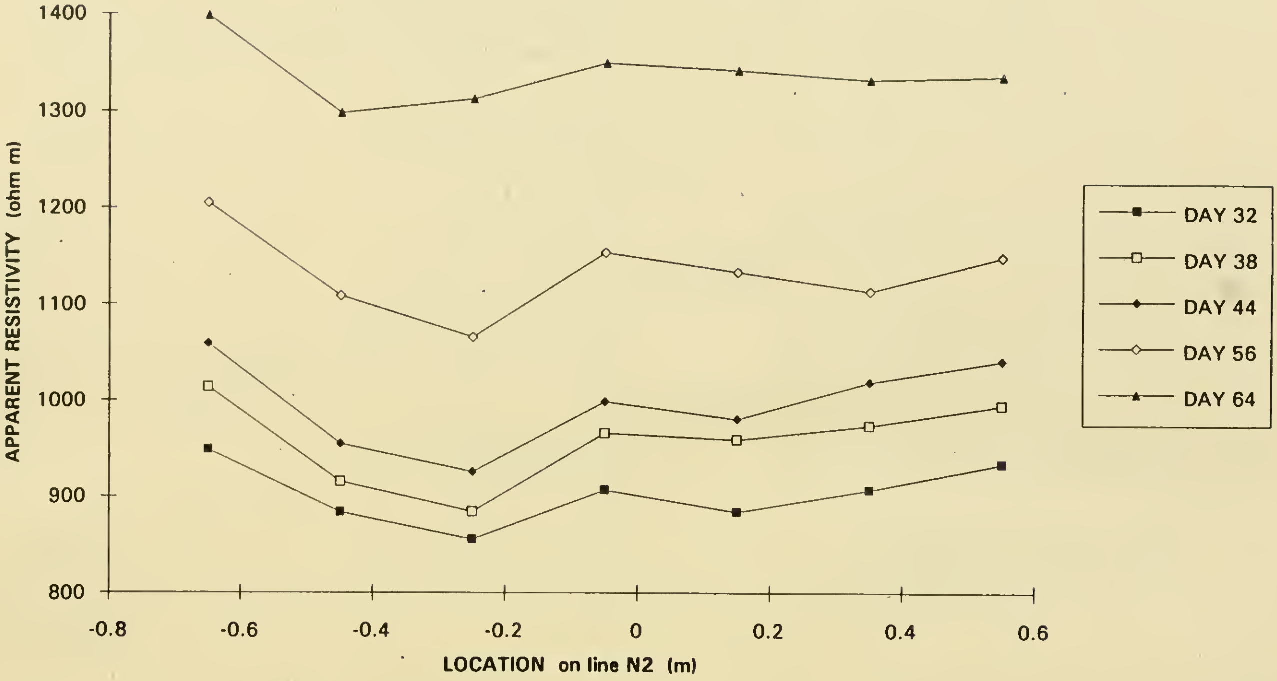

Figure E.2 Surface DC resistivity surveys using a Wenner array with potential electrode spacing of 60 cm. Profiles show changing apparent resistivities with time across the test cell along line N2.

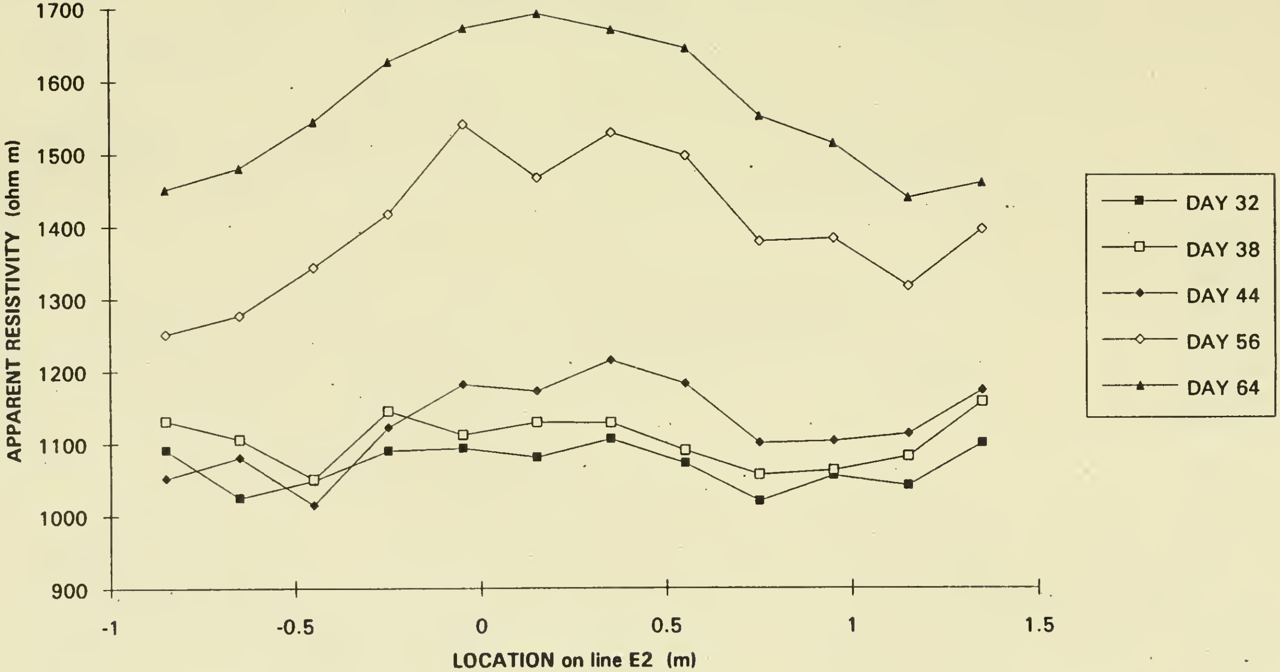

Figure E.3 Surface DC resistivity surveys using a Wenner array with potential electrode spacing of 20 cm. Profiles show changing apparent resistivities with time across the test cell along line E2.

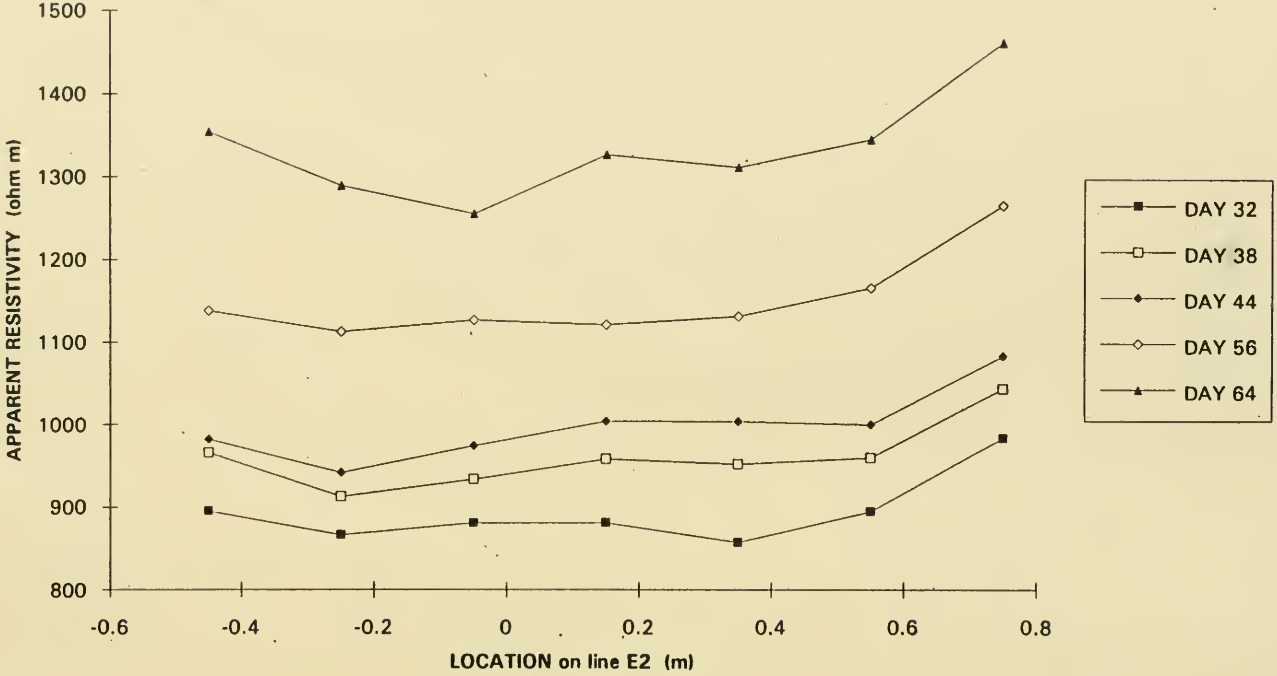

Figure E.4 Surface DC resistivity surveys using a Wenner array with potential electrode spacing of 60 cm. Profiles show changing apparent resistivities with time across the test cell along line E2.

APPENDIX F

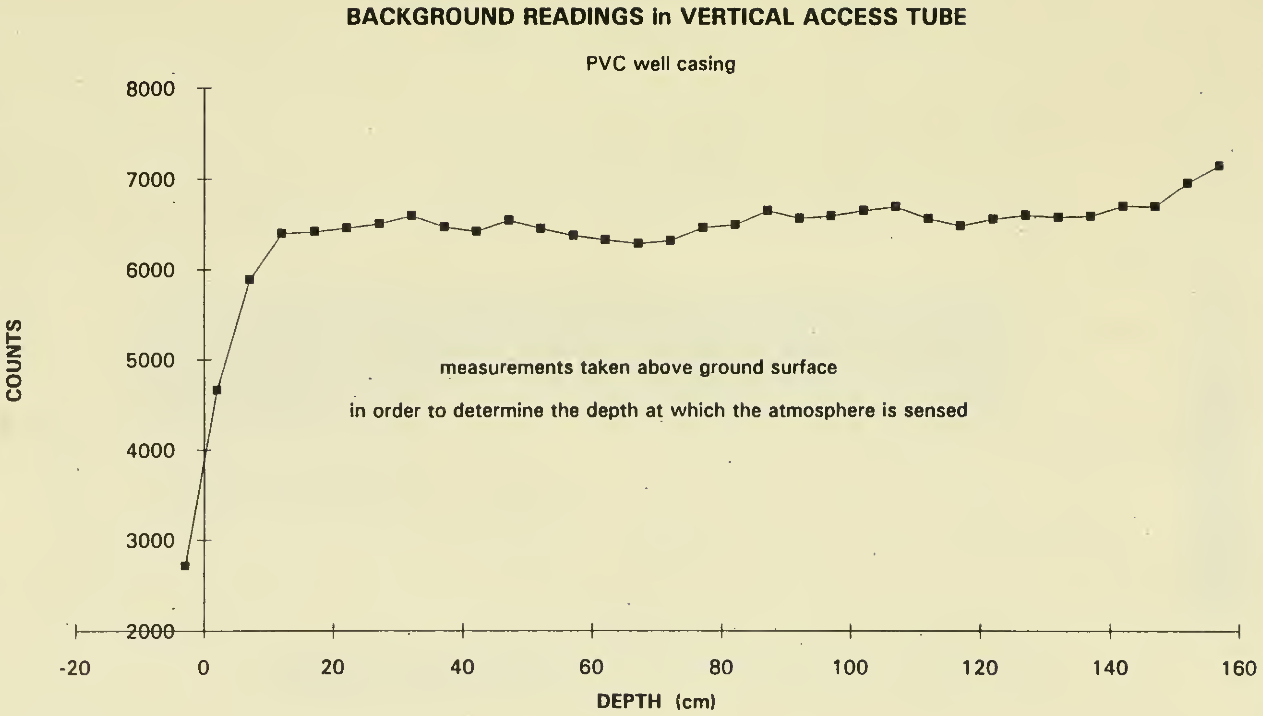

Figure F.1 Neutron measurements in vertical access tube with the test cell saturated to the surface. Determination of the vertical distance which is averaged in each measurement.

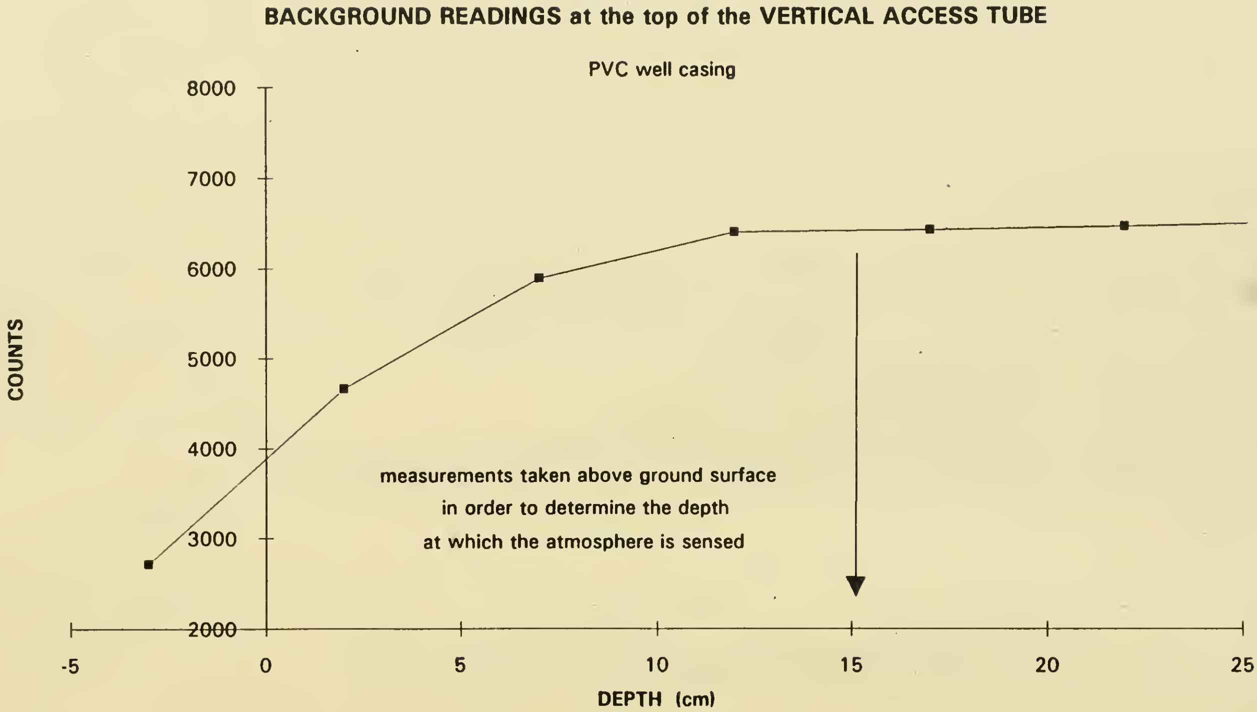

Figure F.2 Neutron measurements in vertical access tube with the test cell saturated to the surface. Determination of the vertical distance which is averaged in each measurement. Near surface readings only.

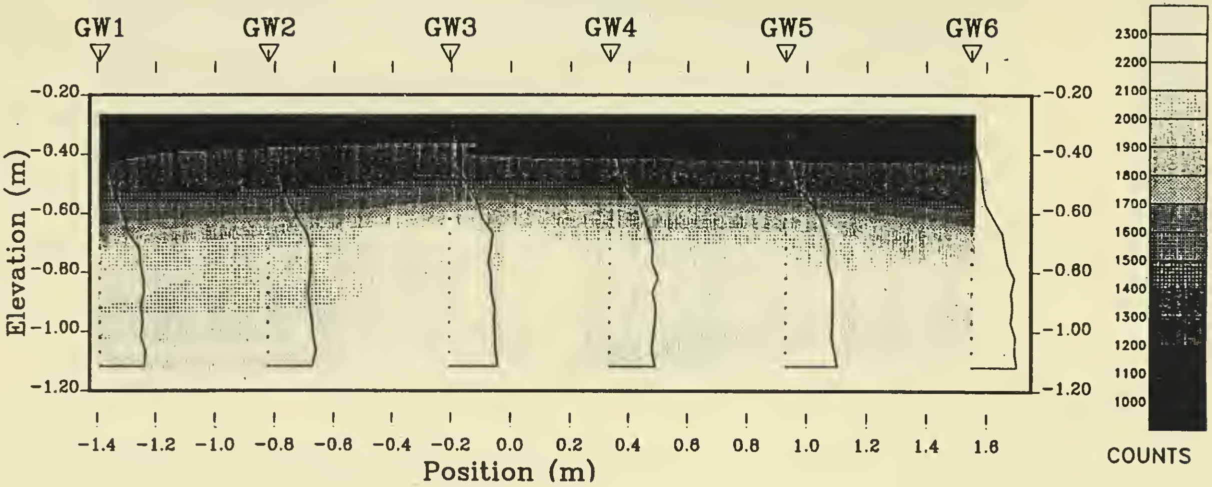

Figure F.3 Cross section of the test cell showing contoured Neutron logging measurements and profiles. Background readings only, that is, with the water table at 1.1 m and no kerosene injected.

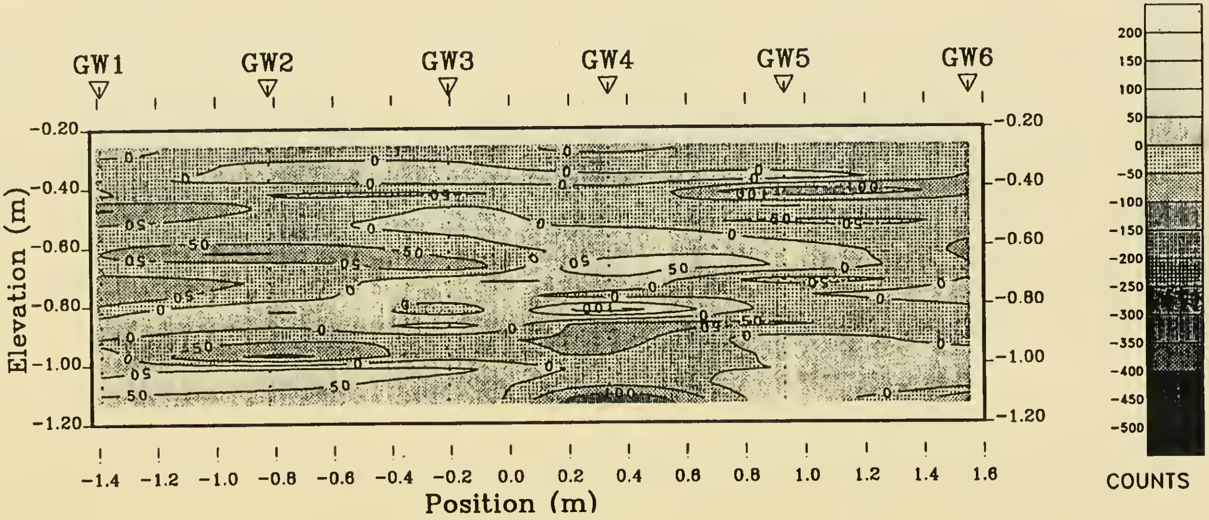

Figure F.4 Cross section of the test cell showing contoured Neutron logging measurements diffenced from background. The water table is at 1.1 m. The readings were made on day 56, after injection #3.

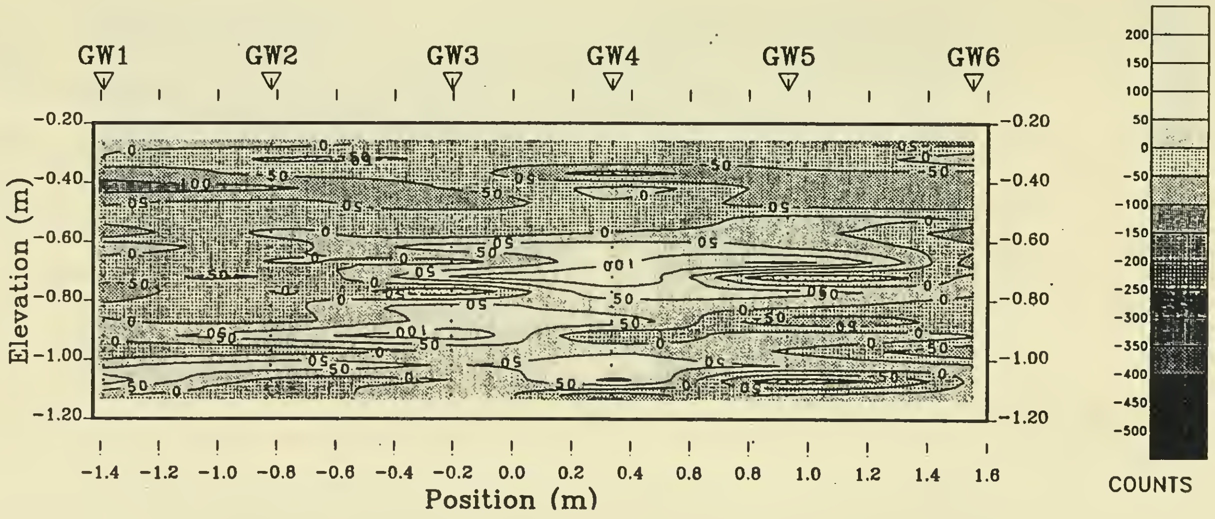

Figure F.5 Cross section of the test cell showing contoured Neutron logging measurements diffenced from background. The water table is at 1.1 m. The readings were made on day 64, after injection #4.

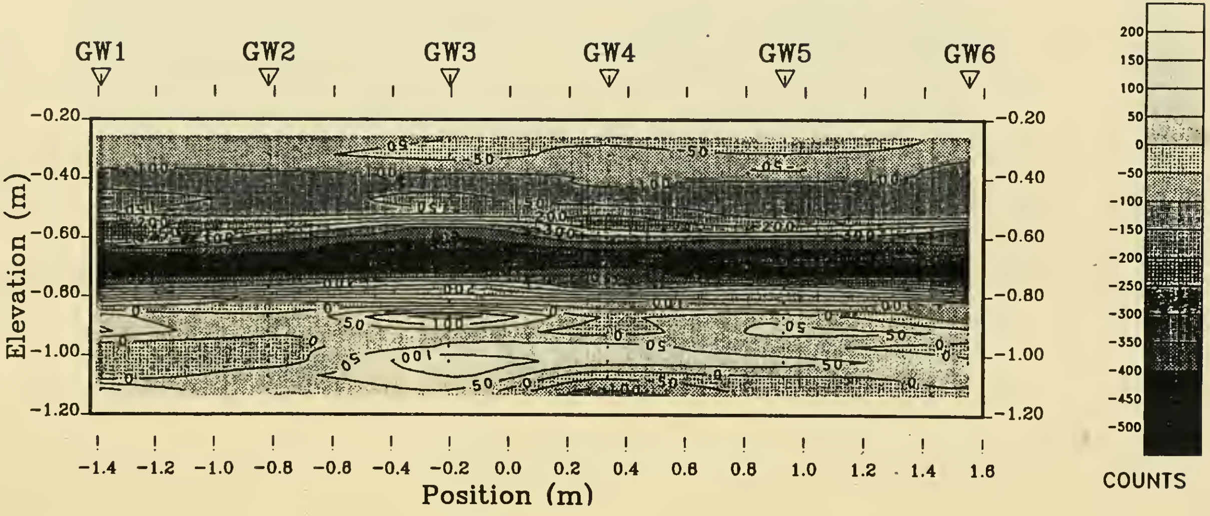

Figure F.6 Cross section of the test cell showing contoured Neutron logging measurements diffenced from background. The water table is at 1.1 m. The readings were made on day 113, after the lowering and raising of the water table in order to trap kerosene.

PVC Radon Access Tube

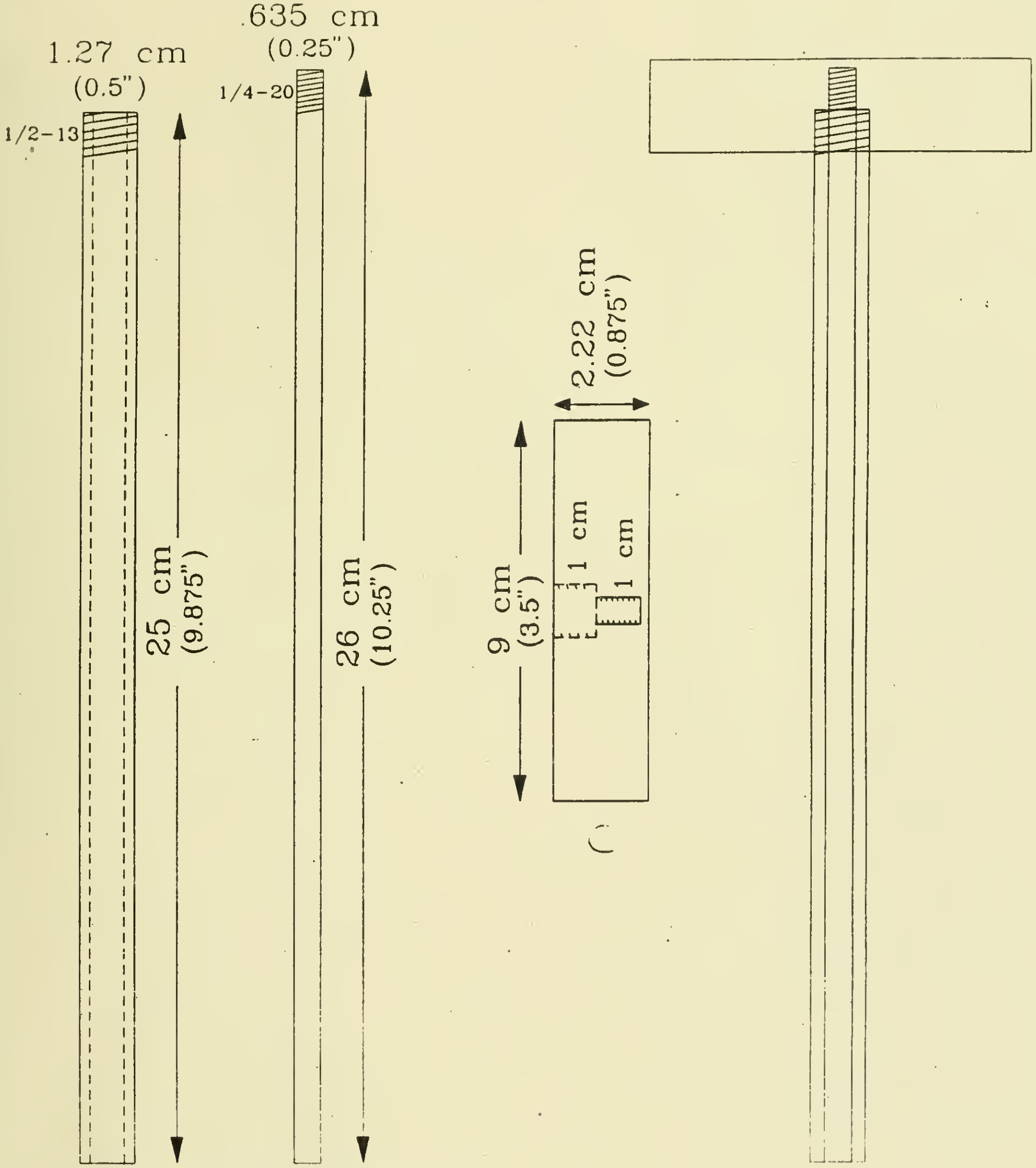

Appendix G Dimensions of Radon Access Tube